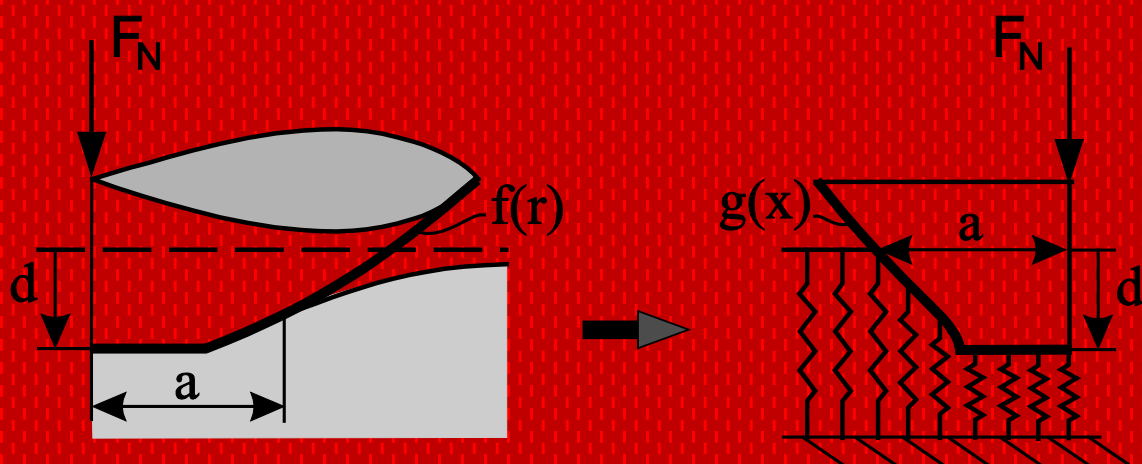


Method of Dimensionality Reduction in Contact Mechanics

User's Manual

Valentin L. Popov
Markus Heß
Emanuel Willert



Valentin L. Popov ◦ Markus Heß ◦
Emanuel Willert

Method of Dimensionality Reduction in Contact Mechanics

User's Manual



Department of System
Dynamics and Friction Physics



Valentin L. Popov
Technische Universität Berlin
Berlin, Germany

Emanuel Willert
Technische Universität Berlin
Berlin, Germany

Markus Heß
Technische Universität Berlin
Berlin, Germany

ISBN 978-3-00-060382-2

© Technische Universität Berlin, Department of System Dynamics and Friction Physics, 2018

Technische Universität Berlin
Department of System Dynamics and Friction Physics
Sekt. C8-4
Str. des 17. Juni 135
10623 Berlin
Germany

The Method of Dimensionality Reduction (MDR) is a method of calculation and simulation of contacts of elastic and viscoelastic bodies. It consists essentially of two simple steps: (a) substitution of the three-dimensional continuum by a uniquely defined one-dimensional linearly elastic or viscoelastic foundation (Winkler foundation) and (b) transformation of the three-dimensional profile of the contacting bodies by means of the MDR-transformation. As soon as these two steps are done, the contact problem can be considered to be solved. For axial symmetric contacts, only a small calculation by hand is required which does not exceed elementary calculus and will not be a barrier for any practically-oriented engineer. Alternatively, the MDR can be implemented numerically, which is almost trivial due to the independence of the foundation elements. In spite of its simplicity, all results are exact. The present book is a collection of open access papers all together covering the most important aspects of the MDR and providing a practical guide for its use.

Author Biographies



Prof. Dr. rer. nat. Valentin L. Popov studied physics (1976-1982) and obtained his doctorate in 1985 from the Moscow State Lomonosov University. He worked at the Institute of Strength Physics of the Russian Academy of Sciences. After a guest-professorship in the field of theoretical physics at the University of Paderborn (Germany) from 1999 to 2002, he has headed since 2002 the department of System Dynamics and the Physics of Friction in the Institute of Mechanics at the Berlin University of Technology.

Address: Technische Universität Berlin, Institute of Mechanics, Sekr. C8-4, Str. des 17. Juni 135, 10623 Berlin, Germany.

E-mail: v.popov@tu-berlin.de



Dr. Markus Heß studied Engineering Science at TU Berlin. He obtained his doctorate in 2011 and in the same year received the research award from the Tribology Society for his dissertation. From 2011 to 2015 he headed the physics department of the preparatory college of the TU Berlin and since 2015 he has been working as an assistant professor in the department of System Dynamics and Friction Physics.

Address: Technische Universität Berlin, Institute of Mechanics, Sekr. C8-4, Str. des 17. Juni 135, 10623 Berlin, Germany.

E-mail: markus.hess@tu-berlin.de



M.Sc. Emanuel Willert studied Engineering Science at the TU Berlin and the Polytechnical University Tomsk. Since 2015 he has been active as a research assistant in the department of System Dynamics and Friction Physics. He is co-author of “Handbuch der Kontaktmechanik” – Springer, 2018.

Address: Technische Universität Berlin, Institute of Mechanics, Sekr. C8-4, Str. des 17. Juni 135, 10623 Berlin, Germany.

E-mail: e.willert@tu-berlin.de

Table of Contents

Preface	1
Chapter 1: Foundations of the Method of Dimensionality Reduction	3
Method of dimensionality reduction in contact mechanics and friction:	
I. Axially-symmetric contacts (V.L. Popov and M. Heß).....	4
Method of dimensionality reduction in contact mechanics and friction:	
II. Power-law graded materials (M. Heß and V.L. Popov).....	18
Method of dimensionality reduction in contact mechanics and friction:	
III. Viscoelastic contacts (V.L. Popov, M. Heß and E. Willert).....	36
Chapter 2: Numerical Aspects of the MDR	51
Fast numerical implementation of the MDR transformations (J. Benad).....	52
Chapter 3: Application of the MDR to Selected Non-Axisymmetrical Contact Problems	64
Indentation of flat-ended and tapered indenters with polygonal cross-sections (Q. Li, V.L. Popov).....	65
Normal line contact of finite-length cylinders (Q. Li, V.L. Popov)	74
Chapter 4: Applications of the MDR	83
The influence of viscoelasticity on velocity-dependent restitutions in the oblique impact of spheres (E. Willert, S. Kusche, V.L. Popov).....	84
Dugdale-Maugis adhesive normal contact of axisymmetric power-law graded elastic bodies (E. Willert).....	100
Limiting profile of axisymmetric indenter due to the initially displaced dual-motion fretting wear (Q. Li).....	110
Chapter 5: Further Generalizations of the MDR	117
Application of the MDR to contacts under normal and torsional loading (E. Willert, M. Hess, V.L. Popov).....	118
Chapter 6: Approximate Solutions using the MDR	128
Simulation of frictional dissipation under biaxial tangential loading with the MDR (A.V. Dimaki, R. Pohrt, V.L. Popov).....	129
Analysis of impact on composite structures with the MDR (V.L. Popov).....	141

Preface

The present book is a collection of open-access papers describing the foundations and applications of the Method of Dimensionality Reduction (MDR), first published in the Journal “Facta Universitatis. Series Mechanical Engineering” in the years 2014-2018.

The Method of Dimensionality Reduction (MDR) is a method of calculation and simulation of contacts of elastic and viscoelastic bodies. It consists essentially of two simple steps: (a) substitution of the three-dimensional continuum by a uniquely defined one-dimensional linearly elastic or viscoelastic foundation (Winkler foundation) and (b) transformation of the three-dimensional profile of the contacting bodies by means of the MDR-transformation. As soon as these two steps are done, the contact problem can be considered to be solved. For axial symmetric contacts, only a small calculation by hand is required which does not exceed elementary calculus and will not be a barrier for any practically-oriented engineer. Alternatively, the MDR can be implemented numerically, which is almost trivial due to the independence of the foundation elements. In spite of its simplicity, all results are exact. The present book brings together papers covering the most important aspects of the MDR and providing a practical guide for its use.

The book comprises the following papers:

- VL Popov, M Hess: *Method of dimensionality reduction in contact mechanics and friction: a users handbook. I. Axially-symmetric contacts*, Facta Universitatis, Series: Mechanical Engineering 12 (1), 1-14, 2014.
- M Hess, VL Popov: *Method of dimensionality reduction in contact mechanics and friction: a user's handbook. II. Power-law graded materials*, Facta Universitatis, Series: Mechanical Engineering 14 (3), 251-268, 2016.
- VL Popov, E Willert, M Heß, *Method of dimensionality reduction in contact mechanics and friction: a user's handbook. III. Viscoelastic contacts*, Facta Universitatis, Series: Mechanical Engineering, 16 (2), 99-113, 2018.
- J Benad, *Fast numerical implementation of the MDR transformations*, Facta Universitatis, Series: Mechanical Engineering, 16 (2), 127-138, 2018.
- Q Li, VL Popov, *Indentation of flat-ended and tapered indenters with polygonal cross-sections*, Facta Universitatis, Series: Mechanical Engineering 14 (3), 241-249, 2016.
- Q Li, VL Popov, *Normal line contact of finite-length cylinders*, Facta Universitatis, Series: Mechanical Engineering 15 (1), 63-71, 2017.
- E Willert, S Kusche, VL Popov, *The influence of viscoelasticity on velocity-dependent restitutions in the oblique impact of spheres*, Facta Universitatis, Series: Mechanical Engineering 15 (2), 269-284, 2017.
- E Willert, *Dugdale-Maugis adhesive normal contact of axisymmetric power-law graded elastic bodies*, Facta Universitatis, Series: Mechanical Engineering 16 (1), 9-18, 2018.
- Q Li, *Limiting profile of axisymmetric indenter due to the initially displaced dual motion fretting wear*, Facta Universitatis, Series: Mechanical Engineering 14 (1), 55-61, 2016.

- E Willert, M Hess, VL Popov, *Application of the method of dimensionality reduction to contacts under normal and torsional loading*, Facta Universitatis, Series: Mechanical Engineering 13 (2), 81-90, 2015.
- AV Dimaki, R Pohrt, VL Popov, *Simulation of frictional dissipation under biaxial tangential loading with the method of dimensionality reduction*, Facta Universitatis, Series: Mechanical Engineering 15 (2), 295-306, 2017.
- VL Popov, *Analysis of impact on composite structures with the method of dimensionality reduction*, Facta Universitatis, Series: Mechanical Engineering 13 (1), 39-46, 2015.

The target audiences:

This book is geared towards engineers working in e.g. mechanical engineering, the tire industry, the automotive industry, polymer- and elastomer manufacturing. Additionally, it functions as a reference work for research and teaching.

Valentin L. Popov, Markus Heß und Emanuel Willert

Berlin, August 2018

Chapter 1

Foundations of the Method of Dimensionality Reduction

**METHOD OF DIMENSIONALITY REDUCTION IN CONTACT
MECHANICS AND FRICTION: A USERS HANDBOOK.
I. AXIALLY-SYMMETRIC CONTACTS**

UDC (539.3)

Valentin L. Popov, Markus Hess

Technical University Berlin

Abstract. *The Method of Dimensionality Reduction (MDR) is a method of calculation and simulation of contacts of elastic and viscoelastic bodies. It consists essentially of two simple steps: (a) substitution of the three-dimensional continuum by a uniquely defined one-dimensional linearly elastic or viscoelastic foundation (Winkler foundation) and (b) transformation of the three-dimensional profile of the contacting bodies by means of the MDR-transformation. As soon as these two steps are completed, the contact problem can be considered to be solved. For axial symmetric contacts, only a small calculation by hand is required which does not exceed elementary calculus and will not be a barrier for any practically-oriented engineer. Alternatively, the MDR can be implemented numerically, which is almost trivial due to the independence of the foundation elements. In spite of their simplicity, all the results are exact. The present paper is a short practical guide to the MDR.*

Key Words: *Normal Contact, Tangential Contact, Adhesion, Friction, Partial Slip, Stress*

1. INTRODUCTION

In the recently published book [1], the so-called method of dimensionality reduction (MDR) is described for the first time in detail. MDR can be traced back to the solution of the normal contact problem by Galin (Russian Academy of Sciences) in the 1940s [2]. His results were later published by Sneddon and, in this way, made public to the western world [3]. The method of dimensionality reduction takes these results and puts them into such a form that even a layman in the field of contact mechanics can use them for a multitude of contact mechanical problems. In doing this, it merges the ideas and results from Cattaneo [4], Mindlin [5], Jaeger [6], and Ciavarella [7] about a close relationship between normal and tangential contacts, the solutions of Galanov and Borodich [8, 9, 10]

Received February 20, 2014

Corresponding author: Valentin Popov

TU Berlin, Department of System Dynamics and Physics of Friction, Berlin, Germany

E-mail: v.popov@tu-berlin.de

for adhesive contacts of axially-symmetric profiles of power functions (later found independently by Yao and Gao [11]), as well as the theory of Lee and Radok about the relationship between elastic and viscoelastic contacts [12, 13].

The book [1] contains all of the necessary evidence and many examples of how to apply the MDR. However, it has proven to be too comprehensive for practical users. There is a need for the fundamental ideas and "recipes" of the MDR to be presented in a concise way without extensive reasoning or proof, a sort of "user's handbook." This work is dedicated to exactly such a practical instruction for the method of dimensionality reduction.

2. TWO INTRODUCTORY STEPS OF THE MDR

We consider a contact between two elastic bodies with moduli of elasticity of E_1 and E_2 , Poisson's numbers of ν_1 and ν_2 , and shear moduli of G_1 and G_2 , accordingly. In this work, we restrict ourselves to the axially-symmetric profiles, which is not necessarily required. A generalization to profiles that are not axially-symmetric is possible, but is not considered in this work. We denote the difference between the profiles of bodies as $z = f(r)$. In the framework of the MDR, two independent steps are conducted:

The first step: First, the three-dimensional elastic (or viscoelastic) bodies are replaced by a one-dimensional linearly elastic foundation. This is considered to be a linear array of elements having independent degrees of freedom and a sufficiently small separation distance Δx , Fig. 1.

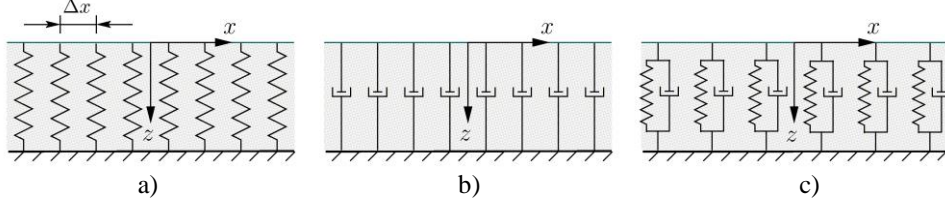


Fig. 1 One-dimensional foundation of different materials: elastic foundation (a), purely viscous foundation (b), and viscoelastic foundation (c) with an example rheology according to Kelvin-Voigt

In the simplest case of the elastic contact, the foundation consists of linearly elastic spring elements that have normal stiffness Δk_z and tangential stiffness Δk_x (Fig. 1a):

$$\Delta k_z = E^* \Delta x \quad \text{with} \quad \frac{1}{E^*} = \frac{1-\nu_1^2}{E_1} + \frac{1-\nu_2^2}{E_2}, \quad (1)$$

$$\Delta k_x = G^* \Delta x \quad \text{with} \quad \frac{1}{G^*} = \frac{2-\nu_1}{4G_1} + \frac{2-\nu_2}{4G_2}. \quad (2)$$

Starred values E^* and G^* denote the effective elastic moduli. Incompressible linearly viscous materials are presented by a linear damping element with damping coefficient $\Delta \gamma$ (Fig. 1b), which is dependent on the viscosity η of the viscoelastic partner according to:

$$\Delta\gamma = 4\eta\Delta x. \quad (3)$$

Arbitrary combinations of these two base elements are also possible in order to satisfy the most complicated elastomers – Fig. 1c, for example, shows a viscoelastic foundation built out of elements of in parallel connected springs and dampers (Kelvin-Voigt model). In this paper, we will restrict ourselves to the case of "elastically similar" materials:

$$\frac{1-2\nu_1}{G_1} = \frac{1-2\nu_2}{G_2}, \quad (4)$$

which guarantees the independence of the normal and tangential contact problems [14]. This condition is always met in important cases of contacts between the bodies with the same elastic properties or those between a rigid body and an elastomer.

The second step: In the second step, three-dimensional profile $z = f(r)$ (Fig. 2, left) is transformed into a one-dimensional profile (Fig. 2, right) according to:

$$g(x) = |x| \int_0^{|x|} \frac{f'(r)}{\sqrt{x^2 - r^2}} dr. \quad (5)$$

The reverse transformation is:

$$f(r) = \frac{2}{\pi} \int_0^r \frac{g(x)}{\sqrt{r^2 - x^2}} dx. \quad (6)$$

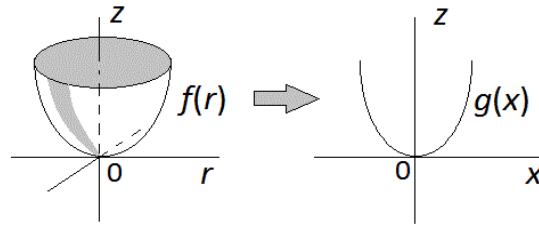


Fig. 2 The three-dimensional profile is transformed into a one-dimensional profile using the MDR

For a less trivial example, we consider the contact of a *parabolic profile with a worn tip* (Fig. 3):

$$f(r) = \begin{cases} 0 & \text{for } 0 \leq r \leq b \\ \frac{r^2 - b^2}{2R} & \text{for } b \leq r \leq a \end{cases}. \quad (7)$$

The MDR transformed profile according to Eq. (5) is given by:

$$g(x) = \begin{cases} 0 & \text{for } 0 \leq |x| \leq b \\ \frac{|x|}{R} \sqrt{x^2 - b^2} & \text{for } b \leq |x| \leq a \end{cases}. \quad (8)$$

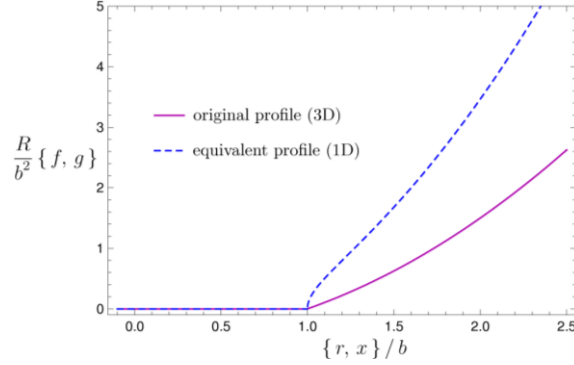


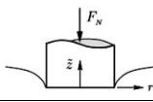
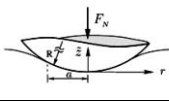
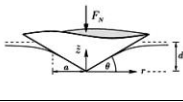
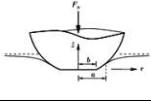
Fig. 3 Parabolic indenter with a "worn" tip: original (solid line) and equivalent (dashed line) profiles for comparison

Examples for the MDR transformation

By inserting profiles into Eq. (5) that correspond to a cylinder, paraboloid, cone, or an arbitrary power function $z \sim r^n$, we obtain the MDR transformed one-dimensional profiles which are summarized in Table 1, where:

$$k_n = \frac{\sqrt{\pi}}{2} \frac{n\Gamma\left(\frac{n}{2}\right)}{\Gamma\left(\frac{n}{2} + \frac{1}{2}\right)} \quad \text{and} \quad \Gamma(n) := \int_0^{\infty} t^{n-1} e^{-t} dt \quad \text{is the gamma function.}$$

Table 1 The three-dimensional profile is transformed into a one-dimensional profile using the MDR

				arbitrary n	
$f(r)$	$\begin{cases} 0, & r < a \\ \infty, & r > a \end{cases}$	$r^2 / 2R$	$r \tan \theta$	$c_n r^n$	Eq. (7)
$g(x)$	$\begin{cases} 0, & x < a \\ \infty, & x > a \end{cases}$	x^2 / R	$\frac{\pi}{2} x \tan \theta$	$\kappa_n c_n x ^n$	Eq. (8)

3. CALCULATION STEP OF THE MDR USING THE EXAMPLE OF A NORMAL CONTACT WITHOUT ADHESION

The one-dimensional profile according to Eq. (5) is now pressed into an elastic foundation corresponding to Eq. (1) with normal force F_N (see Fig. 4). The normal surface displacement at point x within the contact area results from the difference between indentation depth d and profile form g :

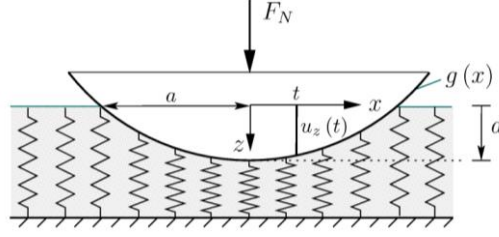


Fig. 4 Equivalent model for a Hertzian contact

$$u_z(x) = d - g(x). \quad (9)$$

At the edge of non-adhesive contact $x = \pm a$, the surface displacement must be zero:

$$u_z(\pm a) = 0 \Rightarrow d := g(a). \quad (10)$$

This equation determines the relationship between the indentation depth and contact radius a . It should be noted that this relationship is independent of the rheology of the medium. The force of a spring at the point x is proportional to the displacement at this point:

$$\Delta F_z(x) = \Delta k_z u_z(x) = E^* u_z(x) \Delta x, \quad (11)$$

and the sum of all spring forces must correspond to the normal force in equilibrium. In the limiting case of very small spring separation distances $\Delta x \rightarrow dx$, the summation becomes the integral:

$$F_N := E^* \int_{-a}^a u_z(x) dx = 2E^* \int_0^a (d - g(x)) dx. \quad (12)$$

Equation (12) provides the normal force in dependence on the contact radius and on the indentation depth, if Eq. (10) is taken into account.

We now define linear force density $q_z(x)$:

$$q_z(x) := \frac{\Delta F_z(x)}{\Delta x} = E^* u_z(x). \quad (13)$$

The stress distribution in the original three-dimensional system can be determined with the help of the one-dimensional distributed load using the integral transformation [15]:

$$p(r) = -\frac{1}{\pi} \int_r^\infty \frac{q'(x)}{\sqrt{x^2 - r^2}} dx. \quad (14)$$

The normal surface displacement (both inside and outside of the contact area) is given by the transformation:

$$u_z(r) = \frac{2}{\pi} \int_0^r \frac{u_z(x)}{\sqrt{r^2 - x^2}} dx. \quad (15)$$

We point out once more that one-dimensional values contain the independent variable x , while three-dimensional values contain radial variable r ; function $u_z(x)$ inside the integrand of Eq. (15) means the surface displacement of the linearly elastic foundation. We will carry out the last two transformations using the example of a cone. The three-dimensional profile in this case is $f(r) = r \cdot \tan \theta$; the MDR transformed profile is $g(x) = \frac{\pi}{2} |x| \tan \theta$. The displacement within the contact area is $u_z(x) = d - \frac{\pi}{2} |x| \tan \theta$. The linear force density is $q(x) = E^* \left(d - \frac{\pi}{2} |x| \tan \theta \right)$ and its derivative is $q'(x) = -\frac{\pi}{2} E^* \tan \theta$ (for positive x). Insertion into Eq. (14) and Eq. (15) results in:

$$p(r) = \frac{E^*}{2} \tan \theta \int_r^a \frac{dx}{\sqrt{x^2 - r^2}} = \frac{E^*}{2} \tan \theta \cdot \ln \left(\frac{a}{r} + \sqrt{\left(\frac{a}{r}\right)^2 - 1} \right), \quad (16)$$

$$u_z(r) = \frac{2}{\pi} \int_0^a \frac{d - (\pi/2)x \tan \theta}{\sqrt{r^2 - x^2}} dx = \frac{2d}{\pi} \left[\arcsin \left(\frac{a}{r} \right) - \left(\frac{r}{a} - \sqrt{\left(\frac{r}{a}\right)^2 - 1} \right) \right]. \quad (17)$$

Equation (17) gives the normal surface displacement outside of the contact area. A similar calculation for a parabolic profile $f(r) = r^2/(2R)$ initially provides $u_z(x) = d - x^2/R$ and, after insertion into Eq. (15), results in:

$$u_z(r) = \frac{d}{\pi} \left[\left(2 - \left(\frac{r}{a}\right)^2 \right) \cdot \arcsin \left(\frac{a}{r} \right) + \sqrt{\left(\frac{r}{a}\right)^2 - 1} \right]. \quad (18)$$

For the contact of a flattened paraboloid, Eq. (7), we obtain the contact radius by using Eq. (10):

$$u_z(a) = 0 \Rightarrow d := g(a) = \frac{a}{R} \sqrt{a^2 - b^2}. \quad (19)$$

and the normal force using Eq.(12):

$$F_N = 2E^* \int_0^a d dx - \frac{2E^*}{R} \int_0^a x \sqrt{x^2 - b^2} dx = \frac{2E^*}{3R} (2a^2 + b^2) \cdot \sqrt{a^2 - b^2}. \quad (20)$$

These results correspond of course with those of Eijke [18] from the three-dimensional theory.

Examples for normal contacts

Insertion of the MDR transformed profiles into Eqs. (10) and (12) and an elementary integration provides the results for the "classical profiles" of a cylinder [17], sphere [16], and cone [3] as well as the general power profile [2], which are summarized in Table 2. The order of the rows corresponds to the order of the calculation steps.

Table 2 Solutions to the normal contact problem for simple profiles

3D profile $f(r)$	$\begin{cases} 0, & r < a \\ \infty, & r > a \end{cases}$	$r^2 / 2R$	$r \tan \theta$	$c_n r^n$
1D profile $g(x)$	$\begin{cases} 0, & x < a \\ \infty, & x > a \end{cases}$	x^2 / R	$\frac{\pi}{2} x \tan \theta$	$\kappa_n c_n x ^n$
contact radius a , according to (10)	a	\sqrt{Rd}	$\frac{2}{\pi} \frac{d}{\tan \theta}$	$\left(\frac{d}{\kappa_n c_n} \right)^{1/n}$
normal force F_N , according to (12)	$2aE^*d$	$\frac{4}{3} E^* R^{1/2} d^{3/2}$	$\frac{2}{\pi} E^* \frac{d^2}{\tan \theta}$	$\frac{2n}{n+1} \frac{E^* d^{n+1}}{(c_n \kappa_n)^{1/n}}$
stress distribution $p(r)$, according to (14)	$\frac{E^* d}{\pi a} \frac{1}{\sqrt{1 - \left(\frac{r}{a}\right)^2}}$	$\frac{2E^*}{\pi} \left(\frac{d}{R}\right)^{1/2} \sqrt{1 - \left(\frac{r}{a}\right)^2}$	Eq. (16)	
displacement $u_z(r)$ according to (15) for $r > a$	$\frac{2d}{\pi} \arcsin\left(\frac{a}{r}\right)$	Eq. (18)	Eq. (17)	

4. ADHESIVE NORMAL CONTACT

The MDR rule for the mapping of adhesive contacts will be formulated in the following. As with the non-adhesive contact, the MDR transformed one-dimensional profile is brought into contact with the linearly elastic foundation defined in Section 2. Now, it will be assumed that all of the springs in the contact adhere to the indenter, then the contact radius remains the same after a successive decrease in the normal force. From the edge of the contact towards the middle, however, more and more springs will be loaded in tension. As soon as the change in length of the outer springs reaches the maximum allowable value:

$$\Delta l(\pm a) = \Delta l_{\max}(a) := \sqrt{\frac{2\pi a \Delta \gamma}{E^*}}, \quad (21)$$

there will be a state of indifference between adhesion and separation (Fig. 5). Here, $\Delta \gamma$ is the separation energy of the contacting bodies per unit area. This state corresponds exactly to the equilibrium state of the three-dimensional adhesive contact [15].

In contrast to the algorithm for non-adhesive contact, Equation (10) must only be replaced by:

$$u_z(\pm a) = -\Delta l_{\max}(a) \Rightarrow d := g(a) - \Delta l_{\max}(a) \quad (22)$$

in order to calculate the indentation depth. The normal force is given as before by Eq. (12):

$$F_N = 2E^* \int_0^a (d - g(x)) dx = 2E^* \left[ad - \int_0^a g(x) dx \right] = 2E^* \left[ag(a) - \int_0^a g(x) dx - a \Delta l_{\max}(a) \right] \quad (23)$$

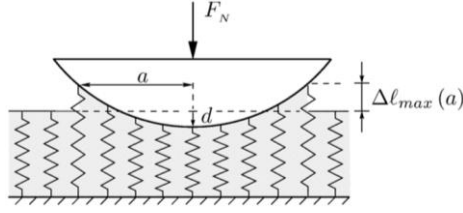


Fig. 5 Illustration for the MDR rule for an adhesive contact

or

$$F_N = 2E^* \left[\int_0^a xg'(x)dx - a\Delta l_{\max}(a) \right]. \quad (24)$$

If the force is controlled during the separation, then critical value a_c of the contact radius at the moment of the loss of stability is determined by condition $dF_N/da = 0$:

$$\frac{dg(a)}{da} = \sqrt{\frac{9\pi\Delta\gamma}{2aE^*}}. \quad (25)$$

Inserting the critical radius obtained from this equation into Eq. (23) results in the maximum negative force. We will call its magnitude the adhesion force F_A :

$$F_A = 2E^* \left[a_c \Delta l_{\max}(a_c) - \int_0^{a_c} xg'(x)dx \right]. \quad (26)$$

The simplest example is calculating the adhesion force between a cylinder with the radius a and an elastic half-space. In this case, the integral in Eq. (26) is equal to zero and the adhesion force is only given by the first term: $F_A = 2E^* a \Delta l_{\max}(a) = \sqrt{8\pi a^3 E^* \Delta\gamma}$, which corresponds to the result of Kendall [20]. Calculations for other profiles are just as simple and are summarized in Table 3.

In order to stress the generality and simplicity of the calculation method, we will now conduct the calculation for a *parabolic profile with a worn tip* (Fig. 6). If we take the equivalent profile from Equation (8) into account, the resulting indentation depth is:

$$d(a) := g(a) - \Delta l_{\max}(a) = \frac{a}{R} \sqrt{a^2 - b^2} - \sqrt{\frac{2\pi a \Delta\gamma}{E^*}}, \quad (27)$$

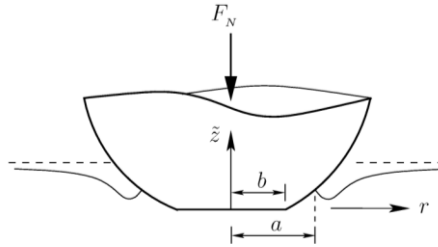


Fig. 6 Qualitative presentation of the adhesive contact of a parabolic profile with a flattened tip

and from Eq. (12), the normal force is:

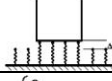
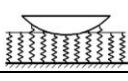
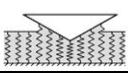
$$F_N(a) = E^* \int_{-a}^a u_z(x) dx = \frac{2E^*}{3R} (2a^2 + b^2) \sqrt{a^2 - b^2} - \sqrt{8\pi a^3 E^* \Delta\gamma}. \quad (28)$$

This equation corresponds to the results from the three-dimensional theory [22].

Examples for adhesive normal contacts

Inserting the MDR transformed profiles into Eqs. (25) and (26) and conducting an elementary integration provides the results summarized in Table 3 for the "classical profiles" of the cylinder [20], sphere [19], and cone [21], as well as the general power function profile [10, 11]. The order of the rows corresponds to the order of the calculation steps.

Table 3 Solutions for adhesive contacts for simple profiles

				arbitrary n
3D profile $f(r)$	$\begin{cases} 0, & r < a \\ \infty, & r > a \end{cases}$	$r^2 / 2R$	$r \tan \theta$	$c_n r^n$
1D profile $g(x)$	$\begin{cases} 0, & x < a \\ \infty, & x > a \end{cases}$	x^2 / R	$\frac{\pi}{2} x \tan \theta$	$\kappa_n c_n x ^n$
critical contact radius a_c , according to (25)	a	$\left(\frac{9\pi\Delta\gamma R^2}{8E^*} \right)^{1/3}$	$\frac{18\Delta\gamma}{\pi E^* \tan^2 \theta}$	$\left(\frac{9\pi\Delta\gamma}{2E^* n^2 \kappa_n^2 c_n^2} \right)^{1/2n-1}$
Adhesive force F_A , according to (26)	$\sqrt{8\pi a^3 E^* \Delta\gamma}$	$\frac{3}{2} \pi \Delta\gamma R$	$\frac{54\Delta\gamma^2}{\pi \tan^3 \theta \cdot E^*}$	$\frac{2n-1}{n+1} \left[\left(\frac{3}{2n\kappa_n c_n} \right)^3 (2\pi\Delta\gamma)^{n+1} E^{*n-2} \right]^{\frac{1}{2n-1}}$

5. TANGENTIAL CONTACT

We now consider an axially-symmetric indenter that is initially pressed into an elastic half-space with normal force F_N and subsequently loaded with tangential force F_x in the x -direction (Fig. 7). We assume that Coulomb's law of friction is valid in the simplest

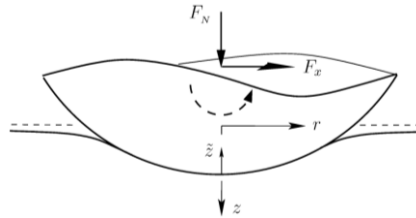


Fig. 7 Qualitative presentation of the tangential contact

form in the contact: as long as tangential stress τ is smaller than the coefficient of friction μ times normal stress p , the surface is in a state of sticking. After slip sets in, the tangential stress remains constant and equal to μp :

$$\tau(r) \leq \mu p(r) \text{ for stick,} \quad (29)$$

$$\tau(r) = \mu p(r) \text{ for slip.} \quad (30)$$

It is known that for a small tangential force at the edge of the contact, a ring-shaped slip domain develops, which expands inwards for increasing force until the complete slip is exhibited. We denote the inner radius of the slip domain (or the radius of the stick domain) with c .

The MDR is applied to the tangential contact as follows. The modified profile $g(x)$ is pressed into the linearly elastic foundation with force F_N and then tangentially displaced by $u_x^{(0)}$. The linearly elastic foundation is denoted by the stiffnesses according to (1) and (2). Every spring sticks to the indenter and is displaced along with it as long as the tangential force $\Delta F_x = k_x u_x^{(0)}$ is smaller than $\mu \Delta F_z$. After the adhesion force is reached, the spring begins to slip and the force remains constant and equal to $\mu \Delta F_z$. This rule can also be incrementally formulated so that it can be applied for arbitrary loading histories: for a small displacement of indenter of $\Delta u_x^{(0)}$, we obtain:

$$\begin{aligned} \Delta u_x(x) &= \Delta u_x^{(0)}, & \text{if } |k_x u_x(x)| < \mu f_z \\ u_x(x) &= \pm \frac{\mu \Delta F_z(x)}{k_x}, & \text{in a state of slip} \end{aligned} \quad (31)$$

The sign of the last equation is dependent on the direction of motion of the indenter. By following the incremental changes in the position of the indenter, we can explicitly determine the displacement of all the springs in the contact area; with this, all tangential forces:

$$\Delta F_x = k_x u_x(x) = G^* \Delta x \cdot u_x(x). \quad (32)$$

and the linear force density (distributed load):

$$q_x(x) = \frac{\Delta F_x}{\Delta x} = G^* u_x(x) \quad (33)$$

are also known. The distribution of tangential stress $\tau(r)$ as well as displacements $u_x(r)$ in the original three-dimensional contact are determined as follows [1]:

$$u_x(r) = \frac{2}{\pi} \int_0^r \frac{u_x(x)}{\sqrt{r^2 - x^2}} dx. \quad (34)$$

$$\tau(r) = -\frac{1}{\pi} \int_r^\infty \frac{q'_x(x)}{\sqrt{x^2 - r^2}} dx = -\frac{G^*}{\pi} \int_r^\infty \frac{u'_x(x)}{\sqrt{x^2 - r^2}} dx. \quad (35)$$

If the indenter is displaced in one direction from the equilibrium position, then radius c of the stick domain is determined from the condition that tangential force $k_x u_x^{(0)}$ is equal to μ times normal force $k_z u_z(c)$ (Fig. 8):

$$G^* u_x^{(0)} = \mu E^* (d - g(c)). \quad (36)$$

The tangential displacement is equal to:

$$u_x(x) = \begin{cases} u_x^{(0)}, & \text{for } x < c \\ \mu \left(\frac{E^*}{G^*} \right) (d - g(x)), & \text{for } c < x < a \end{cases}, \quad (37)$$

the distributed load is:

$$q(x) = \begin{cases} G^* u_x^{(0)}, & \text{for } x < c \\ \mu E^* (d - g(x)), & \text{for } c < x < a \end{cases}, \quad (38)$$

and the resulting tangential force is²:

$$F_x = 2 \int_0^a q_x(x) dx = 2\mu E^* \left[c(d - g(c)) + \int_c^a (d - g(x)) dx \right]. \quad (39)$$

The normal force is still given by Equation (12) and ratio $F_x/(\mu F_N)$ is given by:

$$\frac{F_x}{\mu F_N} = \frac{\int_c^a x g'(x) dx}{ag(a) - \int_0^a g(x) dx}. \quad (40)$$

The relative displacement $\Delta u_x = u_x^{(0)} - u_x(x)$ of the surfaces in contact is obtained by subtracting $u_x^{(0)}$ from Eq. (37):

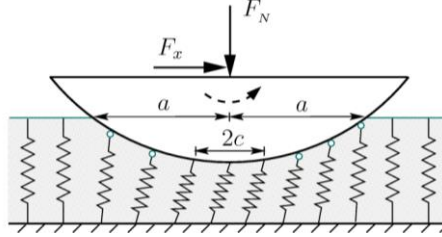


Fig. 8 Equivalent model for the classical tangential contact according to Cattaneo and Mindlin

$$\Delta u_x = \begin{cases} 0, & \text{for } x < c \\ \mu \left(\frac{E^*}{G^*} \right) (g(c) - g(x)), & \text{for } c < x < a \end{cases}. \quad (41)$$

² We stress once more that all macroscopic values obtained using the procedure described above correspond exactly to the three-dimensional solutions of Cattaneo [4], Mindlin [5], Jaeger [6] and Ciavarella [7].

The relative displacement in the original three-dimensional system is calculated using Eq. (34) as:

$$u_x(r) = \frac{2}{\pi} \mu \left(\frac{E^*}{G^*} \right) \int_0^r \frac{g(c) - g(x)}{\sqrt{r^2 - x^2}} dx, \quad \text{for } c < r < a. \quad (42)$$

For example, for a conical, we obtain:

$$u_x(r) = \mu \left(\frac{E^*}{G^*} \right) c \tan \theta \left[-\sqrt{\left(\frac{r}{c} \right)^2 - 1} - \arcsin \left(\frac{c}{r} \right) + \frac{\pi}{2} \right], \quad \text{for } c < r < a. \quad (43)$$

Examples for tangential contacts

Inserting the MDR transformed profiles into Eqs. (36) and (40), results in the relationships between radius c of the stick domain, ratio $F_x / (\mu F_N)$, and tangential displacement $u_x^{(0)}$. The results for the "classical profiles" of the sphere [4, 5], cone [23], as well as the power function profile are summarized in Table 4. The order of the rows corresponds to the order of the calculation steps.

Table 4 Solutions for the tangential contacts of simple profiles

3D profile $f(r)$	$r^2 / 2R$	$r \tan \theta$	$c_n r^n$
1D profile $g(x)$	x^2 / R	$\frac{\pi}{2} x \tan \theta$	$\kappa_n c_n x ^n$
$u_x^{(0)}$ according to (36)	$\mu \frac{E^*}{G^*} \left(d - \frac{c^2}{R} \right)$	$\mu \frac{E^*}{G^*} \left(d - \frac{\pi}{2} c \tan \theta \right)$	$\mu \frac{E^*}{G^*} \left(d - \kappa_n c_n c^n \right)$
$F_x / (\mu F_N)$ according to (40)	$1 - \left(\frac{c}{a} \right)^3$	$1 - \left(\frac{c}{a} \right)^2$	$1 - \left(\frac{c}{a} \right)^{n+1}$
Maximum static displacement according to (36)	$\mu d \left(E^* / G^* \right)$	$\mu d \left(E^* / G^* \right)$	$\mu d \left(E^* / G^* \right)$

6. CONCLUSIONS

In the present paper, we have limited ourselves to the essential rules and procedures of the method of dimensionality reduction. Evidence for the statements herein can be found in the works [1] and [15].

The possibilities of the MDR are much more expansive as presented in this composition. Further successful applications have been found for the rolling contact [24, 25], contacts with elastomers [26], contacts of rough surfaces [27, 28], elastomer friction [29], thermal effects in contacts [1], acoustic emission in rough contacts [31], and wear [32]. Interested readers are referred to the cited literature as well as the book [1]. In many cases, the MDR allows an analytical solution to the problem, as shown in this work.

However, it can also be easily implemented numerically and used for the investigation of systems with complex dynamic loadings [33].

Let us stress that the presented form of the MDR is only applicable to contacts with homogeneous elastic or viscoelastic half-spaces and it does not take into account size effects [34]. However, extensions to contacts with finite bodies or heterogeneous media are also possible [35]. The application of the MDR to rough contacts requires a separate paper.

REFERENCES

1. Popov, V.L., Hess, M., 2013, *Method of Dimensionality Reduction in Contact Mechanics and Friction*, Berlin Heidelberg: Springer-Verlag
2. Galin, L.A., 1961, *Contact Problems in the Theory of Elasticity*, North Carolina State College, USA
3. Sneddon, I.N., 1965, *The relation between load and penetration in the axisymmetric Boussinesq problem for a punch of arbitrary profile*, Int. J. Eng. Sci., 3(1), pp. 47-57.
4. Cattaneo, C., 1938, *Sul contatto di due corpi elastici: distribuzione locale degli sforzi*, Rendiconti dell'Accademia nazionale dei Lincei, 27, pp. 342-348, 434-436, 474-478.
5. Mindlin, R.D., 1949, *Compliance of elastic bodies in contact*, Journal of Applied Mechanics., 16, pp. 259-268.
6. Jaeger, J., 1995, *Axi-symmetric bodies of equal material in contact under torsion or shift*, Archive of Applied Mechanics, 65, pp. 478-487.
7. Ciavarella M., 1998, *Tangential Loading of General Three-Dimensional Contacts*. *Journal of Applied Mechanics*, 65, pp. 998-1003.
8. Galanov, B.A., 1993, *Development of analytical and numerical methods for study of models of materials*, Report for the project 7.06.00/001-92, 7.06.00/015-92. Kiev, Institute for Problems in Materials Science, (in Ukrainian)
9. Borodich, F.M., Galanov, B.A., 2004, *Molecular adhesive contact for indenters of nonideal shapes*, in: ICTAM04, Abstracts book and CD-Rom Proceedings, Warsaw, IPPT PAN
10. Borodich, F.M., 2008, *Hertz type contact problems for power-law shaped bodies*, in: Galin, L.A., Gladwell, G.M.L. (Eds.) "Contact Problems. The Legacy of L.A. Galin", Springer, 2008, pp. 261-292.
11. Yao, H., Gao, H., 2006, *Optimal shapes for adhesive binding between two elastic bodies*, Journal of colloid and interface science, 298(2), pp. 564-572.
12. Lee, E.H., 1955, *Stress analysis in viscoelastic bodies*, Quart. Appl. Math, 13, pp. 183-190.
13. Radok, J.R.M., 1957, *Viscoelastic stress analysis*, Quart. Appl. Math, 15, pp. 198-202.
14. Johnson, K.L., 1987, *Contact Mechanics*, Cambridge University Press
15. Hess, M., 2011, *Über die exakte Abbildung ausgewählter dreidimensionaler Kontakte auf Systeme mit niedrigerer räumlicher Dimension*, Cuvillier, Berlin, Germany
16. Hertz, H., 1882, *Über die Berührung fester elastischer Körper*, Journal für die reine und angewandte Mathematik, 92, pp. 156-171.
17. Boussinesq, V.J., 1885, *Application des Potentiels à l'étude de l'équilibre et du Mouvement des Solids Elastiques*, Gautier-Villar, Paris, France
18. Eijike, U.B.C.O., 1981, *The stress on an elastic half-space due to sectionally smooth-ended punch*, Journal of elasticity, 11(4), pp. 395-402.
19. Johnson, K.L., Kendall, K., Roberts A.D., 1971, *Surface energy and the contact of elastic solids*. Proceedings of the Royal Society of London, Series A, Mathematical and Physical Sciences, 324(1558), pp. 301-313.
20. Kendall, K., *The adhesion and surface energy of elastic solids*, Journal of Physics D: Applied Physics. 1971, 4, pp. 1186-1195.
21. Maugis, D., Barquins, M., 1981, *Adhesive contact of a conical punch on an elastic half-space*, Le Journal de Physique Lettres, 42(5), pp. 95-97.
22. Maugis, D., Barquins, M., 1983, *Adhesive contact of sectionally smooth-ended punches on elastic half-spaces: theory and experiment*, Journal of Physics D: Applied Physics, 16, pp. 1843-1874.
23. Truman, C.E., Sackfield, A., Hills, D.A., 1995, *Contact mechanics of wedge and cone indenters*, Int. J. Mech. Sci., 37, pp. 261-275.

24. Wetter, R., 2012, *Shakedown and induced microslip of an oscillating frictional contact*, Physical Mesomechanics, 2012, 15(5-6), pp. 293-299.
25. Wetter, R., Popov, V.L., 2014, *Shakedown limits for an oscillating, elastic rolling contact with Coulomb friction*. International Journal of Solids and Structures, 2014, 51(5), pp. 930-935.
26. Kürschner, S., Popov, V.L., 2013, *Penetration of self-affine fractal rough rigid bodies into a model elastomer having a linear viscous rheology*, Phys. Rev. E, 87, 042802.
27. Pohrt, R., Popov, V.L., Filippov, A.E., 2012, *Normal contact stiffness of elastic solids with fractal rough surfaces for one- and three-dimensional systems*, Phys. Rev. E, 86, 026710.
28. Pohrt, R., Popov, V.L., 2013, *Contact stiffness of randomly rough surfaces*. Sci. Rep. 3, 3293.
29. Li, Q., Popov, M., Dimaki, A., Filippov, A.E., Kürschner, S., Popov, V.L., 2013, *Friction Between a Viscoelastic Body and a Rigid Surface with Random Self-Affine Roughness*, Physical Review Letters, 111, 034301.
30. Popov, V.L., Voll, L., Li, Q., Chai, Y.S., Popov, M., 2014, *Generalized law of friction between elastomers and differently shaped rough bodies*, Sci. Rep. 2014, 4, 3750.
31. Popov, M., 2012, *Contact force resulting from rolling on self-affine fractal rough surface*. Physical Mesomechanics, 15(5-6), pp. 342-344.
32. Popov, V.L., 2014, *Analytic solution for the limiting shape of profiles due to fretting wear*, Sci. Rep., 4, 3749.
33. Teidelt, E., Willert, E., Filippov, A.E., Popov V.L., 2012, *Modeling of the dynamic contact in stick-slip micro-drives using the method of reduction of dimensionality*, Physical Mesomechanics, 15(5-6), pp. 287-292.
34. Argatov, I., 2010, *Frictionless and adhesive nanoindentation: Asymptotic modeling of size effects*, Mechanics of Materials, 42 (8), pp. 807-815.
35. Popov, V.L., 2014, *Method of dimensionality reduction in contact mechanics and tribology. Heterogeneous media*, Physical Mesomechanics, 17(1), pp. 50-57.

Original scientific paper

METHOD OF DIMENSIONALITY REDUCTION IN CONTACT MECHANICS AND FRICTION: A USER'S HANDBOOK. II. POWER-LAW GRADED MATERIALS

UDC 539.3

Markus Hess, Valentin L. Popov

Department of System Dynamics and the Physics of Friction, TU Berlin, Germany

Abstract. *Until recently, the only way of solving contact problems was to apply three-dimensional contact theories. However, this presupposes higher mathematical and numerical knowledge, which usually only research groups possess. This has changed drastically with the development of the method of dimensionality reduction (MDR), which allows every practically oriented engineer an access to the solution of contact problems. The simple and contact-type dependent rules are summarized in the first part of the user manual; they require contacts between elastically homogeneous materials. The present paper forms the second part of the user handbook and is dedicated to the solution of contact problems between power-law graded materials. All the MDR-rules are listed with which normal, tangential and adhesive contacts between such high-performance materials can be calculated in a simple manner.*

Key Words: *Normal Contact, Tangential Contact, Adhesion, Power-law Graded Materials, Partial Slip, Method of Dimensionality Reduction*

1. INTRODUCTION

The classical dimensionality reduction method is designed to solve contact problems between elastically homogeneous materials. Although it does not appear at first sight, the MDR unites all three-dimensional contact theories and transforms them in such a way that only simple rules remain which have to be applied to equivalent, one-dimensional contact problems [1]. These rules are summarized in the first part of the user handbook [2], assuming axisymmetric profiles and compact contact areas. However, Argatov et al. [3] showed that the MDR is also valid for arbitrarily shaped and non-compact contact areas.

Received October 24, 2016 / Accepted November 29, 2016

Corresponding author: Markus Hess

Institute of Mechanics, Berlin Institute of Technology, Strasse des 17. Juni 135, 10623 Berlin, Germany

E-mail: markus.hess@tu-berlin.de

The enormous technological progress in recent times is closely linked to the development of high-performance materials. In order to meet the increased demands, functionally graded materials (FGM) are used, which include the elastically power-law graded materials. They are characterized by a modulus of elasticity which increases perpendicularly to the half-space surface according to the power law:

$$E(z) = E_0 \left(\frac{z}{c_0} \right)^k \quad \text{with} \quad 0 \leq k < 1. \quad (1)$$

where c_0 denotes the characteristic depth in which elastic modulus E_0 prevails independently of the exponent of the elastic inhomogeneity (see Fig. 1).

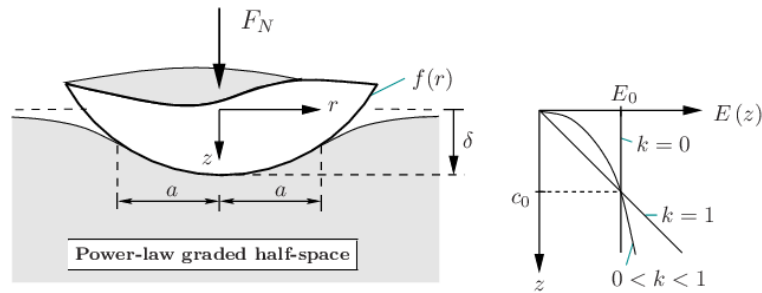


Fig. 1 Axisymmetric contact between a rigid indenter and an elastically power-law graded half-space

Contact mechanics of such materials were mainly developed by Booker et al. [4, 5] and Giannakopoulos and Suresh [6] for normal contacts without adhesion and Chen et al. [7] and Jin et al. [8] for adhesive contacts. Due to the interest in investigating the behavior of elastically inhomogeneous, biological structures as well as the adhesive material behavior in micro- and nanosystem technology the latter is still a subject of current research. An analytical solution of the tangential contact has not yet been published, but Hess [9] presented the solution at a recent workshop. The basic ideas were also mentioned in a further conference paper [10]. The key to the solution of the tangential contact lies once more in the superposition principle of Ciavarella [11] and Jäger [12]. Analogously to contact mechanics of homogeneous materials, all the above-mentioned contact theories for the calculation of contacts between power-law graded materials can again be suitably transformed by means of MDR, so that equivalent one-dimensional models are created which satisfy simple rules. The general foundations for the mapping of contacts between heterogeneous materials were given by Popov [13]. The derivation of all MDR-rules for the exact mapping of non-adhesive and adhesive normal contacts between power-law graded materials goes back to Hess [14, 15]. In this paper, all the rules are listed and their easy handling for the solution of normal, tangential and adhesive contacts is explained by means of examples.

2. TWO INTRODUCTORY STEPS OF THE MDR

The basic procedure for solving contact problems by MDR is independent of whether we consider homogeneous or inhomogeneous materials. Only the rules look a bit different. Again, we would like to assume axisymmetric contacts. Furthermore, the exponent of elastic inhomogeneity k and characteristic depth c_0 of the contacting bodies should be the same. The two solids should thus be able to distinguish themselves only in the Poisson's ratios ν_1, ν_2 and / or in the moduli of elasticity E_{01}, E_{02} prevailing in the characteristic depth.

2.1. The first step: Mapping of material properties

The power-law graded properties of the contacting bodies are taken into account within the MDR by linear elastic springs of suitable stiffness. In addition to a normal stiffness, each spring also has an independent tangential stiffness. The spring stiffnesses related to the distance of springs Δx are called foundation moduli c_N , respectively c_T . These have to be chosen as follows:

$$c_N(x) = \left(\frac{1-\nu_1^2}{h_N(k, \nu_1)E_{01}} + \frac{1-\nu_2^2}{h_N(k, \nu_2)E_{02}} \right)^{-1} \left(\frac{|x|}{c_0} \right)^k, \quad (2)$$

$$c_T(x) = \left(\frac{1}{h_T(k, \nu_1)E_{01}} + \frac{1}{h_T(k, \nu_2)E_{02}} \right)^{-1} \left(\frac{|x|}{c_0} \right)^k. \quad (3)$$

Coefficients h_N and h_T in the foundation moduli according to Eqs. (2) and (3) are complicated but well-defined functions depending on Poisson's ratio ν and exponent k of the elastic inhomogeneity. They are given in the appendix. The decisive factor at the foundation moduli is that they depend on coordinate x (see Fig. 2). Both stiffnesses increase with the lateral distance from the center point of the contact to exactly the same power law according to which, in the original problem, the elastic modulus increases perpendicularly to the half-space surface. In the special case of homogeneous half-space $k = 0$, the following holds:

$$h_N(0, \nu_i) = 1 \quad \text{and} \quad h_T(0, \nu_i) = \frac{2}{(1+\nu_i)(2-\nu_i)}. \quad (4)$$

Then coefficients c_N and c_T are constant and equal to effective elastic moduli E^* and G^* [2].

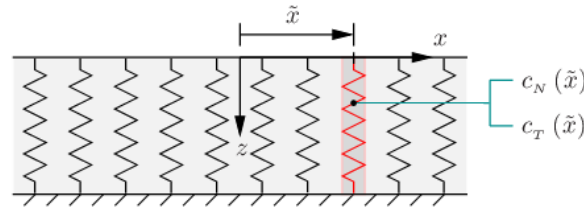


Fig. 2 Series of infinitesimally adjacent, linear spring elements whose normal and tangential stiffness increase with the lateral distance from the midpoint of contact

2.2. The second step: Transformation of profile

The second preliminary step involves the transformation of given three-dimensional contact profile $f(r)$ into an equivalent plane profile $g(x)$. The transformation and reverse transformation for the profile functions are [14]:

$$g(x) = |x|^{1-k} \int_0^{|x|} \frac{f'(r)}{(x^2 - r^2)^{\frac{1-k}{2}}} dr, \quad (5)$$

$$f(r) = \frac{2 \cos\left(\frac{k\pi}{2}\right)}{\pi} \int_0^r \frac{x^k g(x)}{(r^2 - x^2)^{\frac{1+k}{2}}} dx. \quad (6)$$

For better understanding, Fig. 3 visualizes the transformation of the profile. It should be noted that the equivalent plane profile is sometimes called equivalent 1D profile since it belongs to the equivalent 1D system.

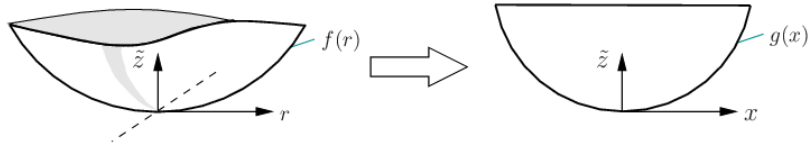


Fig. 3 Transformation of the 3D-profile into an equivalent plane profile

2.3. Example for the MDR transformation

As an example we consider the transformation of a profile whose shape is described by the power function:

$$f(r) = A_n r^n \quad \text{with } n \in \mathbb{R}^+, A_n = \text{const}. \quad (7)$$

Application of Eq. (5) to the profile according to Eq. (7) leads to the following equivalent profile:

$$g(x) = \kappa(n, k) A_n |x|^n = \kappa(n, k) f(|x|), \quad (8)$$

with

$$\kappa(n, k) = \int_0^1 \frac{n \zeta^{n-1}}{(1-\zeta^2)^{\frac{1-k}{2}}} d\zeta = \frac{n}{2} \int_0^1 t^{\frac{n}{2}-1} (1-t)^{\frac{k+1}{2}-1} dt =: \frac{n}{2} B\left(\frac{n}{2}, \frac{k+1}{2}\right), \quad (9)$$

where $B(x, y)$ is the complete beta function. Eq. (8) clearly indicates that the equivalent profile results from a simple, vertical scaling of the original profile. The scaling factor $\kappa(n, k)$ is dependent on the exponent of the power function and the exponent of the elastic inhomogeneity. The scaling factor increases with increasing exponent of the power-law profile (see Fig. 4).

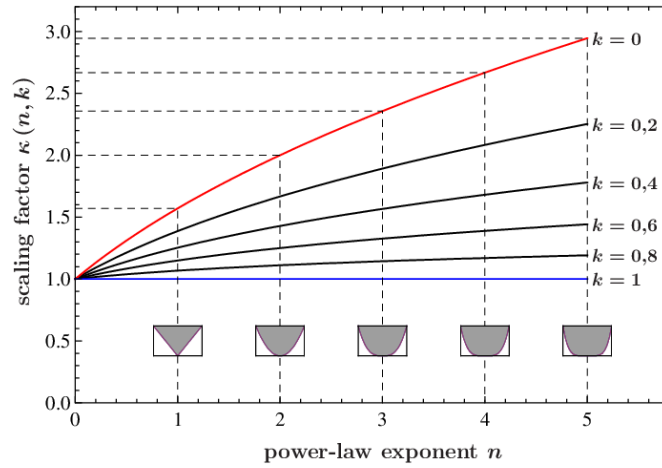


Fig. 4 Dependence of scaling factor κ on power-law exponent n for different exponents k of the power-law graded material (adopted from [14])

In the homogeneous case, the known values $\kappa(1,0)=\pi/2$ for the conical and $\kappa(2,0)=2$ for the parabolic indenter are obtained. The equivalent one-dimensional profiles of the basic contact profiles are listed in Table 1.

Table 1 Basic three-dimensional profiles and their equivalent one-dimensional profiles

	Flat-ended	Parabolic	Conical	Power-law
				...with exponent n
$f(r)$	$\begin{cases} 0, & r < a \\ \infty, & r > a \end{cases}$	$\frac{r^2}{2R}$	$r \tan \theta$	$A_n r^n$
$g(x)$	$\begin{cases} 0, & x < a \\ \infty, & x > a \end{cases}$	$\frac{x^2}{(1+k)R}$	$\frac{1}{2} \mathbf{B}\left(\frac{1}{2}, \frac{1+k}{2}\right) x \tan \theta$	$\kappa(n, k) A_n x ^n$

3. CALCULATION RULES OF MDR FOR SOLVING NORMAL CONTACTS BETWEEN POWER-LAW GRADED MATERIALS WITHOUT ADHESION

The MDR procedure for solving contact problems between power-law graded materials is the same as in the classical MDR for homogeneous materials.

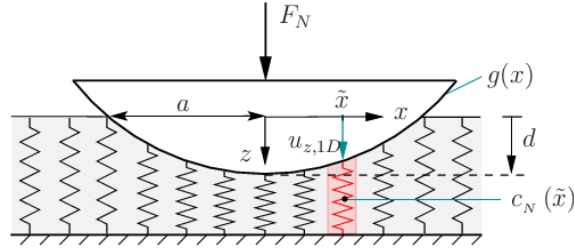


Fig. 5 Equivalent 1D contact problem of the 3D contact problem between two power-law graded half-spaces

The one-dimensional profile according to Eq. (5) is pressed into an elastic foundation of normal modulus given by Eq. (2) (see Fig. 5). The normal surface displacement at point x within the contact area results from the difference between indentation depth d and profile form g :

$$u_{z,1D}(x) := d - g(x) . \quad (10)$$

At the edge of non-adhesive contact $|x|=a$ the surface displacement must be zero:

$$u_{z,1D}(a) = 0 \Rightarrow d = g(a) . \quad (11)$$

This equation determines the relationship between indentation depth d and contact radius a . The sum of all spring forces must correspond to the normal force in equilibrium:

$$F_N(a) = \int_{-a}^a c_N(x) u_{z,1D}(x) dx = 2 \int_0^a c_N(x) [d - g(x)] dx . \quad (12)$$

Eqs. (11) and (12) provide the penetration depth and the normal force as a function of the contact radius. The pressure distribution in the original three-dimensional system can be determined with the help of the one-dimensional displacement using the integral transformation:

$$p(r, a) = -\frac{c_N(c_0)}{\pi c_0^k} \int_r^\infty \frac{u'_{z,1D}(x)}{(x^2 - r^2)^{\frac{1-k}{2}}} dx . \quad (13)$$

The foundation modulus at position c_0 takes into account the elastic parameters of the elastically inhomogeneous materials in contact. From Eq. (2) follows:

$$c_N(c_0) = \left(\frac{1 - \nu_1^2}{h_N(k, \nu_1) E_{01}} + \frac{1 - \nu_2^2}{h_N(k, \nu_2) E_{02}} \right)^{-1} . \quad (14)$$

The normal surface displacement outside of the contact area is given by the transformation:

$$u_z(r, a) = \frac{2 \cos\left(\frac{k\pi}{2}\right)}{\pi} \int_0^a \frac{x^k u_{z,1D}(x)}{(r^2 - x^2)^{\frac{1+k}{2}}} dx \quad \text{for } r > a . \quad (15)$$

3.1. Examples for normal contacts without adhesion

3.1.1. Parabolic contact

As the first example we consider a rigid, parabolic indenter, which is pressed into a power-law graded half-space. The shape function of the parabolic contact is defined by:

$$f(r) = \frac{r^2}{2R} . \quad (16)$$

Using the transformation formula (5) yields the shape function of the equivalent one-dimensional profile (see also Table 1):

$$g(x) = \frac{x^2}{(k+1)R} . \quad (17)$$

Thereby the displacement of the Winkler foundation is known, so that the indentation depth immediately emerges from Eq. (11):

$$u_{z,1D}(a) = 0 \Rightarrow d(a) = g(a) = \frac{a^2}{(k+1)R} . \quad (18)$$

According to Eq. (12), the normal force results from the sum of the spring forces, taking into account the increasing foundation modulus from the center of the contact line according to Eq. (2):

$$F_N(a) = \int_{-a}^a c_N(x) \left(\frac{a^2}{(1+k)R} - \frac{x^2}{(1+k)R} \right) dx = \frac{4E_0}{(1-\nu^2)} \frac{h_N(k, \nu)}{c_0^k (k+1)^2 (k+3)} \frac{a^{k+3}}{R} . \quad (19)$$

To calculate the pressure distribution in the contact area, we need the first derivative of the 1D displacement:

$$u_{z,1D}(x) = d - \frac{x^2}{(k+1)R} \Rightarrow u'_{z,1D}(x) = -\frac{2x}{(k+1)R} \quad (20)$$

and the adjusted elastic parameter (one body was assumed to be rigid):

$$c_N(c_0) = \frac{h_N(k, \nu)E_0}{1-\nu^2} . \quad (21)$$

From Eq. (13) by taking Eqs. (20) and (21) into account, the pressure distribution is:

$$p(r, a) = \frac{2h_N(k, \nu)E_0 a^{k+1}}{\pi(1-\nu^2)c_0^k (k+1)^2 R} \left[1 - \left(\frac{r}{a} \right)^2 \right]^{\frac{1+k}{2}} . \quad (22)$$

The application of Eq. (15) provides the normal displacement of the surface outside of the contact area:

$$u_z(r, a) = \frac{a^2 \cos\left(\frac{k\pi}{2}\right)}{(k+1)\pi R} \left[\mathbf{B}\left(\frac{a^2}{r^2}, \frac{1+k}{2}, \frac{1-k}{2}\right) - \frac{r^2}{a^2} \mathbf{B}\left(\frac{a^2}{r^2}, \frac{3+k}{2}, \frac{1-k}{2}\right) \right], \quad (23)$$

with the incomplete beta function:

$$\mathbf{B}(z, x, y) := \int_0^z t^{x-1} (1-t)^{y-1} dt \quad \forall x, y \in \mathbb{R}^+. \quad (24)$$

It is easy to verify that from Eqs. (18), (19) as well as Eqs. (22), (23) in the particular case $k = 0$ the solutions of the Hertzian contact exactly follow.

3.1.2. Conical contact

For the conical contact, the profile functions of the original and the equivalent system are listed in Table 1. They are:

$$f(r) = r \tan \theta \quad \Rightarrow \quad g(x) = \frac{1}{2} \mathbf{B}\left(\frac{1}{2}, \frac{1+k}{2}\right) |x| \tan \theta. \quad (25)$$

Table 2 summarizes the solutions of the conical contact, which results from the MDR rules Eqs. (10)-(13) and (15). Again, one body was assumed to be rigid.

Table 2 Solutions to the normal contact between a rigid conical indenter and a power-law graded half-space

Conical contact	
$d(a)$	$\frac{1}{2} a \tan \theta \mathbf{B}\left(\frac{1}{2}, \frac{1+k}{2}\right)$
$F_N(a)$	$\frac{h_N(k, \nu) \tan \theta \mathbf{B}\left(\frac{1}{2}, \frac{1+k}{2}\right) E_0 a^{k+2}}{(1-\nu^2) c_0^k (k+1)(k+2)}$
$p(r, a)$	$\frac{h_N(k, \nu) \tan \theta \mathbf{B}\left(\frac{1}{2}, \frac{1+k}{2}\right) E_0}{4\pi(1-\nu^2) c_0^k} r^k \left[\mathbf{B}\left(\frac{-k}{2}, \frac{1+k}{2}\right) - \mathbf{B}\left(\frac{r^2}{a^2}, \frac{-k}{2}, \frac{1+k}{2}\right) \right]$
$u_z(r, a)$	$\frac{\tan \theta \mathbf{B}\left(\frac{1}{2}, \frac{1+k}{2}\right) \cos\left(\frac{k\pi}{2}\right) a}{2\pi} \left[\mathbf{B}\left(\frac{a^2}{r^2}, \frac{1+k}{2}, \frac{1-k}{2}\right) - \frac{r}{a} \mathbf{B}\left(\frac{a^2}{r^2}, \frac{3+k}{2}, \frac{1-k}{2}\right) \right]$

Since the beta function in the pressure distribution contains some negative arguments, we extend the definition according to Eq. (24), in which we make use of its representation by hypergeometric series:

$$B(z, x, y) = \frac{z^x}{x} {}_2F_1(x, 1-y; 1+x; z) \quad (26)$$

where

$${}_2F_1(a, b; c; z) = \sum_{n=0}^{\infty} \frac{(a)_n (b)_n}{(c)_n} \frac{z^n}{n!} \quad \text{with} \quad (x)_n := \frac{\Gamma(x+n)}{\Gamma(x)}.$$

4. ADHESIVE NORMAL CONTACT BETWEEN POWER-LAW GRADED MATERIALS

For the solution of the normal contact with adhesion between two power-law graded materials by means of MDR, there is only a small change to the non-adhesive normal contact: the rule according to Eq. (11) for calculating the indentation depth as a function of the contact radius must simply be replaced by rule [14]:

$$u_{z,1D}(a) = -\Delta\ell_{\max}(a) \quad \text{with} \quad \Delta\ell_{\max}(a) := \sqrt{\frac{2\pi\Delta\gamma a}{c_N(a)}}. \quad (27)$$

Clearly, this means that the equilibrium state of the contact with adhesion is found when the elongations of the springs at the edge of contact reach defined value $\Delta\ell_{\max}(a)$ (see Fig. 6).

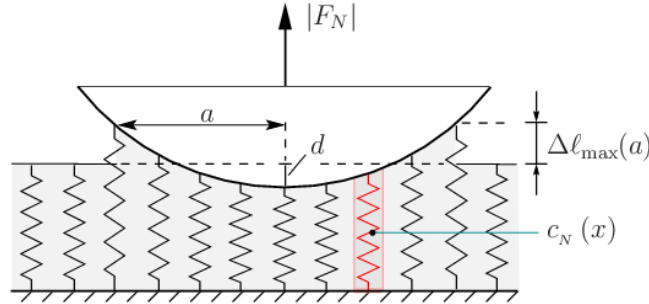


Fig. 6 Illustration of the MDR rule for an adhesive contact between power-law graded materials

In addition, the MDR solution provides a simple way to calculate the critical contact radii, and thus the (maximum) pull-off force as well as the minimum indentation depth. The critical contact radii must fulfill the following condition:

$$\frac{\Delta\ell_{\max}(a_c)}{a_c} = \tilde{C}(k) \left. \frac{\partial g(a)}{\partial a} \right|_{a_c} \quad \text{with} \quad \tilde{C}(k) := \begin{cases} \frac{2}{3+k} & \text{for fixed-load} \\ \frac{2}{1-k} & \text{for fixed-grips} \end{cases}. \quad (28)$$

Thus, the slope of the equivalent profile at the contact edge is decisive for reaching the critical states. The different definition of coefficient $\tilde{C}(k)$ is linked to whether a fixed-load or fixed-grips condition is present. With conditions (27), (28) and the general rules of the MDR procedure (10), (12), (13) and (15), every standard contact problem with adhesion can be easily solved. A few examples are presented below.

4.1. Examples for adhesive normal contacts

4.1.1. Parabolic contact

We refrain from re-calculating the equivalent profile for the parabolic contact at this point and adopt the result of Eq. (17):

$$f(r) = \frac{r^2}{2R} \Rightarrow g(x) = \frac{x^2}{(k+1)R}. \quad (29)$$

Considering the definition of the displacement of the Winkler foundation from Eq. (10), the indentation depth as a function of the contact radius for the adhesive contact follows from the separation criterion (27):

$$d(a) = \frac{a^2}{(k+1)R} - \sqrt{\frac{2\pi\Delta\gamma c_0^k a^{1-k}}{E^* h_N(k, \nu)}}, \quad (30)$$

where we abbreviated $E^* := E_0 / (1-\nu^2)$. According to Eq. (12), the normal force must again correspond to the sum of all spring forces. It differs from the normal force in the case of the non-adhesive contact only by a part which results from an additional rigid-body translation $-\Delta\ell_{\max}(a)$ of all springs:

$$\begin{aligned} F_N(a) &= \frac{2}{(1+k)R} \int_0^a c_N(x)(a^2 - x^2) dx - 2 \int_0^a c_N(x) \Delta\ell_{\max}(a) dx \\ &= \frac{4h_N(k, \nu) E^* a^{k+3}}{c_0^k (k+1)^2 (k+3) R} - \sqrt{\frac{8\pi\Delta\gamma h_N(k, \nu) E^* a^{3+k}}{(k+1)^2 c_0^k}}. \end{aligned} \quad (31)$$

For the calculation of the critical contact radii from condition (28) (limit stability), only the slope of the equivalent profile at the contact edge is required. From Eq. (29) it follows $g'(a) = 2a / [(1+k)R]$ and with it from Eq. (28):

$$a_c = \left(\frac{\pi(1+k)^2 R^2 \Delta\gamma c_0^k}{2\tilde{C}(k)^2 h_N(k, \nu) E^*} \right)^{\frac{1}{3+k}}. \quad (32)$$

Inserting the critical contact radii according to Eq. (32) into Eqs. (30) and (31) provides the critical indentation depths and normal forces:

$$d_c = \frac{1-2\tilde{C}(k)}{(1+k)R} \left(\frac{\pi(1+k)^2 R^2 \Delta\gamma c_0^k}{2\tilde{C}(k)^2 h_N(k, \nu) E^*} \right)^{\frac{2}{3+k}}, \quad (33)$$

$$F_c = \left(\frac{1-\tilde{C}(k)(3+k)}{\tilde{C}(k)^2(3+k)} \right) 2\pi \Delta\gamma R = \begin{cases} -\frac{k+3}{2} \pi \Delta\gamma R & \text{(fixed-load)} \\ -\frac{(1-k)(5+3k)}{2(3+k)} \pi \Delta\gamma R & \text{(fixed-grips)} \end{cases}. \quad (34)$$

It is needless to say that Eqs. (30)-(34) developed by MDR agree exactly with solutions from three-dimensional theory by Chen et al. [7]. They drew attention to the fact that, according to Eq. (34), the maximum pull-off force is independent of the elastic parameters and independent of the characteristic depth as in the homogeneous case. For the calculation of the pressure distribution according to Eq. (13), we need the one-dimensional displacement respectively its derivative, which we specify here again to clarify the treatment of the finite jump at the contact edge (see Fig. 6):

$$u_{z,1D}(x) = \left(\frac{a^2 - x^2}{(k+1)R} - \Delta\ell_{\max}(a) \right) [H(x+a) - H(x-a)] \quad \text{with } x \in \mathbb{R}, \quad (35)$$

$$\begin{aligned} u'_{z,1D}(x) = & -\frac{2x}{(k+1)R} [H(x+a) - H(x-a)] \dots \\ & \dots + \left(\frac{a^2 - x^2}{(k+1)R} - \Delta\ell_{\max}(a) \right) [\delta(x+a) - \delta(x-a)] \end{aligned}. \quad (36)$$

In Eqs. (35) and (36) $H(\dots)$ denote the Heaviside function and $\delta(\dots)$ the delta distribution. After insertion of Eq. (36) in Eq. (13) and taking into account the filter property of the delta distribution, the pressure distribution results in:

$$p(r, a) = \frac{2h_N(k, \nu) E^* a^{k+1}}{\pi c_0^k (k+1)^2 R} \left[1 - \left(\frac{r}{a} \right)^2 \right]^{\frac{1+k}{2}} - \sqrt{\frac{2h_N(k, \nu) \Delta\gamma E^* a^{k-1}}{\pi c_0^k}} \left[1 - \left(\frac{r}{a} \right)^2 \right]^{\frac{k-1}{2}}. \quad (37)$$

4.1.2. Power-law contact profile

The equivalent profile of an indenter whose shape is a power function according to Eq. (7) has already been calculated in Eq. (8):

$$f(r) = A_n r^n \Rightarrow g(x) = \kappa(n, k) A_n |x|^n, \quad n \in \mathbb{R}^+ \quad (38)$$

wherein $\kappa(n, k)$ has been defined in Eq. (9). The solutions of the adhesive contact between a power-law graded half-space and a rigid indenter whose profile is given by Eq. (38) using MDR are summarized in Table 3.

Table 3 Solutions to the adhesive contact between a rigid indenter whose shape is a power function and a power-law graded half-space

Adhesive contact of power-law profile	
$d(a)$	$\kappa(n, k) A_n a^n - \sqrt{\frac{2\pi \Delta\gamma c_0^k a^{1-k}}{E^* h_N(k, \nu)}}$
$F_N(a)$	$\frac{2h_N(k, \nu)\kappa(n, k)nA_n E^* a^{n+k+1}}{(k+1)(n+k+1)c_0^k} - \sqrt{\frac{8\pi h_N(k, \nu)\Delta\gamma E^* a^{3+k}}{(k+1)^2 c_0^k}}$
a_c	$\left(\frac{2\pi \Delta\gamma c_0^k}{h_N(k, \nu)E^* \tilde{C}(k)^2 \kappa(n, k)^2 n^2 A_n^2}\right)^{\frac{1}{2n+k-1}}$
$d(a_c)$	$\left[\left(\frac{2\pi \Delta\gamma c_0^k}{h_N(k, \nu)E^*}\right)^n \left(\frac{1}{\tilde{C}(k)n\kappa(n, k)A_n}\right)^{1-k}\right]^{\frac{1}{2n+k-1}} \left(\frac{1-n\tilde{C}(k)}{n\tilde{C}(k)}\right)$
$F(a_c)$	$2\left(\frac{1-\tilde{C}(k)(n+k+1)}{\tilde{C}(k)(n+k+1)(k+1)}\right) \left[(2\pi \Delta\gamma)^{n+k+1} \left(\frac{c_0^k}{h_N(k, \nu)E^*}\right)^{2-n} \dots \dots \left(\frac{1}{\tilde{C}(k)n\kappa(n, k)A_n}\right)^{k+3}\right]^{\frac{1}{2n+k-1}}$

5. TANGENTIAL CONTACT BETWEEN TWO POWER-LAW GRADED HALF-SPACES

We now consider a partial-slip problem between two power-law graded half-spaces with the same exponent k of elastic inhomogeneity, but different elastic parameters E_0 and ν . The solids are initially pressed against each other with a normal force F_N and subsequently loaded with a tangential force F_x in the x -direction (see Fig. 7). The axisymmetric gap function is given by $f(r)$. Let us assume that normal and tangential contacts are uncoupled, which is strictly permitted only if either [9]:

- both materials are equal: $\nu_1 = \nu_2 =: \nu \wedge E_{01} = E_{02} =: E_0$,
- one material is rigid and the other one has a Poisson's ratio equal to the Holl-ratio [16]: $E_{0i} \rightarrow \infty \wedge \nu_j = 1/(2+k)$ with $i \neq j$ or
- both materials have a Poisson's ratio which corresponds to the Holl-ratio: $\nu_1 = \nu_2 = 1/(2+k)$.

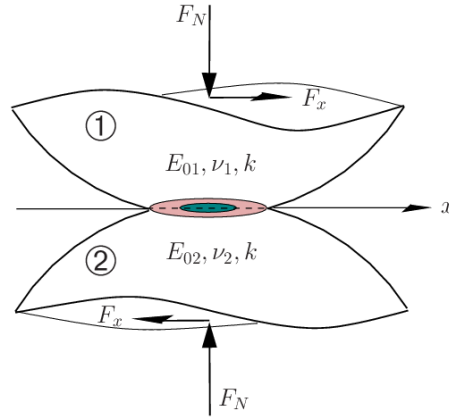


Fig. 7 Tangential contact between two power-law graded half-spaces

It is well-known that the contact region consists of an inner stick and outer slip region. In the stick domain all points undergo the same tangential displacement δ_x . The (unidirectional assumed) tangential stresses are determined by Coulomb's law of friction:

$$|\tau(r)| \leq \mu p(r) \quad \text{for } (x, y) \in A_{\text{stick}} \quad (39)$$

$$|\tau(r)| = \mu p(r) \quad \text{for } (x, y) \in A \setminus A_{\text{stick}} \quad (40)$$

We denote the radius of the stick domain by c .

The equivalent model for the tangential contact is shown in Fig. 8. As already mentioned, each spring has normal and tangential stiffness according to Eqs. (2) and (3). We note once again that these stiffnesses depend on the lateral coordinate according to a power law.

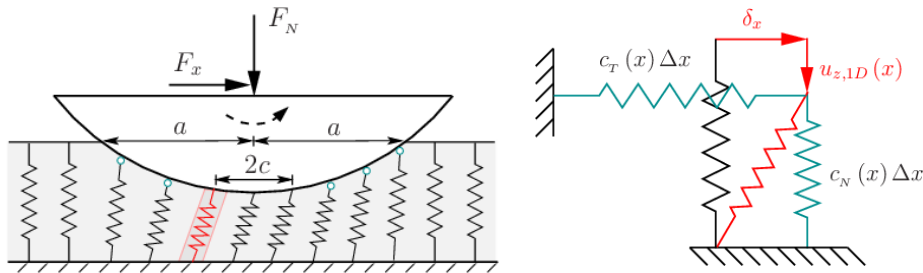


Fig. 8 Equivalent model for the partial-slip problem between two power-law graded half-spaces; each spring has normal and tangential stiffness, which are independent of each other

Due to the uncoupled normal and tangential contact, we assume the solution of the normal contact problem according to Section 3 as already known. The MDR-rules for the solution of the tangential contact require Amonton's law for each spring. The tangential line load is thus defined as follows:

$$q_x(x) = \begin{cases} c_T(x)\delta_x & \text{for } |x| \leq c \text{ (stick)} \\ \mu \underbrace{c_N(x)u_{z,1D}(x)}_{=q_z(x)} & \text{for } c < |x| \leq a \text{ (slip)} \end{cases} . \quad (41)$$

It takes into account both the rigid-body translation of the stick area and the Coulomb friction in the sliding area. The calculation of the stick radius is based on the continuity of the tangential line load at the transition between stick and slip domain:

$$\lim_{x \rightarrow c^-} q_x(x) = \lim_{x \rightarrow c^+} q_x(x) = q_x(c) \Rightarrow \delta_x = \mu \frac{c_N(c)}{c_T(c)} u_{z,1D}(c) . \quad (42)$$

Analogously to the normal contact problem, the tangential force results from the sum of the tangential spring forces. If, instead of the spring forces, the line load from Eq. (41) is used, the calculation formula is:

$$F_x(a) = \int_{-a}^a q_x(x) dx = 2 \int_0^c c_T(x) \delta_x dx + 2 \int_c^a \mu c_N(x) u_{z,1D}(x) dx . \quad (43)$$

It is also possible to deduce the pressure distribution of the original contact problem from the equivalent model. For this purpose, the knowledge of the tangential line load is sufficient since:

$$\tau(r) := -\tau_{zx}(r) = -\frac{1}{\pi r} \frac{d}{dr} \int_r^\infty \frac{x^{1-k} q_x(x)}{(x^2 - r^2)^{\frac{1-k}{2}}} dx . \quad (44)$$

It should be noted that the tangential line load according to Eq. (41) can also be expressed as a difference of the vertical line loads:

$$q_x(x) = \mu [q_z(x, a) \cdot \mathbf{H}(a - |x|) - q_z(x, c) \cdot \mathbf{H}(c - |x|)] . \quad (45)$$

where $q_z(x, a)$ is the normal line load actually acting in the equivalent model, and $q_z(x, c)$ is one that belongs to a smaller contact radius, stick radius c .

5.1. Example: Parabolic tangential contact between power-law graded half-spaces

In the following the same power-law graded materials are assumed which allow uncoupling of normal and tangential contact. The normal contact problem has already been described by means of the MDR in the examples of Section 3. The only difference is that one solid is assumed to be rigid. In order to be able to adopt the solution, we only have to adjust the stiffness, which is half as large, since both bodies are elastic. Regardless of it, the stiffness is shown here again:

$$c_N(x) = \frac{h_N(k, \nu) E_0}{2(1 - \nu^2)} \left(\frac{|x|}{c_0} \right)^k , \quad (46)$$

$$c_T(x) = \frac{1}{2} h_T(k, \nu) E_0 \left(\frac{|x|}{c_0} \right)^k . \quad (47)$$

The one-dimensional normal displacement of the Winkler foundation has already been determined (see Eqs. (20), (18)) so that the tangential line load can be specified:

$$q_x(x) = \begin{cases} c_T(x)\delta_x & \text{for } |x| \leq c \text{ (stick)} \\ \mu c_N(x) \frac{a^2 - x^2}{(1+k)R} & \text{for } c < |x| \leq a \text{ (slip)} \end{cases} \quad (48)$$

From the continuity requirement Eq. (42) at the points $|x|=c$ of the tangential line load it follows:

$$\delta_x = \mu \frac{h_N(k, \nu) a^2}{(1-\nu^2) h_T(k, \nu) (1+k) R} \left(1 - \frac{c^2}{a^2} \right). \quad (49)$$

The maximum displacement before macroscopic sliding (full slip) begins is thus:

$$\delta_{x,\max} = \frac{\mu h_N(k, \nu) a^2}{(1-\nu^2) h_T(k, \nu) (1+k) R}. \quad (50)$$

Integration of the tangential line load (48) over contact length $2a$ according to Eq. (43) yields:

$$\frac{F_x}{\mu F_N} = 1 - \left(\frac{c}{a} \right)^{k+3} = 1 - \left(1 - \frac{\delta_x}{\delta_{x,\max}} \right)^{\frac{k+3}{2}}, \quad (51)$$

where we have taken into account Eqs. (49) and (50) on the right.

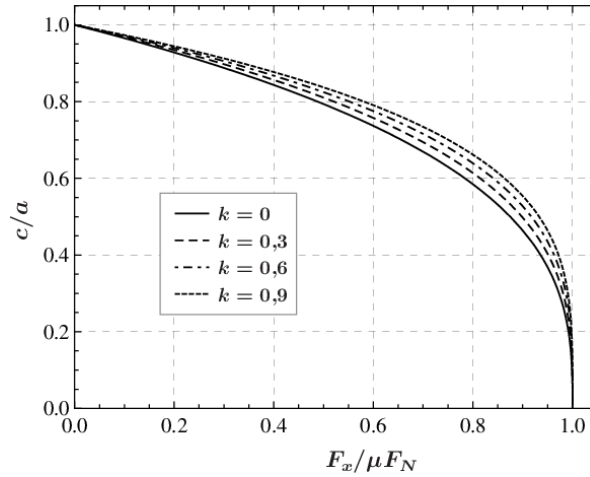


Fig. 9 Stick radius as a function of tangential force in normalized representation for different exponents of elastic inhomogeneity k

Fig. 9 shows the dependence of the stick radius on the tangential force for different exponents k . The tangential force as a function of the tangential displacement for the spe-

cial case $\nu_1 = \nu_2 = 1/(2+k)$ is depicted in Fig. 10. In this case, the prefactor in the maximum displacement deflates and from Eq. (50) it follows:

$$\delta_{x,\max} = \mu \frac{3+k}{2} \frac{a^2}{R}. \quad (52)$$

In Fig. 10 the tangential shift was normalized to the maximum tangential displacement in the homogeneous case. As can be seen from Eq. (52), the tangential shift increases with increasing k . When the state of full-slip is reached, a 30% larger displacement is obtained for $k=0.9$ in comparison to the homogeneous case.

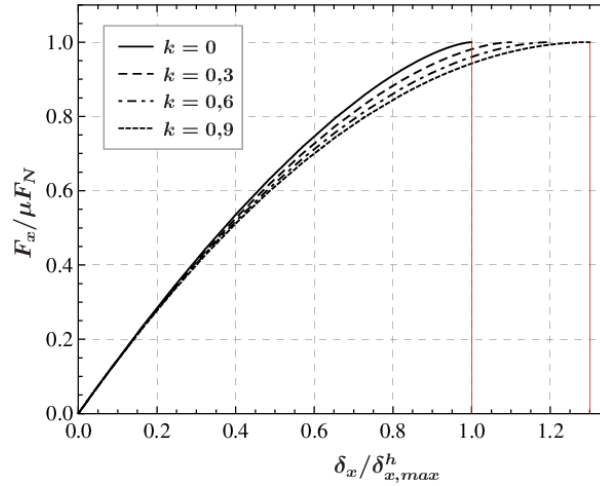


Fig. 10 Normalized representation of the dependence between tangential force and tangential displacement for different exponents of elastic inhomogeneity and specification of $\nu_1 = \nu_2 = 1/(2+k)$

Finally, it should be noted that we have assumed the usual approximations which are already contained in the classic solution of Cattaneo [17] and Mindlin [18] and have been discussed in detail by Ciavarella [11]. With reference to the corresponding paper we therefore waive an explicit listing.

6. CONCLUSIONS

This paper presents all the essential rules of the MDR that allow the solution of contact problems between power-law graded materials. We have carefully distinguished between normal, tangential and adhesive contacts and explained the simple application of the rules by means of examples. It does not need to be mentioned that despite its simplicity the MDR reproduces exactly all the results of the complicated three-dimensional theory. We would like to emphasize that the analytical solution of the tangential contact between power-law graded materials is an absolute novelty, since a derivation from the three-dimensional theory was missing so far. It was only in the run-up to the present pub-

lication that this gap could be closed [9]. Clearly, all MDR rules for solving contact problems between elastically homogenous materials are a special case of the rules presented here. The presented extension of the MDR is of interest to a number of current research areas since functionally-graded materials are gaining in importance. These include tribology, nanotechnology, biostructure mechanics and medicine. Completely analogous to the calculation of wear profiles between homogeneous materials [19, 20], the investigation of fretting between elastically inhomogeneous materials should no longer constitute a barrier.

The same applies to the extension of the current numerically simulated impact problems between elastically homogeneous spheres [21, 22] onto elastically inhomogeneous ones. Based on the MDR-rules presented here, which are comprehensible to everyone, the development of asymptotic solutions [23] for complicated contact configurations between power-law graded materials is also likely to be much easier.

We would like to point out that the theory presented here is limited to power-law graded materials. The extent to which the theory can be applied to other laws of elastic inhomogeneity remains a challenging, future task.

APPENDIX

The coefficients contained in the foundation moduli according to Eqs. (2), (3) are defined as follows [9, 15]:

$$h_N(k, \nu) = \frac{2(1+k) \cos\left(\frac{k\pi}{2}\right) \Gamma\left(1 + \frac{k}{2}\right)}{\sqrt{\pi} C(k, \nu) \beta(k, \nu) \sin\left(\frac{\beta(k, \nu)\pi}{2}\right) \Gamma\left(\frac{1+k}{2}\right)}, \quad (53)$$

$$h_T(k, \nu) = \frac{4\beta(k, \nu) \cos\left(\frac{k\pi}{2}\right) \Gamma\left(1 + \frac{k}{2}\right)}{(1-\nu^2)(1+k) \sqrt{\pi} C(k, \nu) \sin\left(\frac{\beta(k, \nu)\pi}{2}\right) \Gamma\left(\frac{1+k}{2}\right) + 2\beta(k, \nu)(1+\nu) \Gamma\left(1 + \frac{k}{2}\right)} \quad (54)$$

with

$$C(k, \nu) = \frac{2^{1+k} \Gamma\left(\frac{3+k+\beta(k, \nu)}{2}\right) \Gamma\left(\frac{3+k-\beta(k, \nu)}{2}\right)}{\pi \Gamma(2+k)} \quad (55)$$

and

$$\beta(k, \nu) = \sqrt{(1+k) \left(1 - \frac{k\nu}{1-\nu}\right)}. \quad (56)$$

REFERENCES

1. Popov, V.L. and Hess, M., 2015, *Method of dimensionality reduction in contact mechanics and friction*. Berlin Heidelberg: Springer-Verlag
2. Popov, V.L. and Hess, M., 2014, *Method of dimensionality reduction in contact mechanics and friction: a users handbook. I. Axially-symmetric contacts*, Facta Universitatis, Series: Mechanical Engineering, 12(1), pp. 1-14.
3. Argatov, I., Hess, M., Pohrt, R., Popov, V.L., 2016, *The extension of the method of dimensionality reduction to non-compact and non-axisymmetric contacts*. ZAMM-Journal of Applied Mathematics and Mechanics, 96(10), pp. 1144–1155, doi:10.1002/zamm.201600057
4. Booker, J.R., Balaam, N.P., Davis, E.H., 1985, *The behaviour of an elastic non-homogeneous half-space. Part I—line and point loads*, International Journal for Numerical and Analytical Methods in Geomechanics, 9(4), pp. 353-367.
5. Booker, J.R., Balaam, N.P., Davis, E.H., 1985, *The behaviour of an elastic non-homogeneous half-space. Part II—circular and strip footings*, International journal for numerical and analytical methods in geomechanics, 9(4), pp. 369-381.
6. Giannakopoulos, A. E., Suresh, S., 1997, *Indentation of solids with gradients in elastic properties: Part II, Axisymmetric indentors*, International Journal of Solids and Structures, 34(19), pp. 2393-2428.
7. Chen, S., Yan, C., Zhang, P., Gao, H., 2009, *Mechanics of adhesive contact on a power-law graded elastic half-space*, Journal of the Mechanics and Physics of Solids, 57(9), pp. 1437-1448.
8. Jin, F., Guo, X. and Zhang, W., 2013, *A unified treatment of axisymmetric adhesive contact on a power-law graded elastic half-space*, Journal of Applied Mechanics, 80(6), p. 061024.
9. Hess, M., 2016, *Normal, tangential and adhesive contacts between power-law graded materials*, Presentation at the Workshop on Tribology and Contact Mechanics in Biological and Medical Applications, TU-Berlin, 14.-17. Nov. 2016
10. Hess, M., Popov, V.L., 2016, *Die Renaissance der Winklerschen Bettung in der Kontaktmechanik und Reibungsphysik – Eine Anwendung auf Kontaktprobleme funktioneller Gradientenwerkstoffe*, Conference Paper, Tribologie-Fachtagung, 04, pp. 1-11
11. Ciavarella M., 1998, *Tangential Loading of General Three-Dimensional Contacts*. Journal of Applied Mechanics, 65, pp. 998-1003.
12. Jaeger, J., 1995, *Axi-symmetric bodies of equal material in contact under torsion or shift*, Archive of Applied Mechanics, 65, pp. 478-487.
13. Popov, V.L., 2014, *Method of dimensionality reduction in contact mechanics and tribology. Heterogeneous media*, Physical Mesomechanics, 17(1), pp. 50-57.
14. Hess, M., 2016, *A simple but precise method for solving axisymmetric contact problems involving elastically graded materials*, arXiv preprint arXiv:1602.04720.
15. Hess, M., 2016, *A simple method for solving adhesive and non-adhesive axisymmetric contact problems of elastically graded materials*, International Journal of Engineering Science, 104, pp. 20-33.
16. Holl, D.L., 1940, *Stress transmission in earths*, Highway Research Board Proceedings, 20, pp. 709-721.
17. Cattaneo, C., 1938, *Sul contatto di due corpi elastici: distribuzione locale degli sforzi*, Rendiconti dell'Accademia nazionale dei Lincei, 27, pp. 342-348, 434-436, 474-478.
18. Mindlin, R.D., 1949, *Compliance of elastic bodies in contact*, Journal of Applied Mechanics, 16(3), pp. 259–268.
19. Popov, V.L., 2014, *Analytic solution for the limiting shape of profiles due to fretting wear*, Sci. Rep., 4, 3749.
20. Li, Q., 2016, *Limiting profile of axisymmetric indenter due to the initially displaced dual-motion fretting wear*, Facta Universitatis, Series: Mechanical Engineering, 14(1), pp. 55-61.
21. Lyashenko, I.A., Willert, E., Popov, V.L., 2016, *Adhesive impact of an elastic sphere with an elastic half space: Numerical analysis based on the method of dimensionality reduction*, Mechanics of Materials, 92, pp. 155-163.
22. Willert, E., Popov, V.L., 2016, *Impact of an elastic sphere with an elastic half space with a constant coefficient of friction: Numerical analysis based on the method of dimensionality reduction*, ZAMM-Journal of Applied Mathematics and Mechanics, 96(9), pp. 1089–1095, DOI: 10.1002/zamm.201400309
23. Argatov, I., Li, Q., Pohrt, R., Popov, V.L., 2016, *Johnson–Kendall–Roberts adhesive contact for a toroidal indenter*, Proc. R. Soc. A, 472(2919): 20160218

METHOD OF DIMENSIONALITY REDUCTION IN CONTACT MECHANICS AND FRICTION: A USER'S HANDBOOK. III. VISCOELASTIC CONTACTS

UDC 539.3

Valentin L. Popov^{1,2,3}, Emanuel Willert¹, Markus Heß¹

¹Technische Universität Berlin, Berlin, Germany

²National Research Tomsk Polytechnic University, Tomsk, Russia

³National Research Tomsk State University, Tomsk, Russia

Abstract. *Until recently the analysis of contacts in tribological systems usually required the solution of complicated boundary value problems of three-dimensional elasticity and was thus mathematically and numerically costly. With the development of the so-called Method of Dimensionality Reduction (MDR) large groups of contact problems have been, by sets of specific rules, exactly led back to the elementary systems whose study requires only simple algebraic operations and elementary calculus. The mapping rules for axisymmetric contact problems of elastic bodies have been presented and illustrated in the previously published parts of The User's Manual, I and II, in Facta Universitatis series Mechanical Engineering [5, 9]. The present paper is dedicated to axisymmetric contacts of viscoelastic materials. All the mapping rules of the method are given and illustrated by examples.*

Key Words: *Contact, Friction, Viscoelasticity, Rheology, Method of Dimensionality Reduction*

1. INTRODUCTION

In recent years the Method of Dimensionality Reduction (MDR) has been developed to efficiently deal with axisymmetric [1] and non-axisymmetric contacts [2]. The scope of applicability includes normal contacts with and without adhesion as well as tangential contacts [1], torsional contacts [3], contacts of Functionally Graded Materials [4-5] and viscoelastic contacts [6-8]. In preceding papers the mapping rules of MDR have been

Received March 27, 2018 / Accepted May 11, 2018

Corresponding author: Emanuel Willert

Technische Universität Berlin, Sekr. C8-4, Straße des 17. Juni 135, D-10623 Berlin

E-mail: e.willert@tu-berlin.de

© 2018 by University of Niš, Serbia | Creative Commons Licence: CC BY-NC-ND

summarised and illustrated for axisymmetric contacts with a compact contact area for homogeneous [9] and power-law graded [5] elastic materials. The present publication gives a similar “user’s manual” for the treatment of viscoelastic contacts.

2. BASIC ASSUMPTIONS

Let us in the beginning briefly clarify the fundamental assumptions, which define the framework of our method. The results of the set of simple rules given in this paper to solve axisymmetric contact problems of viscoelastic materials will be exactly correct, if all assumptions are met. Yet the method can also be used if some of the assumptions are broken although in this case the obtained solutions might exhibit smaller or larger errors, depending on the precise circumstances.

Firstly, we only consider homogeneous, isotropic, linear-viscoelastic media. Moreover, the deformations have to be small to ensure kinematic linearity. In this case we are also allowed to work within the half-space approximation. Throughout most of the paper we will additionally demand incompressible material behaviour, i.e. Poisson ratio ν shall be equal to 0.5. The treatment of compressible materials will, as far as possible, be covered in a separate section.

Under these assumptions the viscoelastic material can be described by a single time-dependent shear relaxation function $G(t)$, which gives the material’s stress response to a unit strain increment. Stress response $\sigma(t)$ to an arbitrary deformation history $\gamma(t)$ is due to the superposition principle given by the sum of stresses for all past strain increments ([10], p.257),

$$\sigma(t) = \int G(t-t')d\gamma = \int_{-\infty}^t G(t-t')\dot{\gamma}(t')dt'. \quad (1)$$

As the convolution (1) in the time domain corresponds to a product in the Laplace domain, Eq. (1) can alternatively be written in the following way:

$$\sigma^*(s) = G^*(s)s\gamma^*(s), \quad (2)$$

whereas a star denotes the Laplace transform into the s -domain, i.e.

$$G^*(s) := \int_0^{\infty} G(t)\exp(-st)ds, \quad (3)$$

and similarly for all others.

Also, a time-dependent shear creep function $J(t)$, i.e. the strain response to a unit stress increment, can be defined ([11], p.215). The strain response to an arbitrary stress history is, analogously to Eq. (1), given by

$$\gamma(t) = \int_{-\infty}^t J(t-t')\dot{\sigma}(t')dt', \quad (4)$$

or, equivalently, in the Laplace domain

$$\gamma^*(s) = J^*(s)s\sigma^*(s). \quad (5)$$

Hence both the material functions are coupled by the relation

$$s^2 G^*(s)J^*(s) \equiv 1. \quad (6)$$

In case of harmonic oscillations, or put generally, in the frequency domain, for any linear viscoelastic material there is a linear proportionality between (shear) stress and (shear) strain – this directly follows from the material law in Eq. (1). The coefficient of proportionality is called “complex dynamic modulus”

$$\hat{G}(\omega) := i\omega \int_0^{\infty} G(t) \exp(-i\omega t) dt = i\omega G^*(s = i\omega). \quad (7)$$

Its real part is referred to as “storage modulus” and the imaginary part as “loss modulus”.

For the contact of two viscoelastic bodies with creep functions J_1 and J_2 both the creep functions simply have to be linearly superposed,

$$J(t) = J_1(t) + J_2(t). \quad (8)$$

Then a combined shear relaxation function $G(t)$ can also be defined *via* Eq. (6).

Finally, we will only consider quasi-static processes, i.e. all characteristic velocities of the contact problem must be much smaller than the smallest speed of wave propagation in the viscoelastic medium, and neglect adhesion or plasticity.

3. RHEOLOGICAL MODELS

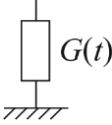


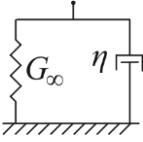
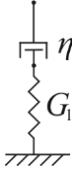
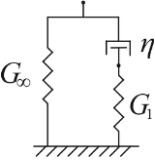
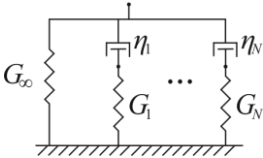
The viscoelastic properties of materials, as they have been briefly introduced in the previous section, are often represented in terms of rheological models. The basic elements of those models are a spring, representing ideally elastic properties, and a dashpot, representing ideally viscous properties.

Combining a sufficiently large set of those basic elements, any arbitrarily complex (linear-) viscoelastic behaviour can be captured. Thereby only two fundamental rules of superposition exist: for two elements in parallel to each other, the respective relaxation functions have to be linearly superposed; for two elements in series the creep functions are superposed. The rheological model, which reproduces a given relaxation function $G(t)$ shall henceforth in this paper be denoted with a simple box accompanied by the respective relaxation function (see Tab. 1).

We should point out that all the values of stiffness and damping in these models are to be understood as continuum variables, i.e. per unit volume, which is why we will always speak of moduli and viscosities.

Tab. 1 shows a compilation of the most commonly used viscoelastic material models and their rheological representations as well as the associated relaxation and creep functions. Thereby $\delta(t)$ denotes the Dirac δ -distribution while all the other designations are self-explanatory, based on the depicted rheological models.

Table 1 Rheological representations and material functions for the most common linear viscoelastic material models (δ denotes the Dirac δ -distribution)

Material Model		Material Functions
Elastic Body		$G(t) \equiv G,$ $J(t) \equiv \frac{1}{G}$
Viscous Body		$G(t) = \eta\delta(t),$ $J(t) = \frac{t}{\eta}$
Kelvin-Voigt Body		$G(t) = G_\infty + \eta\delta(t),$ $J(t) = \frac{1}{G_\infty} \left[1 - \exp\left(-\frac{G_\infty}{\eta} t\right) \right]$
Maxwell Body		$G(t) = G_1 \exp\left(-\frac{G_1}{\eta} t\right),$ $J(t) = \frac{1}{G_1} + \frac{t}{\eta}$
Standard Body		$G(t) = G_\infty + G_1 \exp\left(-\frac{G_1}{\eta} t\right),$ $J(t) = \frac{1}{G_\infty} \left[1 - \frac{G_1}{G_1 + G_\infty} \exp\left(-\frac{G_1 G_\infty t}{(G_1 + G_\infty)\eta}\right) \right]$
Prony Series (Generalised Maxwell Body)		$G(t) = G_\infty + \sum_{i=1}^N G_i \exp\left(-\frac{G_i}{\eta_i} t\right),$ no closed-form analytical expression for $J(t)$

4. TWO PREPARATORY STEPS OF THE METHOD

We consider the contact of two incompressible viscoelastic bodies with combined shear relaxation function $G(t)$ (or, equivalently, combined creep function J). The non-deformed gap between both the bodies shall be an axisymmetric function $z = f(r)$. To solve contact problems of this configuration within the MDR two introductory steps are necessary.

Firstly, the axisymmetric gap has to be transformed into an equivalent (rigid) plain profile $g(x)$ by the integral transform [9]

$$g(x) = |x| \int_0^{|x|} \frac{f'(r) dr}{\sqrt{x^2 - r^2}}. \quad (9)$$

This relation is the same as in the elastic case and is thus explained and illustrated by several examples in the first part of this user's manual. The inverse transform of Eq. (9) reads [9]

$$f(r) = \frac{2}{\pi} \int_0^r \frac{g(x) dx}{\sqrt{r^2 - x^2}}. \quad (10)$$

Secondly, a one-dimensional foundation of independent, linear-viscoelastic elements, each in distance Δx of each other, must be initialised, as demonstrated in Fig. 1.

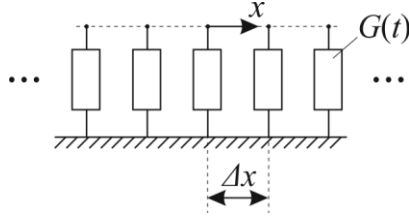


Fig. 1 One-dimensional foundation of linear-viscoelastic elements

A single element of the foundation is given by the rheological model for relaxation function $G(t)$, as shown in the previous section. For example, if the relaxation behaviour can be captured by a three-element standard solid, a single element of the viscoelastic foundation is given by a spring in series with a dashpot, the pair in parallel with another spring, as described above. The elements will have time-dependent values of normal and tangential stiffness (note that we assume incompressibility, i.e. $\nu = 0.5$),

$$\begin{aligned} \Delta k_z(t) &= \frac{2}{1-\nu} G(t) \Delta x = 4G(t) \Delta x, \\ \Delta k_x(t) &= \frac{4}{2-\nu} G(t) \Delta x = \frac{8}{3} G(t) \Delta x, \end{aligned} \quad (11)$$

or in the frequency domain,

$$\begin{aligned}\Delta\hat{k}_z(\omega) &= 4\hat{G}(\omega)\Delta x, \\ \Delta\hat{k}_x(\omega) &= \frac{8}{3}\hat{G}(\omega)\Delta x.\end{aligned}\tag{12}$$

5. NORMAL CONTACT OF AXISYMMETRIC BODIES

The equivalent profile defined by Eq. (9) is now pressed into the viscoelastic foundation defined by Eq. (11) by an indentation depth $d(t)$. Without loss of generality we will assume that the indentation starts at time $t = 0$, and that the viscoelastic medium previously was stress-free and non-deformed. Vertical displacement w_{ID} of an element at position x within the contact area of radius a is enforced by the indentation,

$$w_{\text{ID}}(x, t) = d(t) - g(x), \quad |x| \leq a.\tag{13}$$

An element comes into contact (geometrically) if the displacement of the non-contacting surface equals the displacement enforced by the indentation, i.e.

$$w_{\text{ID}}^{\text{n.c.}}(a(t), t) = d(t) - g(a(t)).\tag{14}$$

For a monotonically increasing contact radius the non-contacting surface is not deformed. In this case the contact radius is therefore simply given by the relation

$$d(t) = g(a(t)),\tag{15}$$

which, for a monotonically increasing contact radius, is a universal relation independent of the material rheology, as proven by Lee & Radok [12]. If the contact radius has extremal values the creep behaviour of the area without direct contact must be traced and inserted into Eq. (14) to give correct results [6].

The normal force in a single element of the foundation is due to the superposition principle given by

$$\Delta F_N(x, t) = 4\Delta x \int_0^t G(t-t') \frac{\partial w_{\text{ID}}(x, t')}{\partial t'} dt',\tag{16}$$

or in the frequency domain

$$\Delta\hat{F}_N(x, \omega) = 4\Delta x \hat{G}(\omega) \hat{w}_{\text{ID}}(x, \omega).\tag{17}$$

Note that if the rheological model contains separate dashpots, like the Kelvin-Voigt model, stress relaxation function $G(t)$ includes Dirac-distributions, which have to be evaluated in the integral using their filter properties. Instead of evaluating Eq. (16), which under some circumstances may require the knowledge about the entire loading history, one can also apply the complete set of equilibrium conditions for the single element, including the inner degrees of freedom. For example, the standard element shown on the left of Fig. 2 has one inner degree of freedom representing the material relaxation. The equilibrium conditions for the outer and inner degree of freedom are

$$\begin{aligned}\Delta F_N &= 4\Delta x(G_\infty w_{1D} + G_1 \tilde{w}_{1D}), \\ 0 &= \eta(\dot{\tilde{w}}_{1D} - \dot{w}_{1D}) + G_1 \tilde{w}_{1D}.\end{aligned}\quad (18)$$

For both force- or displacement-controlled conditions this gives a closed ordinary differential equation system with a unique solution.

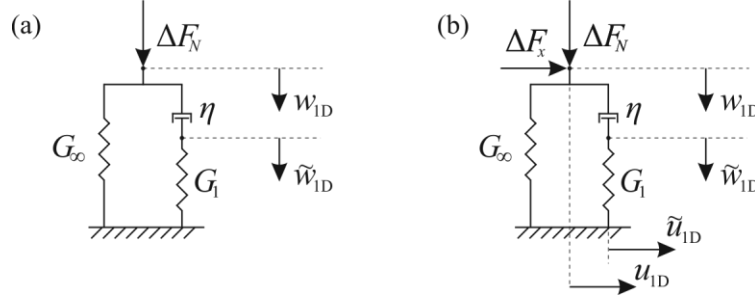


Fig. 2 Rheological standard element of the viscoelastic foundation under normal load (left, a) and superimposed normal and tangential load (right, b)

Note that under force-controlled conditions Eq. (16) can be inverted to give

$$w_{1D}(x, t) = \frac{1}{4\Delta x} \int_0^t J(t-t') \frac{\partial \Delta F_N(x, t')}{\partial t'} dt'. \quad (19)$$

The elements outside the contact area are, of course, free of forces, i.e.

$$\Delta F_N(x, t) = 0, \quad |x| \geq a. \quad (20)$$

An element leaves the contact (dynamically), if the upkeep of contact would require negative normal forces. The total normal force is obtained by summation of all the element normal forces,

$$F_N(t) = \int_{-a(t)}^{a(t)} \frac{\Delta F_N(x, t)}{\Delta x} dx \quad (21)$$

and with the linear force density,

$$q_z(x, t) := \frac{\Delta F_N(x, t)}{\Delta x}, \quad (22)$$

one can also calculate pressure distribution $p(r, t)$ in the original axisymmetric system by the relation

$$p(r, t) = -\frac{1}{\pi} \int_r^\infty \frac{\partial q_z(x, t)}{\partial x} \frac{dx}{\sqrt{x^2 - r^2}}. \quad (23)$$

We would like to stress again that all the results obtained by the described solution scheme will be exactly correct within the stated assumptions.

Let us now illustrate the procedure by some examples.

Displacement-controlled indentation

As the first example we consider the displacement-controlled indentation of a flat three-element standard solid by a rigid cone with slope θ and thus the profile

$$f(r) = r \tan \theta. \quad (24)$$

The indentation depth as a function of time shall be $d(t) = v_0 t$, which corresponds to a simple indentation test to determine the (visco-)elastic properties of a material. We would like to know the total normal force as a function of time and the material properties of the standard solid.

Solution: The equivalent plain profile is given by

$$g(x) = \frac{\pi}{2} \tan \theta |x|. \quad (25)$$

As the contact radius is monotonically increasing Eq. (15) can be applied to determine the contact radius. Hence

$$a(t) = \frac{2v_0 t}{\pi \tan \theta}. \quad (26)$$

An element at position x will therefore come into contact after a time

$$t_c(x) = \frac{\pi}{2} \tan \theta \frac{x}{v_0} = \frac{x t}{a(t)}. \quad (27)$$

The indentation velocity for all the elements in contact is equal v_0 . Hence the application of equation (16) yields the desired normal force:

$$\begin{aligned} F_N(t) &= 8v_0 \int_0^{a(t)} \int_{x/a(t)}^t \left[G_\infty + G_1 \exp\left(-\frac{t-t'}{\tau}\right) \right] dt' dx \\ &= 4v_0 a(t) \left[G_\infty t + 2G_1 \tau \left(1 + \frac{\tau}{t} \left\{ \exp\left(-\frac{t}{\tau}\right) - 1 \right\} \right) \right]. \end{aligned} \quad (28)$$

Force-controlled indentation

As the second example we consider the force-controlled indentation of a Kelvin-Voigt solid by a rigid sphere with radius R . The total normal force shall be kept constant,

$$F(t) = \text{const} = F_0. \quad (29)$$

This loading situation corresponds to the ideal loading protocol of the commonly used Shore hardness test for elastomers. We would like to know the indentation depth as a function of time and the material properties.

Solution: The spherical profile can in the vicinity of the contact be approximated by the parabolic profile

$$f(r) = \frac{r^2}{2R} \quad \Leftrightarrow \quad g(x) = \frac{x^2}{R}. \quad (30)$$

The contact radius will be again, due to creep, a monotonically increasing function with time. Hence

$$d(t) = \frac{a^2(t)}{R}. \quad (31)$$

In a Kelvin-Voigt solid the stress state is a linear superposition of ideally elastic and ideally viscous stress components (this can be easily understood with the respective rheological model shown in Tab. 1). The total normal force is therefore

$$\begin{aligned} F_N(t) &\equiv F_0 = \frac{16}{3} G_\infty \frac{a^3(t)}{R} + 8\eta \dot{d}(t) a(t) \\ &= \frac{16G_\infty}{3R} \left[a^3(t) + \tau \frac{d}{dt} (a^3(t)) \right], \quad \tau := \frac{\eta}{G_\infty}. \end{aligned} \quad (32)$$

The solution of this equation with initial condition $a(t=0) = 0$ is

$$a^3(t) = \frac{3F_0 R}{16G_\infty} \left[1 - \exp\left(-\frac{t}{\tau}\right) \right]. \quad (33)$$

Application of Eq. (31) will then provide the indentation depth as a function of time. The solution in Eq. (33) can be written in the more general form

$$\frac{F_N^{\text{el}}(a(t))}{F_0} = \hat{J}(t), \quad (34)$$

with the elastic (Hertzian) normal force as a function of the contact radius,

$$F_N^{\text{el}}(a) := \frac{16}{3} G_\infty \frac{a^3}{R}, \quad (35)$$

and the non-dimensional shear creep function for the Kelvin-Voigt solid,

$$\hat{J}(t) := 1 - \exp\left(-\frac{t}{\tau}\right). \quad (36)$$

As it turns out, the general formulation (34) is correct for arbitrary axisymmetric indenters and arbitrary linear-viscoelastic rheologies ([11], p.232) and can therefore be used to analyse general Shore hardness test configurations.

Impact test

As the third example in this section and in order to complete the set of applications of the MDR to commonly used material test of elastomers, we would like to show the application of the described rules to a rebound test: A homogeneous rigid sphere with radius R , mass m , mass density ρ and initial velocity v_0 impacts onto a viscoelastic half-space, whose rheology can be described by a three-element standard solid model. We would like to know the coefficient of restitution e (as a measure of energy dissipation under dynamic loading conditions) as a function of the inbound velocity and the material parameters.

Solution: This problem cannot be solved analytically. However, based on the MDR, a simple numerical algorithm can be implemented to give the solution of the impact problem in the quasi-static limit, i.e. assuming that the viscoelastic medium moves through a series of equilibrium states thus neglecting wave propagation in the viscoelastic material. The equation of motion of the sphere, in terms of indentation depth d , is simply given by

$$m\ddot{d}(t) = F_N(t). \quad (37)$$

For all the foundation elements in contact, the displacement is enforced by the movement of the plain parabolic profile equivalent to the three-dimensional sphere (see Eq. (30)),

$$w_{1D}(x, t) = d(t) - \frac{x^2}{R}, \quad |x| \leq a. \quad (38)$$

Solution of Eqs. (18) will give the corresponding element forces. They can be summed up to give the total normal force, which enters the equation of motion. As stated before, an element gets into contact geometrically and leaves contact if contact upkeep would require negative values of the respective element normal force. The impact ends at time T , if all elements have left contact. Any time integration scheme can be used to solve the described equation system in discrete time steps, by far the easiest one being an explicit Euler method. As the required computational operations are extremely simple, the time step can be set small enough to ensure numerical stability. The solution of the impact problem, i.e. the coefficient of restitution

$$e := -\frac{v(t=T)}{v_0} \quad (39)$$

only depends on two non-dimensional parameters, namely [13]

$$p_1 := \frac{\eta}{R} \left(\frac{v_0}{\rho^2 G_\infty^3} \right)^{1/5}, \quad p_2 = \frac{G_1}{G_\infty}, \quad (40)$$

and is shown in Fig. 3 as a function of p_1 for several different values of p_2 . Note that the physical meaning of p_1 (except for a numerical factor of the order of unity) is a ratio of two characteristic time scales: the viscoelastic relaxation time of the three-element standard solid compared to the elastic impact duration with $G = G_\infty$.

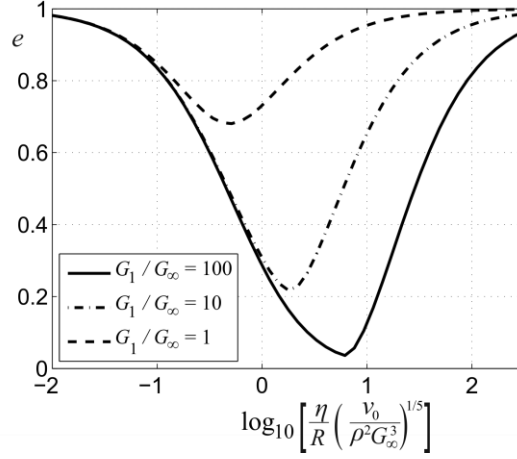


Fig. 3 Coefficient of restitution for the normal impact of a rigid sphere onto a flat standard solid as a function of the two governing parameters

6. TANGENTIAL CONTACT OF AXISYMMETRIC BODIES

We now consider contacts with superimposed normal and tangential loading. Thereby the application of a tangential load is completely analogous to the previous section. The elements of the viscoelastic foundation are vertically and horizontally displaced. *Via* the superposition principle the tangential force in a single element can be calculated from tangential displacement u_{1D} :

$$\Delta F_x(x, t) = \frac{8}{3} \Delta x \int_0^t G(t-t') \frac{\partial u_{1D}(x, t')}{\partial t'} dt', \quad (41)$$

Or, vice versa,

$$u_{1D}(x, t) = \frac{3}{8 \Delta x} \int_0^t J(t-t') \frac{\partial \Delta F_x(x, t')}{\partial t'} dt'. \quad (42)$$

Alternatively, as in the normal contact problem, the equilibrium conditions for all degrees of freedom of the elements can be evaluated. Coming back to the standard element example in Fig. 2 the equilibrium conditions in tangential direction (see the right side of Fig. 2) read

$$\begin{aligned} \Delta F_x &= \frac{8}{3} \Delta x (G_\infty u_{1D} + G_1 \tilde{u}_{1D}), \\ 0 &= \eta (\dot{\tilde{u}}_{1D} - \dot{u}_{1D}) + G_1 \tilde{u}_{1D}. \end{aligned} \quad (43)$$

Note that non-contacting surface areas also relax tangentially. In the frequency domain the convolution (41) reduces to a product,

$$\Delta \hat{F}_x(x, \omega) = \frac{8}{3} \Delta x \hat{G}(\omega) \hat{u}_{1D}(x, \omega). \quad (44)$$

The tangential linear force density,

$$q_x(x, t) := \frac{\Delta F_x(x, t)}{\Delta x}, \quad (45)$$

will provide the total tangential force,

$$F_x(t) = \int_{-a(t)}^{a(t)} q_x(x, t) dx, \quad (46)$$

and the shear stress distribution in the original axisymmetric system,

$$\sigma_{xz}(r, t) = -\frac{1}{\pi} \int_r^\infty \frac{\partial q_x(x, t)}{\partial x} \frac{dx}{\sqrt{x^2 - r^2}}. \quad (47)$$

To account for micro-slip in the contact we assume the validity of a local Amontons-Coulomb friction law in its simplest form for any contact point: if the local shear stress does not exceed the maximum value given by pressure times friction coefficient μ the surfaces are able to stick,

$$|\sigma_{xz}(r, t)| < \mu p(r, t), \quad \text{stick}; \quad (48)$$

Otherwise the surface points will slip and the frictional shear stress is known,

$$|\sigma_{xz}(r, t)| = \mu p(r, t), \quad \text{slip}. \quad (49)$$

Thereby it is clear that the contact area will always consist of an inner stick area with radius c and a slip area propagating inside from the edge of contact.

Accounting for slip in viscoelastic frictional contacts within the framework of MDR is simple (and completely analogous to the elastic case): the elements of the viscoelastic foundation simply have to obey the same local Amontons-Coulomb law! That is, if the indenting plain profile is moved tangentially by an increment $\Delta u^{(0)}$ from a given contact configuration, the contacting elements can either stick or slip, defined by the condition

$$\begin{aligned} \Delta u_{1D}(x, t) &= \Delta u^{(0)}, & \text{if } |\Delta F_x(x, t)| < \mu \Delta F_N(x, t), \\ \Delta F_x(x, t) &= \mu \Delta F_N(x, t) \operatorname{sgn}(u_{1D}), & \text{else.} \end{aligned} \quad (50)$$

Radius c of the stick area is given by the condition

$$|\Delta F_x(c, t)| = \mu \Delta F_N(c, t). \quad (51)$$

Tangential fretting in a viscoelastic contact

As an illustrative example we consider a simple case of tangential fretting: two axisymmetric bodies with combined relaxation function $G(t)$ are pressed together with a fixed indentation depth d_0 . The equivalent plain profile of non-deformed gap $f(r)$ shall be $g(x)$. After the normal stresses have been relaxed to their asymptotic value, small relative tangential harmonic oscillations

$$u^{(0)}(t) = \Delta u^{(0)} \cos(\omega t) \quad (52)$$

are enforced. We would like to know radius c of the permanent stick area.

Solution: Within the permanent stick area the forces in the elements of the viscoelastic foundation are known to be

$$\Delta F_x(t) = \frac{8}{3} \Delta x \Delta u^{(0)} \left| \hat{G}(\omega) \right| \cos(\omega t + \varphi), \quad \varphi = \arg\{\hat{G}(\omega)\}. \quad (53)$$

Here the complex dynamic modulus, introduced in Eq. (7), has been used because the excitation is harmonic. The normal forces in the fully-relaxed (i.e. elastic) state are

$$\Delta F_N(x) = 4 \Delta x G_\infty [d_0 - g(x)]. \quad (54)$$

Hence, the radius of the permanent stick area will be given by the solution of the condition

$$d - g(c) = \frac{2 \left| \hat{G}(\omega) \right|}{3 \mu G_\infty} \Delta u^{(0)}. \quad (55)$$

7. CONTACT OF COMPRESSIBLE MATERIALS

Although many (or even most) technically or biologically relevant viscoelastic media can – at least in good approximation – be considered incompressible, any linear isotropic viscoelastic material has not one but two characteristic material functions: in addition to shear relaxation $G(t)$, already used throughout this paper, there is also bulk relaxation function $K(t)$ giving the stress response to a unit volume strain. Accounting for compressibility in viscoelastic contact problems is, in general, a rather non-trivial task [14]. However, for *normal contact problems* (and only for them) it is easy to show that the compressible contact problem can be traced back to an equivalent incompressible one with the effective shear creep function

$$J_{\text{eff}}(t) = J(t) + \tilde{J}(t), \quad \tilde{J}^*(s) = \frac{3}{s^2 [3K^*(s) + G^*(s)]}. \quad (56)$$

This obviously means that in the MDR model the rheological elements of the viscoelastic foundation simply have to be replaced by the elements shown in Fig. 4. For the diagram we assume two materials with relaxation functions $G_1(t)$, $G_2(t)$, $K_1(t)$ and $K_2(t)$ respectively. A box, as in the section on rheological models, is an abbreviation for the rheological model representing the relaxation function denoted near the box.

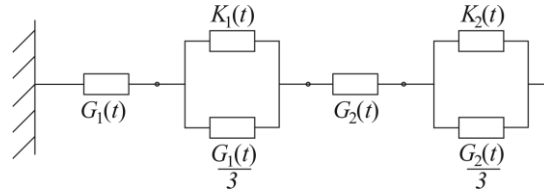


Fig. 4 General rheological element representing two contacting compressible viscoelastic materials. A box is an abbreviation for the rheological model representing the relaxation function denoted near the box

As compressible media are not by necessity elastically similar to each other we would like to stress that this ascription to an equivalent incompressible problem is only exact for either elastically similar materials or frictionless normal contacts.

Displacement-controlled indentation of a compressible medium

As an example let us analyse the frictionless indentation of a general Kelvin-Voigt solid with the relaxation functions

$$\begin{aligned} G(t) &= G_\infty + \eta\delta(t), \\ K(t) &= K_\infty + \xi\delta(t), \end{aligned} \quad (57)$$

with the shear and bulk viscosities, η and ξ , by a rigid flat cylindrical punch with radius a . The indentation depth as a function of time shall be $d(t) = v_0 t$. We would like to know the total normal force as a function of time and the material parameters.

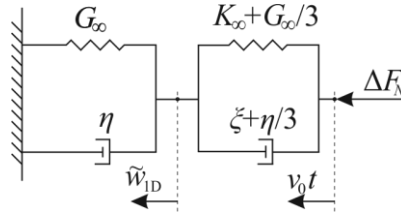


Fig. 5 Displacement-controlled indentation of a compressible Kelvin-Voigt element (based on [8])

Solution: The equivalent MDR-profile of a cylindrical flat stamp is a rectangle of the same length. Hence, all the elements within contact radius a are identically deformed. The equilibrium condition for the inner degree of freedom for each element reads (see Fig. 5)

$$\left(\xi + \frac{4}{3}\eta\right)\dot{\tilde{w}}_{1D} + \left(K_\infty + \frac{4}{3}G_\infty\right)\tilde{w}_{1D} = \left(\xi + \frac{1}{3}\eta\right)v_0 + \left(K_\infty + \frac{4}{3}G_\infty\right)v_0 t. \quad (58)$$

The solution of this ordinary differential equation with initial condition $\tilde{w}_{1D}(t=0) = 0$ is given by

$$\begin{aligned} \tilde{w}_{1D}(t) &= v_0 \tau (b - c) \left[1 - \exp\left(-\frac{t}{\tau}\right) \right] + c v_0 t, \\ \tau &:= \frac{3\xi + 4\eta}{3K_\infty + 4G_\infty}, \quad b := \frac{3\xi + \eta}{3\xi + 4\eta}, \quad c := \frac{3K_\infty + G_\infty}{3K_\infty + 4G_\infty}. \end{aligned} \quad (59)$$

Also, for the total normal force (as the indenting body shall be a rigid flat punch, all the elements of the foundation with $|x| < a$ are displaced in the same way),

$$F_N(t) = 2a \frac{\Delta F_N(t)}{\Delta x} = 8a [G_\infty \tilde{w}_{1D} + \eta \dot{\tilde{w}}_{1D}]. \quad (60)$$

In the limit of fast relaxation $t \gg \tau$ the total normal force will be

$$F_N(t) \approx 8av_0 [G_\infty \tau (b-c) + G_\infty ct + \eta c]. \quad (61)$$

8. CONCLUSIONS

The present paper gives a concise description of the rules for the application of the Method of Dimensionality Reduction to contacts of linear viscoelastic materials. Although the given examples mostly focus on analytical solutions for accessibility, it is, of course, possible to implement the rules in a numerical scheme to efficiently simulate viscoelastic contacts with arbitrary oblique loading histories. For example, based on the method, comprehensive contact-impact solutions for viscoelastic materials have been obtained very recently and cross-checked against respective Boundary-Element simulations [13].

REFERENCES

1. Popov, V.L., Heß, M., 2015, *Method of dimensionality reduction in contact mechanics and friction*, Springer, Berlin Heidelberg.
2. Argatov, I.I., Heß, M., Pohrt, R., Popov, V.L., 2016, *The extension of the method of dimensionality reduction to non-compact and non-axisymmetric contacts*, ZAMM Zeitschrift für Angewandte Mathematik und Mechanik, 96(10), pp. 1144-1155.
3. Willert, E., Popov, V.L., 2017, *Exact one-dimensional mapping of axially symmetric elastic contacts with superimposed normal and torsional loading*, ZAMM Zeitschrift für Angewandte Mathematik und Mechanik, 97(2), pp. 173-182.
4. Heß, M., 2016, *A simple method for solving adhesive and non-adhesive axisymmetric contact problems of elastically graded materials*, International Journal of Engineering Science, 104, pp. 20-33.
5. Heß, M., Popov, V.L., 2016, *Method of Dimensionality Reduction in Contact Mechanics and Friction: A User's Handbook. II. Power-Law Graded Materials*, Facta Universitatis-Series Mechanical Engineering, 14(3), pp. 251-268.
6. Argatov, I.I., Popov, V.L., 2016, *Rebound indentation problem for a viscoelastic half-space and axisymmetric indenter – Solution by the method of dimensionality reduction*, ZAMM Zeitschrift für Angewandte Mathematik und Mechanik, 96(8), pp. 956-967.
7. Kürschner, S., Filippov, A.E., 2012, *Normal contact between a rigid surface and a viscous body: Verification of the method of reduction of dimensionality for viscous media*, Physical Mesomechanics, 15(5-6), pp. 270-274.
8. Willert, E., Popov, V.L., 2018, *Short note: Method of Dimensionality Reduction for compressible viscoelastic media. I. Frictionless normal contact of a Kelvin-Voigt solid*, ZAMM Zeitschrift für Angewandte Mathematik und Mechanik, 98(2), pp. 306-311.
9. Popov, V.L., Heß, M., 2014, *Method of Dimensionality Reduction in Contact Mechanics and Friction: A Users Handbook. I. Axially-Symmetric Contacts*, Facta Universitatis-Series Mechanical Engineering, 12(1), pp. 1-14.
10. Popov, V.L., 2017, *Contact Mechanics and Friction. Physical Principles and Applications*, 2nd Edition, Springer, Berlin Heidelberg.
11. Popov, V.L., Heß, M., Willert, E., 2018, *Handbuch der Kontaktmechanik – Exakte Lösungen axialsymmetrischer Kontaktprobleme*, Springer, Berlin Heidelberg.
12. Lee, E.H., Radok, J.R.M., 1960, *The Contact Problem for Viscoelastic Bodies*, Journal of Applied Mechanics, 27(3), pp. 438-444.
13. Willert, E., Kusche, S., Popov, V.L., 2017, *The influence of viscoelasticity on velocity-dependent restitution in the oblique impact of spheres*, Facta Universitatis-Series Mechanical Engineering, 15(2), pp. 269-284.
14. Greenwood, J.A., 2010, *Contact between an axisymmetric indenter and a viscoelastic half-space*, International Journal of Mechanical Sciences, 52(6), pp. 829-835.

Chapter 2

Numerical Aspects of the Method of Dimensionality Reduction

FAST NUMERICAL IMPLEMENTATION OF THE MDR TRANSFORMATIONS

UDC 539.3

Justus Benad

Berlin University of Technology, Berlin, Germany

Abstract. *In the present paper a numerical implementation technique for the transformations of the Method of Dimensionality Reduction (MDR) is described. The MDR has become, in the past few years, a standard tool in contact mechanics for solving axially-symmetric contacts. The numerical implementation of the integral transformations of the MDR can be performed in several different ways. In this study, the focus is on a simple and robust algorithm on the uniform grid using integration by parts, a central difference scheme to obtain the derivatives, and a trapezoidal rule to perform the summation. The results are compared to the analytical solutions for the contact of a cone and the Hertzian contact. For the tested examples, the proposed method gives more accurate results with the same number of discretization points than other tested numerical techniques. The implementation method is further tested in a wear simulation of a heterogeneous cylinder composed of rings of different material having the same elastic properties but different wear coefficients. These discontinuous transitions in the material properties are handled well with the proposed method.*

Key Words: *Normal Contact, Method of Dimensionality Reduction, Stress, Wear*

1. INTRODUCTION

The Method of Dimensionality Reduction (MDR) is a simple and convenient tool for the calculation of contact forces between elastic and viscoelastic bodies. It is particularly easy to use for the simulation of axially-symmetric contacts. Since it was first proposed in 2007 [1] the MDR has been applied to a wide range of problems [2]. The method maps a given three-dimensional contact problem to an equivalent contact problem of a transformed indentation profile with a one-dimensional elastic or viscoelastic foundation of independent elements. From a numerical perspective, the solution of the contact problem in the transformed MDR domain is then trivial due to the decoupled degrees of freedom. A variety

Received May 26, 2018 / Accepted June 30, 2018

Corresponding author: Justus Benad

TU Berlin, Institut für Mechanik, FG Systemdynamik und Reibungsphysik, Str. d.17. Juni 135, 10623 Berlin, DE

E-mail: mail@jbenad.com

of problems can be solved directly in this domain after the initial transformation to the equivalent problem was performed (see for example [3]). However, there are other problems which require multiple transformations to the MDR domain and back, for example due to a continuously changing indentation profile as it appears in wear simulations, see [4-6]. With such kinds of problems, the main difficulty in achieving an accurate and efficient numerical simulation is the implementation of the MDR transformations. These are given by Abel-like integral equations and it is well known that their numerical treatment is challenging [7, 8].

This work is dedicated to providing a simple and fast numerical method for the implementation of the MDR transformations for axially-symmetric contact problems. The transformations have an integrable singularity which is handled well with the proposed method.

The parts of this work are organized as follows: In Section 2, the MDR transformations are rewritten using integration by parts to a form which is well suited for numerical implementation. In Section 3, this numerical implementation technique is explained in detail. Section 4 gives some advice on optimizing the implementation for maximum speed. Section 5 shows exemplary results of the newly proposed technique and highlights its advantages and weaknesses. In Section 6, a small addition to the method is presented to further improve it. In Section 7, the accuracy of the introduced numerical method is compared to other known implementation techniques which rely on the original form of the transformations. In Section 8, an exemplary wear simulation is conducted with the newly introduced technique and compared to the results of other numerical implementation methods. A conclusion is presented in Section 9.

This work can be regarded as a small addition to the paper “Method of Dimensionality reduction in contact mechanics and friction: A users handbook” [9]. In the following, only homogeneous elastic material is considered. However, the MDR is applicable also to gradient media [10] and to viscoelastic media [11], which can be treated in a similar manner as described in the present paper.

2. FORMULATION OF THE MDR TRANSFORMATIONS FOR SIMPLE NUMERICAL IMPLEMENTATION

The general MDR procedure is fully described in [9]. Three main transformations occur in the method: The transformation of three-dimensional profile $f(r)$ to a one-dimensional profile is

$$g(x) = |x| \int_0^{|x|} \frac{f'(r)}{\sqrt{x^2 - r^2}} dr, \quad (1)$$

the transformation of one-dimensional foundation displacement $w_{1D}(x)$ to three-dimensional normal surface displacement $w(r)$ is

$$w(r) = \frac{2}{\pi} \int_0^r \frac{w_{1D}(x)}{\sqrt{r^2 - x^2}} dx, \quad (2)$$

and the transformation of one-dimensional force density $q(x)$ to three-dimensional pressure distribution $p(r)$ is

$$p(r) = -\frac{1}{\pi} \int_r^\infty \frac{q'(x)}{\sqrt{x^2 - r^2}} dx. \quad (3)$$

The singularity arising at $x = r$ in the numerical summation can be avoided when rewriting Eqs. (1), (2) and (3) to

$$g(x) = \frac{\pi}{2} |x| f'(x) - |x| \int_0^{|x|} \operatorname{atan} \left(\frac{r}{\sqrt{x^2 - r^2}} \right) f''(r) dr, \quad (4)$$

$$w(r) = w_{\text{ID}}(r) - \frac{2}{\pi} \int_0^r \operatorname{atan} \left(\frac{x}{\sqrt{r^2 - x^2}} \right) w'_{\text{ID}}(x) dx, \quad (5)$$

and

$$p(r) = \frac{1}{\pi} \log(r) q'(r) + \frac{1}{\pi} \int_r^\infty \log(\sqrt{x^2 - r^2} + x) q''(x) dx \quad (6)$$

using integration by parts.

The following example shall illustrate a possible numerical implementation of the three transformations (4), (5) and (6).

3. EXEMPLARY NUMERICAL PROCEDURE

Consider a uniform discretization of $r \in [0, L]$ and $x \in [0, L]$ with N points each and the same step size

$$h = \frac{L}{N-1}, \quad (7)$$

so that

$$r_n = h(n-1), \quad x_k = h(k-1), \quad n, k \in \{1, 2, \dots, N\}. \quad (8)$$

The first and second derivatives of a discretized indentation profile $f_n = f(r_n)$ can be obtained via central differences:

$$f'_n = \frac{f_{n+1} - f_{n-1}}{2h}, \quad (9)$$

$$f''_n = \frac{f_{n+1} - 2f_n + f_{n-1}}{h^2}. \quad (10)$$

Some care must be taken at the borders. To obtain f'_1 and f''_1 recall that in the present framework of the MDR profile f is axially-symmetric and $f(0) = 0$. Thus, it is

$$f'_1 = 0, \quad (11)$$

and

$$f''_1 = \frac{2f_2}{h^2}. \quad (12)$$

At the other border the values for f_N' and f_N'' can remain undetermined. One-dimensional profile g_k can now be obtained with Eq. (4). It is

$$g_k = \frac{\pi}{2} x_k f_k' - x_k t_k, \quad \text{for } k = 2, 3, \dots, N-1, \quad (13)$$

where t_k is the result of the integral in (4). Using the trapezoidal rule, it is

$$t_k = \begin{cases} \frac{\pi}{4} f_k'' h, & \text{for } k = 2 \\ \sum_{n=2}^{k-1} \left(\operatorname{atan} \left(\frac{r_n}{\sqrt{x_k^2 - r_n^2}} \right) f_n'' h \right) + \frac{\pi}{4} f_k'' h, & \text{for } k = 3, 4, \dots, N-1 \end{cases} \quad (14)$$

Again, some care must be taken at the borders. To obtain g_1 , recall that in the framework of the MDR it is $g(0) = 0$. Thus, it is

$$g_1 = 0. \quad (15)$$

At the other border the value for g_N can remain undetermined.

In a quite similar fashion, normal surface displacement w_n can be obtained: The first derivative in Eq. (5) can be obtained as in Eq. (9) using central differences, and the integral can be calculated as in Eq. (14) using the trapezoidal rule. Subsequent smoothing of w_n with $w_n := (w_{n-1} + w_n + w_{n+1}) / 3$ increases the accuracy of w_n .

The third transformation to obtain p_n is again similar to the first and second transformation. The derivatives in Eq. (6) can once more be obtained as in Eqs. (9) and (10) using central differences. Then it is

$$p_n = \frac{1}{\pi} \log(r_n) q_n' + \frac{1}{\pi} s_n, \quad \text{for } n = 2, 3, \dots, N-2 \quad (16)$$

where s_n is the result of the integral in (6). Using the trapezoidal rule, it is

$$s_n = \begin{cases} \frac{\log(x_n) q_n'' h}{2} + \sum_{k=n+1}^{N-2} \log(\sqrt{x_k^2 - r_n^2} + x_k) q_k'' h, & \text{for } n = 2, 3, \dots, N-3 \\ \frac{\log(x_n) q_n'' h}{2}, & \text{for } n = N-2 \end{cases} \quad (17)$$

Note that at kinks of q the term $q_k'' h = (q_{k+1} - 2q_k + q_{k-1}) / h$ converges to finite values for decreasing step-sizes h . Note also that the summation in Eq. (17) stops at $N-2$ because q_N'' and q_{N-1}'' are undetermined. This is not problematic because in the framework of the MDR it is $q = 0$ for sufficiently large x in any way ($x > a$, where a is the contact radius). Once again, some care must be taken at the borders. One way to approximate p_1 is via Taylor series. A first order expansion yields simply

$$p_1 = p_2 - \frac{p_3 - p_2}{2}. \quad (18)$$

At the other border the values for p_N and p_{N-1} remain undetermined. Again, this is not problematic as long as it is ensured that these last points lie outside the contact area. Then they can simply be set to

$$p_N = p_{N-1} = 0. \quad (19)$$

4. PERFORMANCE

Often, the MDR transformations need to be performed repeatedly. One example is that of wear simulations where the transformations (1) and (3) need to be performed many times after each other for a changing indentation profile. In such cases, consider optimizing the implementation of the MDR transformations for maximum speed.

For example, when using the transformation technique presented in the example above, note that the summation in Eqs. (13) and (16) can be regarded as a matrix vector product in which the matrix is a kernel which is independent of the indentation profile and can be predefined. This enables full vectorization of the transformations when they are used repeatedly for changing indentation profiles.

Also consider the possibility of calculating the derivatives in the transformations such as (9) and (10) via matrix vector multiplication using predefined sparse matrices.

5. EXEMPLARY RESULTS

Fig. 1 shows the results of the previously described implementation technique for a conic and parabolic indenter at an exemplary indentation depth d . It becomes apparent that already for as few as $N = 51$ discretization points a fairly good approximation of the analytical solutions can be achieved.

The maximum error of g_k , w_n , and p_n with respect to the analytical solutions for g , w , and p decreases when the number of discretization points N is increased as can be seen in Fig. 2.

For most N , the maximum error of pressure distribution p_n (a thin grey oscillating line in Fig. 2) is given by the error at the very last discretization point lying within the contact area (highlighted with a star in Fig. 1). Index n of this particular point shall be denoted with $n = s$. At all other points a much better accuracy is achieved: If point s would be disregarded in the assessment of the maximum error, the upper limit of the grey oscillating line would move down from the dotted line to the dashed one.

In the exemplary case of $N = 51$ which is displayed in Fig. 1 this relatively high error of p_n at the point $n = s$ does not immediately become apparent to the viewer due to the large slope of p at the end of the contact area which puts the numerical value close to the analytical curve even if there is a relatively high error.

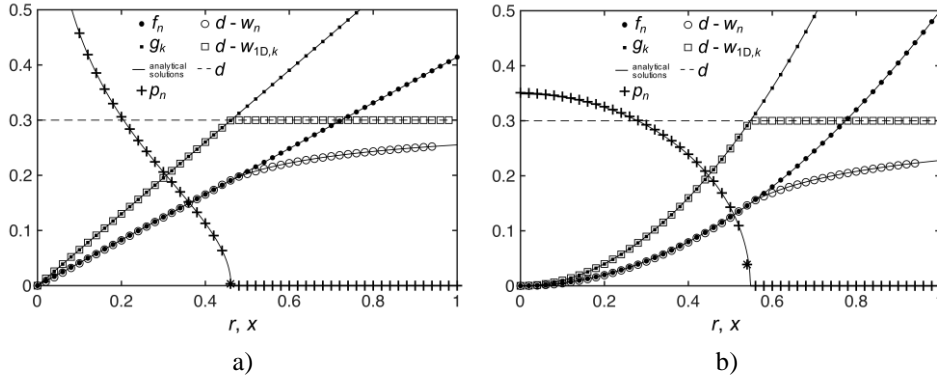


Fig. 1 Results of the MDR transformations carried out with the numerical procedure described above for $N = 51$ discretization points, exemplary input parameters of $L = 1$, $E^* = 1$, $d = 0.3$ and an exemplary conic indenter (left) given with $f(r) = r \tan(\pi/8)$ and an exemplary parabolic indenter (right) given with $f(r) = r^2/2$. The pressure which is obtained at last discretization point within the contact area in this example is highlighted with a star

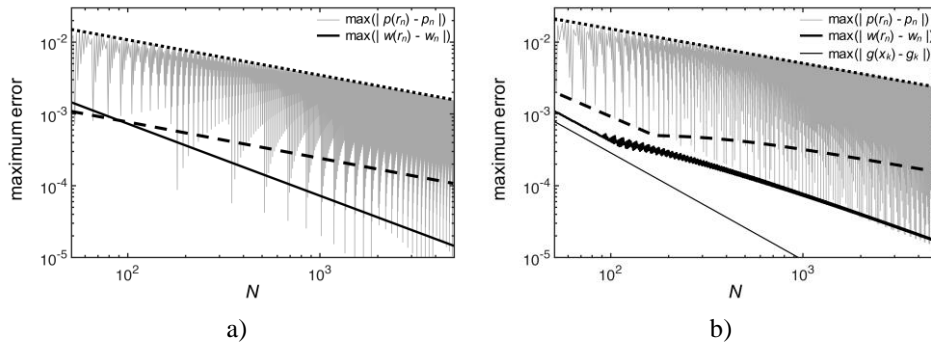


Fig. 2 Maximum error of g_k , w_n , and p_n for a discretization of $N = 51, 52, 53 \dots 5000$, shown for the exemplary inputs $L = 1$, $E^* = 1$, $d = 0.3$ and the exemplary conic indenter (left) given with $f(r) = r \tan(\pi/8)$ and the exemplary parabolic indenter (right) given with $f(r) = r^2/2$. The oscillating thin grey line shows the maximum error of p_n . Its upper limit is marked with the dotted black line. Neglecting the error of p_n at the point $n = s$ in the assessment of the maximum error would cause a much lower upper limit which is marked with the dashed black line. Note also that the maximum error of g_k for the exemplary conic indenter lies at around 10^{-15} and is thus outside the chosen region displayed in the figure

6. ADJUSTMENTS

If needed, one possible way of obtaining better results for p_s is by inserting one or more discretization points on a finer grid after point s so that it is no longer the last point in the contact area.

For example, one can use a technique such as the one illustrated in Fig. 3. Here, a new discretization point is added right at contact radius a , which is approximated from g_k with a simple linear interpolation

$$a = \frac{r_{s+1} - r_s}{g_{s+1} - g_s} (d - g_s) + r_s, \quad (20)$$

another discretization point is added in between r_s and a at $r_s + (a - r_s) / 2$, and at both ends two more points are added, one at $r_s - (a - r_s) / 2$ and one at $a + (a - r_s) / 2$. The values for the one-dimensional profile are interpolated linearly from g_k to these points. The resulting five equally spaced points are marked with crosses in Fig. 3.

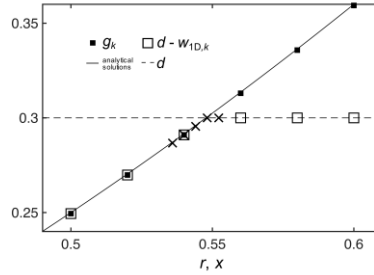


Fig. 3 Detailed view of the graph in Fig. 1b, here with additional discretization points at the end of the contact area which are marked with black crosses

The desired value for the pressure at point s can now be calculated as in Eqs. (16) and (17) using a new refined grid. The three inner points are used for the summation while the two additional outer points are only there to obtain the derivatives with the central difference scheme.

Note that the above method of obtaining a more accurate value for p_s does not practically increase the computational time. It is a simple addition of three values, and the three linear interpolations which are needed are also given with small algebraic equations. Compared to the time for the main transformation steps, the time for these additional steps is negligible. However, the small correction reduces the maximum error norm (see Fig. 4).

At the end of this section it shall be noted that higher order methods for the calculation of the derivatives and for the numerical integration do not necessarily lead to more accurate results. It is observed that the use of more neighboring points than in Eqs. (9) and (10) for calculating the derivatives tends to decrease the accuracy of the transformations for the contact of the cone and the Hertzian contact. It was also observed that using Simpson's rule to perform the summation in Eqs. (13) and (16) instead of the trapezoidal rule decreases the accuracy of the transformations.

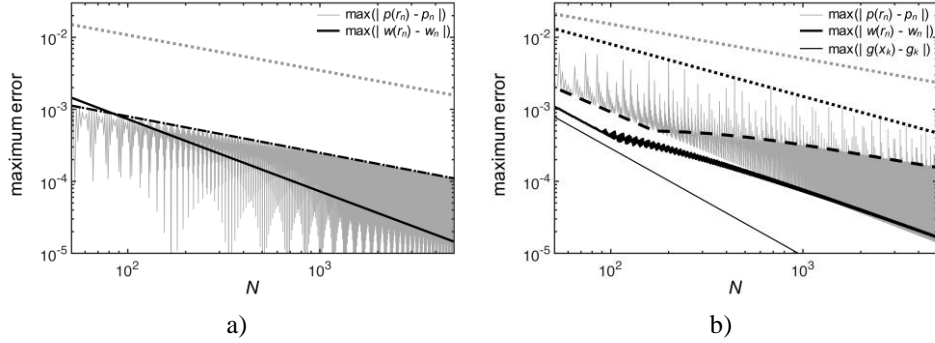


Fig. 4 Maximum error of g_k , w_n , and p_n as displayed in Fig. 2 here however p_s is corrected with the technique explained above. The old upper limit of the maximum error of p_n from Fig. 2 is shown with the grey dotted line. The new upper limit of the maximum error of p_n after the correction of p_s is shown with the black dotted line. In the case of the cone (a) this upper limit falls onto the dashed line marking the maximum error of p_n when the point s is disregarded

7. COMPARISON WITH OTHER NUMERICAL TECHNIQUES

Recall that at the beginning of the numerical scheme presented above the MDR transformations were rewritten using integration by parts. However, the MDR transformations can also be implemented numerically using their original form of Eqs. (1), (2) and (3) without rewriting them to Eqs. (4), (5) and (6). Here, two such methods which will be called “Method I” and “Method II” shall briefly be discussed. Their accuracy will be compared to the partial integration methods introduced above, which are referred to as “Method III” and “Method IV” in the following.

Method I – insertion of h at singularity:

One technique for the implementation of the transformations using their original form of Eqs. (1), (2) and (3) is to insert a single increment h at the singularity where $x = r$, as in

$$g_k = x_k h \left(\sum_{n=1}^{k-1} \left(\frac{f'_n}{\sqrt{x_k^2 - r_n^2}} \right) + \frac{f'_k}{\sqrt{h}} \right), \quad (21)$$

where the first derivative is computed as in Eq. (9) using central differences. This method, however, delivers only very poor results. As can be seen in Fig. 5, the technique requires a number of discretization points which is several orders of magnitude higher in order to reach the accuracy which is achieved by the other implementation techniques. This method is not recommended.

Method II – implementation of the kernel with its antiderivative:

A far better technique for the implementation of the transformations using their original form is to implement the kernel of the transformation using its antiderivative. For the transformation to g_k , this translates to

$$g_k = x_k h \sum_{n=1}^k \left(\frac{\operatorname{atan} \frac{r_n}{\sqrt{x_k^2 - r_n^2}} - \operatorname{atan} \frac{r_{n-1}}{\sqrt{x_k^2 - r_{n-1}^2}}}{h} f_n' \right) \quad (22)$$

and for the transformation to p_n , one can use

$$p_n = -\frac{1}{\pi} h \sum_{k=n}^N \left(\frac{\log(\sqrt{x_{k+1}^2 - r_n^2} + x_{k+1}) - \log(\sqrt{x_k^2 - r_n^2} + x_k)}{h} q_k' \right). \quad (23)$$

The first derivatives can once more be obtained via central differences. As can be seen in Fig. 5, the Method II provides a much better accuracy than Method I.

Method III – partial integration method:

This technique was described in great detail in the first sections of this work. Here the singularity at $x = r$ is avoided through partial integration of the transformations. This leads to alternative formulations of the transformations in which the second derivative of the three-dimensional indentation profile and the deformed elastic foundation occur. Thus, singularities now occur at kinks of these profiles; however, they disappear in the numerical integration, similarly to Method II where small increment h cancels out in Eqs. (22) and (23).

Recall, however, that the singularity which is overcome in Method II occurs in the kernel. Method III, however, overcomes singularities which may occur through the shape of the indentation profile or the deformed one-dimensional foundation.

Also, the singularity in Method II always influences the transformation values at all discretization points whereas in Method III the singularities through kinks may leave transformation values at some discretization points uninfluenced.

In Fig. 5 it can be seen that with Method III the number of discretization points can substantially be reduced to achieve the same accuracy as in Method II. However, it stands out that the maximum error in Method III is still fairly close to the maximum error in Method II. This relatively high maximum error of Method III is generally attained at the end of the contact area.

Method IV – partial integration method with small adjustment:

The previously described relatively high maximum error of Method III is reduced in Method IV. The simple adjustment through the insertion of an additional discretization point at the end of the contact area is described in Section 6 above. In Fig. 5 it can be seen that with the Method IV the number of discretization points can further be reduced to achieve a certain desired accuracy.

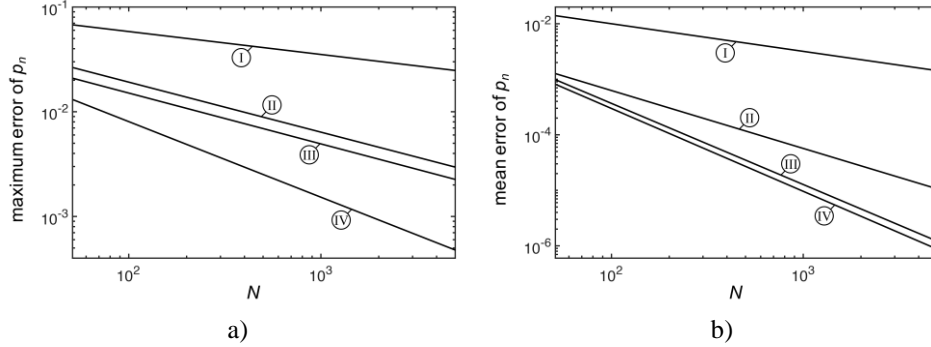


Fig. 5 Upper limits of the maximum absolute error of p_n (left graph a) and the mean absolute error of p_n (right graph b) compared for the different numerical methods: Method I – insertion of h at singularity, Method II – implementation of the kernel with its antiderivative, Method III – partial integration method (technique from this paper), Method IV – partial integration method with small adjustment (refined technique from this paper). As before, the curves are displayed for the exemplary inputs of $L = 1$, $E^* = 1$, $d = 0.3$ and here only for the exemplary parabolic indenter given with $f(r) = r^2/2$

8. EXEMPLARY WEAR SIMULATION

Apart from a high accuracy, Method III and Method IV may also show an advantage when they are used multiple times on a changing indentation profile, such as in wear simulations. As an example, consider a heterogeneous cylinder which is pressed onto an elastic half-space with normal force F_N and moves tangentially with velocity v_0 . The cylinder shall be composed of rings of different material having the same elastic properties but different wear coefficients k_1 and k_2 (see Fig. 6a). This setup has recently been studied with the MDR by Li et al. [6] using Archard's law [12]

$$\Delta V = k_{\text{wear}}(r) \frac{F_N s}{\sigma_0(r)} \quad (24)$$

to model the change of the indentation profile due to wear. Therein, $k_{\text{wear}}(r)$ and $\sigma_0(r)$ are wear coefficient, that is, hardness, and with $k(r) = k_{\text{wear}}(r) / \sigma_0(r)$ the linear wear is

$$\Delta f(r) = k(r) p(r) v_0 \Delta t. \quad (25)$$

In the following, the same procedure is adopted. It shows that the numerical method which is used for the MDR transformations has a significant impact on the quality of the simulation results.

The limiting profile and pressure reached after a long enough wear process are both displayed in Fig. 6b. Profile f is normalized with initial indentation depth $d_0 = F_N / (2aE^*)$ and the pressure distribution is normalized with $p_0 = F_N / (2\pi a^2)$. As can be seen in Fig. 6b, the use of Method II to perform the transformations leads to an oscillating error in the results for both the profile and the pressure (a thin grey jagged line). This error does not occur when Method III or Method IV are used (a smooth bold line). For an increasing

number of discretization points or smaller time steps in the wear simulation the oscillating error which occurs with Method II does not vanish although it can be smoothed out in the post-processing. Method III and IV, however, deliver the undistorted results straight away without the requirement for subsequent corrections.

Note that these raw results of the exemplary simulation obtained using Method III and Method IV also reproduce results obtained for validation purposes in [6] with the Boundary Element Method (BEM) [13].

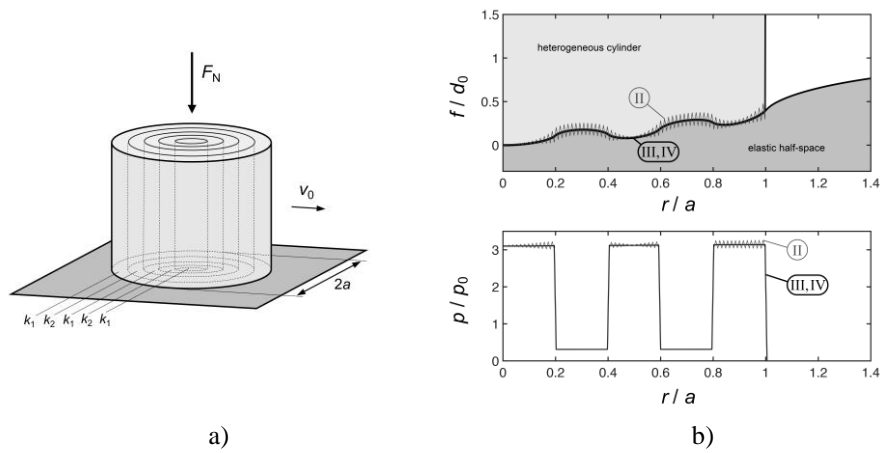


Fig. 6 Left graph a): A heterogeneous cylinder composed of rings of different material having the same elastic properties but different wear coefficients k_1 and k_2 is pressed onto an elastic half-space with the normal force F_N and moves tangentially with velocity v_0 . Right graph b): Simulation results for the limiting profile and pressure after a long enough running-in process as obtained with Method II (a thin grey jagged line), and the techniques from this paper – Method III and Method IV (a smooth bold line) with $N = 201$ discretization points and $k_2/k_1 = 10$

9. CONCLUSION

A simple implementation technique for the MDR transformations is presented in this work. It relies on integration by parts of the transformations, a central difference scheme to obtain the derivatives, and the trapezoidal rule to perform the summation.

It is shown that the results of the method for the contact of a cone and the Hertzian contact converge to the corresponding analytical solutions for an increasing number of discretization points. Therein, the highest error occurs at the border of the contact area. A small refinement to the numerical method has been presented to reduce this error.

The introduced method and its refinement are then compared to other numerical techniques which rely on the original form of the transformations. For the tested examples, the newly introduced method and its refinement deliver more accurate results at the same number of discretization points (see Fig. 5).

Furthermore, it is shown that apart from a higher accuracy when used once, the presented method and its refinement may have another benefit when used multiple times in

wear simulations. In an exemplary simulation, the wear of a heterogeneous cylinder composed of rings of different material having the same elastic properties but different wear coefficients is modeled. These discontinuous transitions in the material properties are handled well by the newly introduced methods, whereas the tested numerical techniques which rely on the original form of the transformations deliver results with a high oscillating error (see Fig. 6).

Acknowledgments: *The author would like to thank V. L. Popov, M. Heß, Q. Li, E. Willert and P. Diercks for many valuable discussions on the topic and critical comments.*

REFERENCES

1. Popov, V.L., Psakhie, S., 2007, *Numerical simulation methods in tribology*, Tribology International, 40(6), pp. 916-923.
2. Popov, V.L., Heß, M., 2016, *Method of dimensionality reduction in contact mechanics and friction*, Springer, Berlin.
3. Popov, M., Benad, J., Popov, V.L., Heß, M., 2015, *Acoustic Emission in Rolling Contacts*, Method of Dimensionality Reduction in Contact Mechanics and Friction, Springer, Berlin, pp. 207-214.
4. Dimaki, A., Dmitriev, A., Chai, Y., Popov, V.L., 2014, *Rapid simulation procedure for fretting wear on the basis of the method of dimensionality reduction*, International Journal of Solids and Structures, 51(25-26), pp. 4215-4220.
5. Dimaki, A., Dmitriev, A., Menga, N., Papangelo, A., Ciavarella, M., Popov, V.L., 2016, *Fast high-resolution simulation of the gross slip wear of axially symmetric contacts*, Tribology Transactions, 59(1), pp. 189-194.
6. Li, Q., Forsbach, F., Schuster, M., Pielsticker, D., Popov, V.L., 2018, *Wear Analysis of a Heterogeneous Annular Cylinder*, Lubricants, 6(1), 28.
7. Murio, D., Hinesroza, D., Mejía, C., 1992, *New stable numerical inversion of Abel's integral equation*, Computers & Mathematics with Applications, 23(11), pp. 3-11.
8. Hansen, E., Law, P., 1985, *Recursive methods for computing the Abel transform and its inverse*, Journal of the Optical Society of America A, 2(4), pp. 510-520.
9. Popov, V.L., Heß, M., 2014, *Method of dimensionality reduction in contact mechanics and friction: A users handbook. I. Axially-symmetric contacts*, Facta Universitatis-Series Mechanical Engineering, 12(1), pp. 1-14.
10. Heß, M., 2016, *A simple method for solving adhesive and non-adhesive axisymmetric contact problems of elastically graded materials*, International Journal of Engineering Science, 104, pp. 20-33.
11. Popov, V.L., Heß, M., Willert, E., 2017, *Handbuch der Kontaktmechanik*, Springer, Berlin.
12. Archard, J., Hirst, W., 1956, *The wear of metals under unlubricated conditions*, Proc. R. Soc. Lond. A, 236(1206), pp. 397-410.
13. Pohrt, R., Li, Q., 2014, *Complete Boundary Element Formulation for Normal and Tangential Contact Problems*, Physical Mesomechanics, 17(4), pp. 334-340.

Chapter 3

Application of the Method of Dimensionality Reduction to Selected Non-Axisymmetrical Contact Problems

Original scientific paper

INDENTATION OF FLAT-ENDED AND TAPERED INDENTERS WITH POLYGONAL CROSS-SECTIONS

UDC 539.3

Qiang Li, Valentin L. Popov

Department of System Dynamics and the Physics of Friction, TU Berlin, Germany

Abstract. *Using the Boundary Element Method, we numerically study the indentation of prismatic and tapered indenters with polygonal cross-sections. The contact stiffness of punches with flat bases in the form of a triangle and a square as well as a number of higher-order polygons is determined. In particular, the classical results of King (1987) for indenters with triangle and square base shapes are revised and more precise numerical results are provided. For tapered indenters, the equivalent transformed profile used in the Method of Dimensionality Reduction (MDR) is determined. It is shown that the MDR-transformed profile of polygon-based indenters with power function side is given by the power function with the same power; it differs from the 3D profile only by a constant coefficient. These coefficients are listed in the paper for various types of indenters, in particular for pyramidal and paraboloid ones. The determined MDR-transformed profiles can be used for study of other contact problems such as tangential contact, normal contact with elastomers, and, in an approximate way, to adhesive contacts.*

Key Words: *Indentation, Contact Stiffness, Polygonal Indenter, Boundary Element Method, MDR Transformed Profile*

1. INTRODUCTION

Indentation test is a very common way of probing mechanical properties of materials such as hardness, contact stiffness, elastic modulus and strain-stress relation [1-3]. There is a variety of indenter geometries used in macro- and microindentation; the most popular are spherical and pyramidal indenters (e.g. for the Vickers hardness test and Brinell hardness test) [4]. The contact stiffness of indenters with regular geometries is also important for the foundation design [5]. The analytical solution for contact between a rigid cylindrical flat punch and an elastic half space was given by Galin in 1953 (English translation see [6]). His results were later published by Sneddon and, in this way, made public to the western world [7]. Based on this

Received September 10, 2016 / Accepted November 04, 2016

Corresponding author: Qiang Li

Institute of Mechanics, Berlin Institute of Technology, Strasse des 17. Juni 135, 10623 Berlin, Germany

E-mail: qiang.li@tu-berlin.de

solution, Oliver and Pharr proposed an analysis method to determine the hardness and elastic modulus from the load-displacement curves of indentation test [8]. General relations among contact stiffness, contact area, and elastic modulus during indentation have been analytically derived only for axisymmetric indenters. For a non-axisymmetrical geometry, a correction coefficient is needed [9], which can be still found only numerically.

In this paper we numerically investigate the indentation of rigid bodies with various geometries: the flat-ended punches in Section 2 and tapered indenters in Section 3. In both cases we consider different polygonal bases including triangle and square. Note that the assumption of a rigid indenter is no restriction as the normal frictionless contact of two elastic bodies with elastic moduli E_1 and E_2 and Poisson numbers ν_1 and ν_2 can always be reduced to the contact of a rigid indenter and an elastic medium with an effective elastic modulus E^* determined as [10]

$$\frac{1}{E^*} = \frac{1-\nu_1^2}{E_1} + \frac{1-\nu_2^2}{E_2}. \quad (1)$$

In the present paper, the indentation test is numerically simulated by the high resolution Boundary Element Method (BEM), which has recently been generalized to arbitrary contact problems including tangential contact and adhesive contact [11, 12].

2. INDENTATION OF PRISMATIC INDENTERS WITH POLYGONAL BASE

The normal contact stiffness between a rigid flat cylinder and an elastic half space is given by $k=2aE^*$ [7], where a is the radius of the cylinder, and E^* is the effective elastic modulus, Eq. (1). In the case of a prismatic indenter with an arbitrary base form, the normal contact stiffness is given by [5]:

$$k = \beta \cdot 2E^* \sqrt{\frac{A}{\pi}}, \quad (2)$$

where A is the contact area of the base. Obviously the value of β is equal to 1 for the flat-ended cylinder. It was proven that Eq. (2) is also valid for indenters which have a cross section other than a circle [5]: $\beta=1.034$ for triangle and $\beta=1.012$ for square. These results were numerically obtained by King in 1987. Due to the limitation of computer technology at that time, King used only 200 elements for simulating a triangle indenter, and the

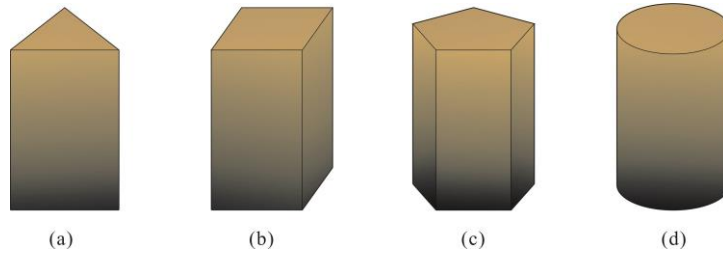


Fig. 1 Prismatic indenters with polygonal bases: $m=3$ (triangle), $m=4$ (square), $m=5$ (pentagon) and $m=\infty$ (circle)

triangular area looked quite ‘rugged’. Note that the stiffness of a flat punch and correspondingly factor β are related to the so-called harmonic capacity of the base form of the punch. This analogy was discussed by Argatov (2010) [13].

Below we repeat the calculations of King using the current high-resolution BEM and provide corrected values.

Using the boundary element method we have numerically carried out the indentation test for different shapes of cross section of indenters: from triangle ($m=3$), square ($m=4$), pentagon ($m=5$) to circle ($m=\infty$) as shown in Fig.1. In the simulation, the whole area was divided into 1024×1024 elements where at least 200000 elements were in the contact area. It is at least 1000 times more than in the King’s simulations; therefore, a much more precise result could be obtained. The values of coefficient β for different m are presented in Fig.2 and Table1. For the two most popular indenter shapes, the values are:

$$\begin{aligned} \beta &= 1.061, \text{ for triangle,} \\ \beta &= 1.021, \text{ for square,} \end{aligned} \tag{3}$$

which is larger than the values reported by King [5]. It can be seen that with the same area of cross section, the stiffness of triangular indenter is for 6% larger than that of a flat cylinder.

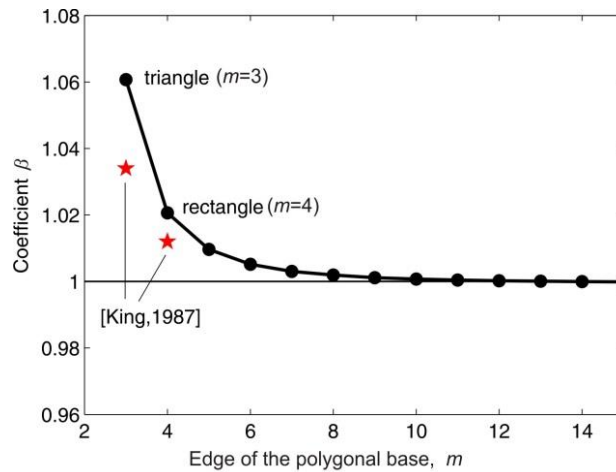


Fig. 2 Factor β for different polygonal indenters. The two stars indicate the results obtained numerically by King in 1987 [5]

Table 1 Values of constant β

m	3	4	5	6	7	8	∞
polygon	(triangle)	(square)					(cylinder)
β	1.061	1.021	1.010	1.005	1.003	1.002	1.000

3. INDENTATION OF TAPERED INDENTERS WITH POLYGONAL BASE AND POWER FUNCTION SIDE SURFACE

Now we consider the tapered indenters which have a regular polygonal base, as shown in Fig. 3. We begin with the most common type – a pyramid, and then extend it to indenters whose side profile is an arbitrary power function.

3.1. Pyramidal indenters

For the contact between a rigid cone with profile $f(r) = \tan\theta \cdot r$ and an elastic half space with effective elastic module E^* , the dependence of normal force on indentation depth was analytically found by Galin [6] (see also Sneddon [7]):

$$F_N = \frac{2}{\pi} \frac{E^*}{\tan\theta} d^2, \quad (4)$$

where d is indentation depth and θ is defined in Fig. 3(c). This solution can be easily reproduced using the method of dimensionality reduction (MDR). In the framework of the MDR [14], any contact problem of an axis-symmetrical profile $f(r)$ with an elastic half-space can be mapped onto a contact of a modified (MDR-transformed) profile $g(x)$:

$$g(x) = |x| \int_0^{|x|} \frac{f'(r)}{\sqrt{x^2 - r^2}} dr, \quad (5)$$

with properly defined elastic foundation. For a conical profile, $f(r) = \tan\theta \cdot r$, the substitution in Eq. (5) and integration provides the MDR-transformed profile:

$$g(x) = (\pi/2) \cdot |x| \cdot \tan\theta. \quad (6)$$

A short calculation (see. e.g. [14]) leads to Eq. (4).

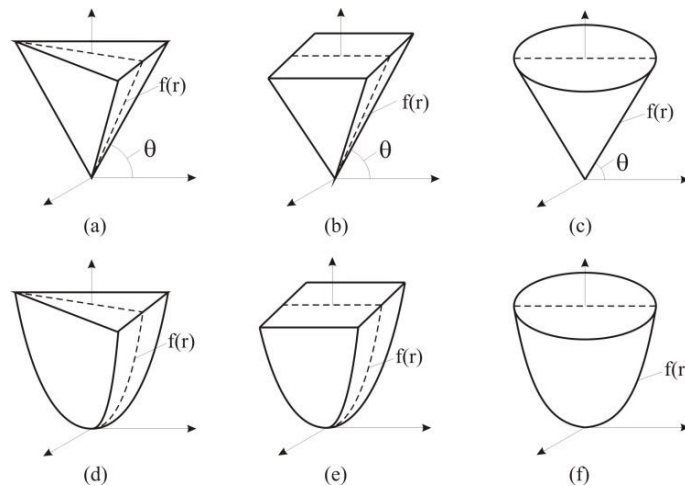


Fig. 3 Pyramid indenters for $n=1$ (a)-(c) and parabolic indenters for $n=2$ (d)-(f) with polygonal base, $m=3$ (triangle), $m=4$ (square), and $m=\infty$ (cycle)

In [15], it was shown that an equivalent MDR-transformed profile does exist not only for axis-symmetrical indenters but also for indenters of arbitrary shape. As shown in [15] and [16], for this sake, quantity $l=k/(2E^*)$ (where $k=dF_N/d$ is the incremental normal stiffness) should be determined numerically as function of indentation depth d . Inverse function $d(l)$ is then exactly the unknown MDR transformed profile $g(x)$. Let us illustrate this simple procedure on the example of conical indenter. By differentiating Eq. (4) with respect of d we get stiffness $k=4E^*d/(\pi \tan \theta)$ and length $l=2d/(\pi \tan \theta)$. Inverse relation $d=l(\pi/2)\tan \theta$ coincides exactly with the MDR transformed profile (6). This procedure is applicable regardless of whether dependence $F_N(d)$ was obtained analytically, numerically or experimentally. In the following, we determine dependence $F_N(d)$ numerically and extract from it the MDR-transformed profiles for a number of tapered profiles with polygonal cross-sections (Fig. 3).

We start with consideration of pyramidal indenters. As shown in Fig. 3(a)(b), the bases of the indenter are regular polygons. Angle θ is defined as the angle between the ground plane and the 3D indenter side surface as shown in Fig.3.

In the simulation we calculated the contacts of pyramid indenters with different polygonal bases varying from $m=3$ to 20, and for each type the angle ranges from $\theta=\pi/64$ to $31\pi/64$. All the simulation results show that the one-dimensional profile is still a linear function which can be formulated as:

$$g(x) = c_{1D} \cdot |x|, \quad (7)$$

with c_{1D} :

$$c_{1D} = \alpha \cdot \tan \theta, \quad (8)$$

where α is dependent only on polygon order m . For the sake of comparison we can define a fictive rotationally symmetric 3D profile with the same inclination angle:

$$f_{3D}(r) = c_{3D} \cdot r = \tan \theta \cdot r. \quad (9)$$

Then we can write $\alpha = c_{1D}/c_{3D}$. The values of α for different shapes of polygons are shown in Fig. 4(a) and Table 2. For a larger m , the shape of the pyramid indenter is close to a cone, the value of α is almost equal to $\pi/2$.

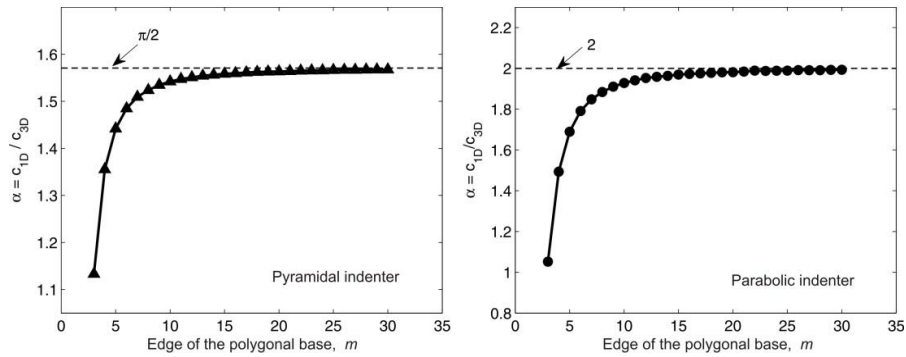


Fig. 4 Coefficient of α for pyramidal indenter $n=1$ (a) and parabolic indenter $n=2$ (b) with different polygonal bases

Table 2 Values of coefficient α

m	3	4	5	6	7	10	20	30	∞
polygon	triangle	square							cycle
α ($n=1$) pyramid	1.133	1.356	1.422	1.485	1.510	1.542	1.564	1.568	$\pi/2$
α ($n=2$) paraboloid	1.052	1.493	1.690	1.791	1.848	1.928	1.981	1.993	2

3.2. Indenters with arbitrary power function geometry

Let us now consider the case when the side surface of the indenter is not flat but is given by a power function. An example of parabolic indenter (shape with power 2) is shown in Fig. 3(d)-(f). We first remember the corresponding solution for an axisymmetric indenter with an arbitrary power function shape $f(r) = c_n \cdot r^n$. According to Eq. (5) its one-dimensional MDR-transformed profile is given by:

$$g(x) = \kappa_n c_n \cdot |x|^n, \quad (10)$$

where:

$$\kappa_n = \frac{\sqrt{\pi}}{2} \cdot \frac{n\Gamma(n/2)}{\Gamma(n/2+1/2)}, \quad (11)$$

and $\Gamma(n)$ is gamma function. In particular, for the cone ($n=1$) $\kappa_1 = \pi/2$ and for a paraboloid ($n=2$) $\kappa_2=2$, corresponding to $\alpha = c_{1D}/c_{3D}$ for $m=\infty$ as shown in Fig. 4 and Table 2.

As in the previous Section, we define an axis-symmetrical shape with the same power-law shape as shown in detail in Fig. 3. To underline that we have to do with a three-dimensional body which is in contact with a three-dimensional half-space, we denote the corresponding reference shape as

$$f_{3D}(r) = c_{3D} \cdot r^n. \quad (12)$$

This shape coincides with the vertical section of the polygonal indenters (shown by dashed lines in Fig. 3).

The numerical indentation tests were carried out for different indenters with power function n from 1 to 20 and the polygonal base parameter m from 3 to 30. The results show that the 1D profile for an arbitrary power function is still a power function with the same power. Coefficient $\alpha = c_{1D}/c_{3D}$ for the same type of indenter (fixed n and m) is constant (independent of coefficient c_{3D}). An example of parabolic indenter ($n=2$) is shown in Fig. 4 (b), where the values of α for triangle, square and further polygonal based profile are presented. In the limiting case the indenter is a spherical cylinder, and $\alpha=2$ corresponding to $\kappa_2=2$ is well-known from the MDR theory [14].

If we use the following parameter instead of α

$$\zeta = \frac{c_{1D}}{\kappa_n c_{3D}}, \quad (13)$$

then in the limiting case $m=\infty$, value ζ for any power function n will be equal to 1, $\zeta_{m=\infty}=1$. Some values of ζ , in particular for pyramid and parabolic indenter with triangle and square base are shown in Fig. 5 and Table 3.

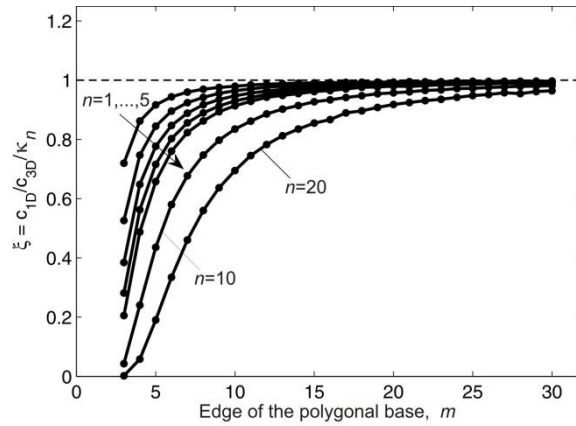


Fig. 5 Coefficient of ζ for indenters with power function profile

Table 3 Values of coefficient ζ

n	m					
	3 (triangle)	4 (square)	5	10	20	30
1 (pyramid)	0.723	0.866	0.923	0.986	1.000	1.000
2 (paraboloid)	0.526	0.747	0.845	0.964	0.991	0.997
3	0.384	0.648	0.777	0.947	0.987	0.994
10	0.043	0.241	0.058	0.835	0.957	0.983
20	0.002	0.058	0.190	0.695	0.918	0.964

3.3. Consideration of indenters with the same base area

In Section 2 it is found that the contact stiffnesses of triangular, rectangular indenters and flat cylinder with the same cross-section area are almost the same, and differ at most by 6%. It thus appears to be sensible to try as “reference” indenters the axisymmetrical profiles with the same area of cross-section. This definition is slightly different from the definition in the previous Section. For both initial polygonal profile and the reference axisymmetrical profile we carry out the MDR transformation and determine the equivalent 1D-MDR profiles. Let us explain the exact procedure on the example of a pyramid indenter ($n=1$). First, we determine the area of the indenter at different height and construct a cone with exactly the same cross-section areas. Then we carry out the three dimensional indentation test of the polygonal indenter by the BEM simulation and extract corresponding MDR profile $g(x)_{m\text{-poly}}$ and corresponding coefficient $c_{1D,m\text{-poly}}$ as described in Section 3. For the reference axisymmetrical profile, the corresponding MDR transformed profile and the corresponding coefficient $c_{1D,m=\infty}$ are determined by (5). Finally we compare this $c_{1D,m\text{-poly}}$ and the coefficient of the axisymmetric conical profile using the ratio

$$\zeta = \frac{c_{1D,m\text{-poly}}}{c_{1D,m=\infty}} . \tag{14}$$

In an absolute similar way comparisons were also carried out for other power function geometries. The results are shown in Fig.6 and Table 4. It can be seen that the coefficient c_{ID} of pyramid indenter is close to that of conical indenter: it differs by at most 7% in the case of triangular base ($c_{ID}=0.927$). It is noted that coefficient c_{ID} cannot directly reflect the contact stiffness. Take an example of triangular indenter with power $n=20$ whose geometry is close to the flat triangular indenter (Fig. 1a), its ζ is very small $\zeta=0.295$ ($m=3, n=20$), but the contact stiffness at the large indentation depth is the same to the flat indenter.

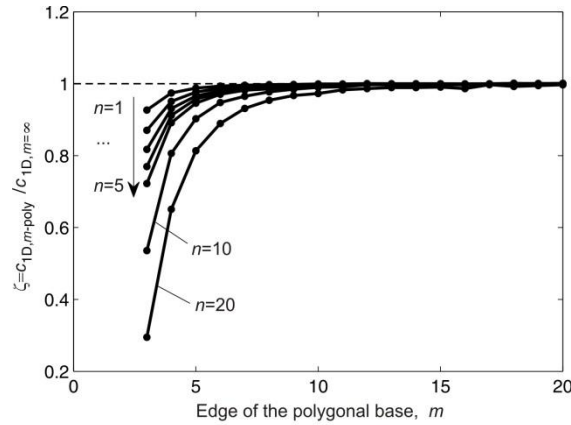


Fig. 6 Comparison of coefficient c_{ID} among different indenters with the same base area

Table 4 Coefficient ζ for different power n and polygon m

n	m					
	3 (triangle)	4 (square)	5	6	10	20
1 (pyramid)	0.927	0.974	0.988	0.994	1.000	1.000
2 (paraboloid)	0.870	0.951	0.977	0.988	0.997	1.000
3	0.817	0.931	0.966	0.981	0.996	1.000
10	0.536	0.806	0.820	0.893	0.990	1.000
20	0.295	0.651	0.814	0.889	0.973	0.997

4. CONCLUSION

Indentation of flat-ended and tapered indenters with polygonal base was numerically simulated using the boundary element method. The contact stiffnesses of prismatic punches with the same cross section area are almost same as the cylindrical indenter, where the triangular punch differs at most by 6%. For pyramidal indenter and others with power function side, the one dimensional MDR transformed profile was generated based on the three dimensional simulation of indentation. It is found that the 1D profile is still a power function with the same power and it differs only by a constant factor. The factor was numerically calculated for the indenters with different power function side and different polygonal base. The generated MDR profiles can be used for the further contact problems, such as tangential contact or contact with linear viscoelastic bodies.

REFERENCES

1. Oliver, W.C., Pharr, G.M., 2011, *Measurement of hardness and elastic modulus by instrumented indentation: Advances in understanding and refinements to methodology*, Journal of Materials Research, 19(1), pp. 3–20.
2. Fischer-Cripps, A.C., 2000, *A review of analysis methods for sub-micron indentation testing*, Vacuum, 58(4), pp.569-585.
3. Hay, J., Agee, P., Herbert, E., 2010, *Continuous stiffness measurement during instrumented indentation testing*, Experimental Techniques, 34, pp. 86–94.
4. Swadener, J.G., George, E.P., Pharr, G.M., 2002, *The correlation of the indentation size effect measured with indenters of various shapes*, Journal of the Mechanics and Physics of Solids, 50(4), pp. 681-694.
5. King, R.B., 1987, *Elastic analysis of some punch problems for a layered medium*, International Journal of Solids and Structures, 23(12), pp. 1657-1664.
6. Galin, L.A., 1961, *Contact Problems in the Theory of Elasticity*, North Carolina State College, USA
7. Sneddon, I.N., 1965, *The relation between load and penetration in the axisymmetric Boussinesq problem for a punch of arbitrary profile*, International Journal of Engineering Science, 23(12), pp. 1657-1664.
8. Oliver, W.C., Pharr, G.M., 1992, *An Improved Technique for Determining Hardness and Elastic-Modulus Using Load and Displacement Sensing Indentation Experiments*, Journal of Materials Research, 7(6), pp. 1564-1583.
9. Pharr, G.M., Oliver, W.C., Brotzen, F.R., 2011, *On the generality of the relationship among contact stiffness, contact area, and elastic modulus during indentation*, Journal of Materials Research, 7(3), pp. 613–617.
10. Popov V.L., 2010, *Contact mechanics and friction: Physical principles and foundations*, Springer, Berlin.
11. Pohrt, R., Li, Q., 2014, *Complete boundary element formulation for normal and tangential contact problems*, Physical Mesomechanics, 17(4), pp. 334-340.
12. Pohrt, R., Popov, V.L., 2015, *Adhesive contact simulation of elastic solids using local mesh-dependent detachment criterion in Boundary Elements Method*, Facta Universitatis series: Mechanical Engineering, 13(1), pp. 3-10
13. Argatov, I., 2010, *Frictionless and adhesive nanoindentation: Asymptotic modeling of size effects*, Mechanics of Materials, 42(8), pp. 807–815.
14. Popov, V.L., Heß, M., 2015, *Method of dimensionality reduction in contact mechanics and friction*, Springer, Berlin.
15. Argatov, I., Heß, M., Pohrt, R., Popov, V.L., 2016, *The extension of the method of dimensionality reduction to non-compact and non-axisymmetric contact*, Journal of Applied Mathematics and Mechanics (ZAMM), 96(10), pp. 1144-1155.
16. Popov, V.L., Pohrt, R., Heß, M., 2016, *General procedure for solution of contact problems under dynamic normal and tangential loading based on the known solution of normal contact problem*, Journal of Strain Analysis for Engineering Design, 51(4), pp. 247-255.

Original scientific paper

NORMAL LINE CONTACT OF FINITE-LENGTH CYLINDERS

UDC 539.3

Qiang Li, Valentin L. Popov

Department of System Dynamics and the Physics of Friction,
Berlin Institute of Technology, Berlin, Germany

Abstract. *In this paper, the normal contact problem between an elastic half-space and a cylindrical body with the axis parallel to the surface of the half-space is solved numerically by using the Boundary Element Method (BEM). The numerical solution is approximated with an analytical equation motivated by an existing asymptotic solution of the corresponding problem. The resulting empirical equation is validated by an extensive parameter study. Based on this solution, we calculate the equivalent MDR-profile, which reproduces the solution exactly in the framework of the Method of Dimensionality Reduction (MDR). This MDR-profile contains in a condensed and easy-to-use form all the necessary information about the found solution and can be exploited for the solution of other related problems (as contact with viscoelastic bodies, tangential contact problem, and adhesive contact problem.) The analytical approximation reproduces numerical results with high precision provided the ratio of length and radius of the cylinder are larger than 5. For thin disks (small length-to-radius ratio), the results are not exact but acceptable for engineering applications.*

Key Words: *Line Contact, Boundary Element Method, Finite-length Cylinder, Contact Stiffness, Method of Dimensionality Reduction*

1. INTRODUCTION

The contact problem of cylinders with parallel axes or of a flat elastic body with a “lying” cylinder is very common in practical engineering applications, in particular in mechanical elements such as roller bearings, gears and cams [1, 2]. In contrast to the Hertz-like contacts of bodies with curvature in two directions which in engineering mechanics are called “point contacts”, the contact of two parallel cylinders is denoted as a “line contact”. Being an immediate two-dimensional analog of the Hertz contact, the line contact between cylinders with parallel axes is one of basic problems in contact mechanics.

Received February 22, 2017 / Accepted March 15, 2017

Corresponding author: Valentin L. Popov

Department of System Dynamics and the Physics of Friction, Berlin Institute of Technology, Str. des 17 Juni 135, 10623 Berlin, Germany

E-mail: v.popov@tu-berlin.de

Even if the effective dimensionality of a line contact is lower than that of the point contact (2D vs. 3D), the line contact is in some sense more complicated than its 3D analog since in the line contact the “indentation depth” cannot be defined unambiguously. This is related to the logarithmic divergence of the 2D fundamental solution in infinity. In other words, the properties of a 2D contact (line contact) are not “local” but depend on the macroscopic shape of the body. This dependence, however, is relatively weak (logarithmic). Therefore, there exist a large number of approximated solutions [3-5], which have been applied in many further studies, for example in elastic hydrodynamic lubrication [6, 7]. The main structure of all approximate solutions is relatively simple: it reproduces the logarithmic divergence and cuts it up at some characteristic distance, at which the contact ceases to be a line-contact. In the case of a true 2D contact, this is the size of the system (e.g. the radius of contacting cylinders).

On the other hand, for any finite contact, e.g. that of a lying cylinder of finite length, the indentation depth can be determined unambiguously. The macroscopic length which in this case limits the “two-dimensionality” of the line contact is the length of the cylinder. One can anticipate that the indentation depth at a given force will be a weak logarithmic function of the cylinder length. Finding the exact form of this function is the main goal of this paper.

As the solution of the underlying two-dimensional contact problem gives the basis for our consideration, we first provide a brief overview of earlier works on this topic. The contact of cylinders with parallel axes was early studied by Prescott [8] and Thomas and Hoersch [9], and later also investigated by many researchers, for example Lundberg et al. [10]. A good review of analytical solution for this contact problem can be found in Norden’s report [11], where the deviation of relationship between the normal load and the indentation depth is given in detail; this relationship is still widely used today. The same analysis is also presented in Puttock and Thwaite’s report [12]. In these solutions, the existing result of pressure distribution for elliptical contact is used for cylindrical contact with parallel axes by assuming one axis of ellipse is infinitely large, and then the contact area is considered as a finite rectangle whose length is much larger than its width. For further reference, here we reproduce their solution of a cylinder with radius R and length L pressed into elastic half space under normal load F [12]: the half width of contact rectangle b is equal to:

$$b = \sqrt{\frac{4RF}{\pi E^* L}} \quad (1)$$

and indentation depth d is:

$$d = \frac{F}{\pi L E^*} \left(1 + \ln \frac{\pi E^* L^3}{RF} \right) = \frac{F}{\pi L E^*} \left(1 + \ln \frac{4L^2}{b^2} \right) \quad (2)$$

where E^* is effective elastic modulus and equal to:

$$\frac{1}{E^*} = \frac{1-\nu_1^2}{E_1} + \frac{1-\nu_2^2}{E_2} . \quad (3)$$

with E_1 and E_2 are elastic module of contacting bodies, ν_1 and ν_2 are Poisson’s ratio. Later Johnson and other authors gave other forms of force-displacement e.g.:

$$d = \frac{F}{\pi L E^*} \left(\ln \frac{4\pi E^* L R}{F} - const \right) \quad (4)$$

where $const=1$ in [4], 0.72 and 0.572 in others [13].

Correspondingly, the experiment investigation consisting of compression of parallel cylinders or indenting a cylinder into an elastic body is carried out in [11, 14]. Empirical equations of load-displacement are provided to verify theoretical solutions. In Thwaite's compression test [15] of a contact between a cylinder and a half-space, the comparison of slopes (or contact stiffness) shows that the solution (2) is the closest to the experimental results. In Kunz's experimental investigation [14], it is found that the approach of parallel cylinders is proportional to the loading force: $F=cE^*Ld$, where c is constant $c=0.175$.

In the last few decades, some numerical studies of the finite length line contact have been carried out to investigate the effect of contact edge and bone shape of the contact area and on stress distribution [16, 17]. However, a more precise solution for the line contact is rarely provided. Recently an analytical solution for contact problem of toroidal indenter is given by Argatov et al. [18] and is validated numerically by the boundary element method. In this paper we propose an analytical approximation of contact stiffness of a rigid cylinder and an elastic half space based on the results of [18]. While we overtake the general form of solution, we let some parameters free and determine them finally by numerical simulation of indentation test using the boundary element method.

2. EFFECTIVE MDR-PROFILE FOR A FINITE LENGTH LYING CYLINDER

2.1. Analytical approximation based on an asymptotic solution

The main physical result of this paper will be the dependence of normal force on the indentation depth for a contact between an elastic half-space and a "lying" cylinder (with the axis parallel to the surface of the half-space.) However, we will "pack" this dependence in the terms of the Method of Dimensionality Reduction (MDR) [19] where the whole information about the system is compressed into effective plane profile $g(x)$. The advantage of this presentation is that $g(x)$ can be used not only to easy reconstruct the dependency of the normal force on the indentation depth but also to solve a variety of other related problems such as tangential contact problem with friction in the interface, adhesive contact problem, and contact of visco-elastic bodies. In this sense, $g(x)$ is, so to say, the "visiting card" of the profile in question which allows multi-purpose use.

Note that the possibility of mapping three-dimensional contacts onto contacts with elastic foundation is well known for axis-symmetric indenters with compact contact area [19]. Less known is that the same concept can also be used to arbitrary other profiles, as e.g. of a torus (not compact contact area) or a rough surface. The corresponding proof as well as examples of MDR-profiles for a number of non-axisymmetric contacts can be found in [18] and [20]. Profile $g(x)$ determines straightforwardly force-indentation dependence $F(d)$. Thus the information content of both dependencies is equal: one can either determine $F(d)$ from $g(x)$ or $g(x)$ from $F(d)$. Even if the information content of both the functions is the same, it is more convenient to have $g(x)$ as it allows to solve much more various problems than $F(d)$.

In [20] the explicit procedure of "extracting" profile $g(x)$ from dependency $F(d)$ is described. The procedure is very trivial: from known dependency $F(d)$ one first determines differential contact stiffness $k_n(d)=dF(d)/dd$ and then determines the dependence of d as function of variable $x=k_n/(2E^*)$. Dependency $d(x)$ is exactly searched-for function $g(x)$. In the present paper, this procedure is carried out numerically: first, dependency $F(d)$ is determined by direct simulation using the boundary element method. Subsequently, the

described procedure is applied to extract $g(x)$. Finally, numerically found profile $g(x)$ is approximated analytically.

For the analytical approximation we use the form of $g(x)$ found in [18] for indentation of a torus. In [18], it is derived by an asymptotic analysis and verified through BEM simulations. The 1D profile for toroidal indenter is given by:

$$g(x) = \frac{R'^2}{4\rho} \left(\frac{\pi^2 R'}{x} + 1 \right) \exp \left(8 \ln 2 - \frac{\pi^2 R'}{x} \right). \quad (5)$$

Here, R' is the distance from the center of the torus tube to the center of the torus, ρ is the radius of the torus tube.

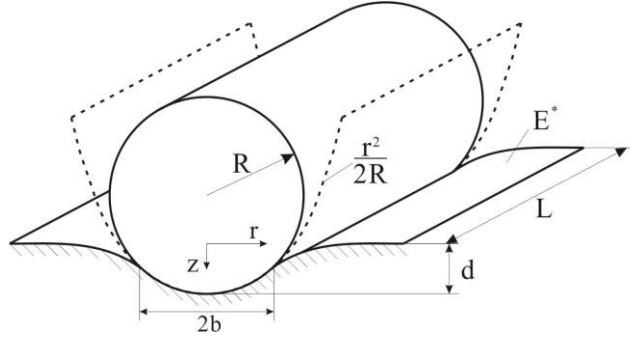


Fig. 1 A rigid cylinder lying on an elastic half space

The contact of the torus is very similar to that of a “lying” cylinder: both contacts are basically line ones and thus two-dimensional contacts whose logarithmic divergence is cut at some distance. For the torus, the role of the cut-off length plays the radius of the torus, while in the case of the lying cylinder this is the length of the cylinder. Equation (5) found for the torus thus can be used for lying cylinder with radius R and length L (Fig. 1) just by replacing $R' \rightarrow L$ and $\rho \rightarrow R$. The differences in two configurations are taken into account by introducing two coefficients c_1 and c_2 which in the case of the torus are equal to 1, but in the case a lying cylinder are allowed to take some other values:

$$g(x) = \frac{L^2}{4R} \left(c_1 \cdot \frac{\pi^2 L}{x} + 1 \right) \exp \left(c_2 \cdot 8 \ln 2 - c_1 \cdot \frac{\pi^2 L}{x} \right). \quad (6)$$

In a more compact form Eq. (6) can be rewritten as:

$$g(x) = \beta \frac{L^2}{R} \left(\frac{\alpha L}{x} + 1 \right) \exp \left(-\frac{\alpha L}{x} \right) \quad (7)$$

where we have introduced two other fitting coefficients α and β (instead of c_1 and c_2). Introducing dimensionless parameters:

$$\tilde{x} = \frac{x}{L} \quad \text{and} \quad \tilde{g}(\tilde{x}) = \frac{g(x)R}{L^2}, \quad (8)$$

Eq. (7) can be written in the dimensionless form:

$$\tilde{g}(\tilde{x}) = \beta \left(\frac{\alpha}{\tilde{x}} + 1 \right) \exp\left(-\frac{\alpha}{\tilde{x}} \right). \quad (9)$$

2.2. Numerical simulation of the indentation test

Two unknown coefficients α and β in Eq. (7) will be determined by numerical simulation of indentation test using the boundary element method which was developed by Pohrt, Li and Popov for various 3D contact problems including the partial sliding contact [21] and adhesive contact [22, 23].

In the simulation, the whole simulation area was divided into 512×512 rectangular elements. The rigid cylinder was modeled as parabolic indenter $f(y) = y^2 / (2R)$, where y is in-plane coordinate perpendicular to the axis of the cylinder. The cylinder was indented in an elastic half space with controlled indentation depth in 100 steps from zero (first contact) to $0.15R$. The pressure distribution as well as the normal load and normal contact stiffness were calculated in each step of indentation. One example of contact configuration and pressure distribution is shown in Fig. 2. The concentration of pressure at the contact edge can be clearly observed in Fig. 2b.

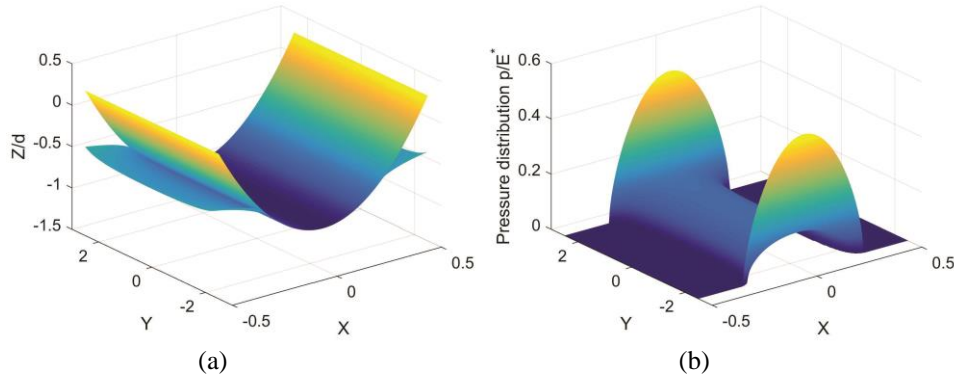


Fig. 2 An example of numerical simulation for $L/R=5$ and $d=0.1R$:
(a) contact state (b) pressure distribution

3. RESULTS AND DISCUSSION

We have performed indentation simulations for cylinders with 29 increasing values of L/R ranging from $L/R = 0.1$ to 20 (10 linearly increasing L/R from 0.1 to 1, and 19 from 2 to 20). Resulting MDR-profiles $g(x)$ are shown with crosses in Fig. 3a. In Fig. 3b, all curves are plotted in dimensionless form in coordinates (8). It is seen that all crosses for different L/R collapse to a single curve thus confirming the basic structure of the solution:

$$g(x) = \frac{L^2}{R} \Phi\left(\frac{x}{L} \right). \quad (10)$$

Fig. 3b provides the numerically determined form of function $\Phi(\cdot)$.

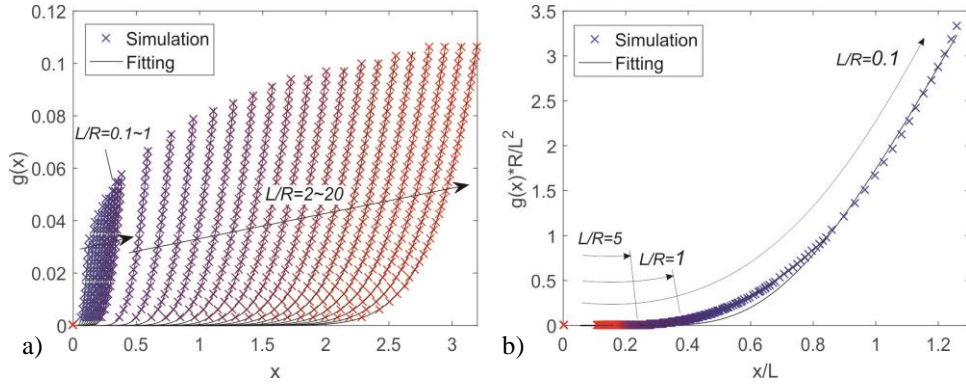


Fig. 3 1D profile of lying cylinder calculated by BEM simulation (cross) and fitting with Eq. (7)

In the following, we provide analytical approximation for this function on the basis of Eq (9). The values of coefficients α and β are calculated by the method of least squares. The agreement of fitting (black solid lines) with numerical simulation can be seen in Fig. 3. Values of α and β are presented in Fig. 4, where we can see that both factors are almost constant for large ratios of L/R but change significantly for small ratios. We thus discuss the cases of “long cylinders” and “short cylinders” separately.

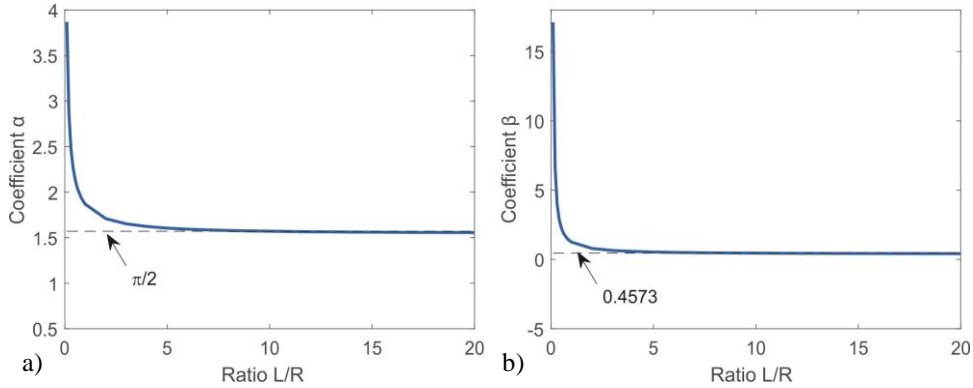


Fig. 4 Values of coefficients of α (a) and β (b) for different ratios of L/R obtained by fitting of Eq. (7) with numerical results

(a) Large ratio L/R (“long cylinder”)

From Fig. 4, one can see that α and β for larger L/R are almost constant: $\alpha = \pi/2$ and $\beta = 0.4573$. Thus, for large ratios in the range of about $L/R \geq 5$ we can give the following approximation:

$$g(x) = 0.4573 \frac{L^2}{R} \left(\frac{\pi L}{2x} + 1 \right) \exp\left(-\frac{\pi L}{2x} \right), \text{ for } L/R \geq 5, \quad (11)$$

or in the dimensionless form:

$$\tilde{g}(\tilde{x}) = 0.4573 \left(\frac{\pi}{2\tilde{x}} + 1 \right) \exp\left(-\frac{\pi}{2\tilde{x}}\right), \text{ for } L/R \geq 5. \quad (12)$$

Numerical results and analytical approximations (11) and (12) in this range of L/R are shown in Fig. 5.

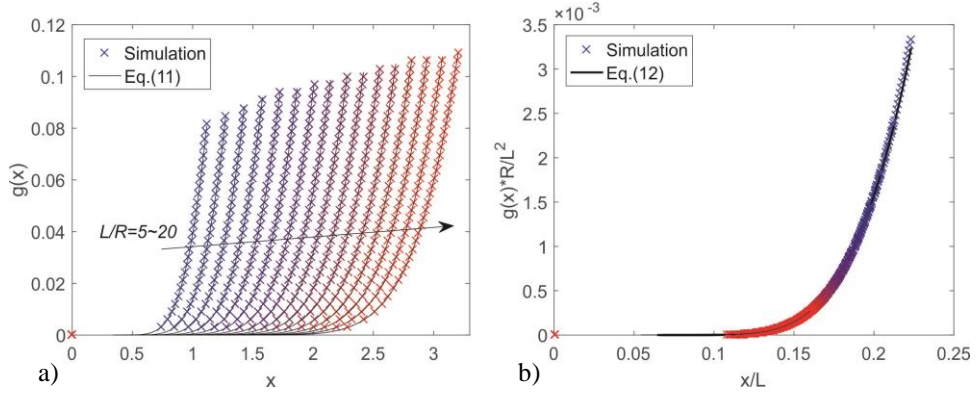


Fig. 5 1D profile of cylinder for larger ratios of L/R :
(a) for different L/R (b) in dimensionless form

(b) *Small ratio of L/R ("short cylinder")*

In practical applications, many line-contact machine elements are thin plates meaning a small value of L/R , as e.g. cams. The results of numerical simulation and fitting for $L/R=0.1\sim 4$ are clearly shown in Fig. 6. Coefficients α and β in this range are different (Fig. 4); however, from the subplot of Fig. 6b we can find that the fittings agree with the numerical results also well, except for very small L/R ($=0.1$ or 0.2) (subplot in Fig. 6b), so we list their values in Tab. 1 for the further studies.

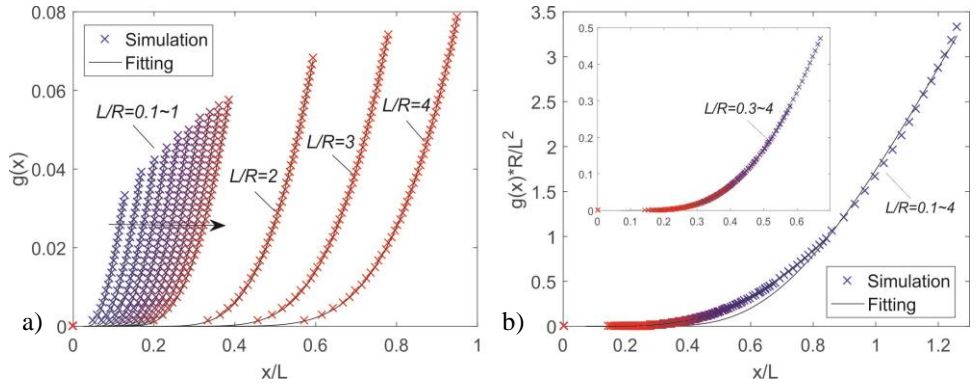


Fig. 6 1D profile of cylinder for small ratios of L/R :
(a) for different L/R (b) in dimensionless form

Table 1 Values of coefficients α and β for small L/R

L/R	A	β	L/R	A	β	L/R	α	β
0.1	3.8695	17.1183	0.6	2.0528	1.9139	2	1.7086	0.7936
0.2	2.8664	6.6132	0.7	1.9928	1.6847	3	1.6518	0.6495
0.3	2.4734	3.9560	0.8	1.9400	1.4963	4	1.6231	0.5799
0.4	2.2714	2.8770	0.9	1.8996	1.3589	5	1.6048	0.5376
0.5	2.1455	2.2975	1	1.8668	1.2517	6	1.5930	0.5091

Finally, let us compare our results with those following from Eq. (2). Differentiation of the force with respect to the indentation depth provides the normal contact stiffness:

$$k_n = \pi LE^* \ln \frac{RF}{\pi E^* L^3} . \quad (13)$$

Together with relation (2) we can obtain 1D profile $g(x)$, which has also a dimensionless form similar to Eq. (12). This dimensionless form is shown with a dashed line in Fig. 7. One can see that it differs substantially from the “numerically exact” result found in the present paper and plotted in Fig. 7 with a bold line.

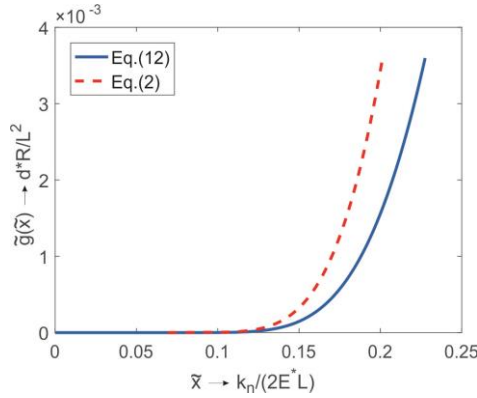


Fig. 7 Comparison of 1D profile obtained from existing solution and in this paper

4. CONCLUSION

We have numerically simulated indentation of the finite-length cylinder lying on an elastic half space. The ratio of the cylinder’s length and radius was varied in a wide range from a thin disk (ratio 0.1) to a long pole (ratio 20). Based on the results of numerical simulation, the equivalent MDR-profiles containing the whole information about the contact problem was “extracted” and subsequently approximated analytically using an equation inspired by an asymptotic solution of the contact problem. For large length-to-radius ratios (larger than about 5), the fitting coefficients are almost constant and a general form with high accuracy is provided in a closed analytical form. For small length-to-radius ratios, analytical solution is provided which contains two constants provided in the form of a table. Comparison of the present solution with the already available analytical approximation shows that the present solution is much more precise.

REFERENCES

1. Harris, T.A., 2001, *Rolling bearing analysis*, John Wiley and Sons, New York.
2. Norton, R., 2009, *Cam Design and Manufacturing Handbook*, Industrial Press.
3. Popov, V.L., 2010, *Contact Mechanics and Friction: Physical Principles and Applications*, Springer, Berlin.
4. Jonson, K.L., 1985, *Contact Mechanics*, Cambridge University Press, Cambridge.
5. Landau, L.D., Lifshitz, E.M., 1970, *Theory of Elasticity*, Course of Theoretical Physics.
6. Venner, C.H., Lubrecht, A.A., 1994, *Transient Analysis of Surface Features in an EHL Line Contact in the Case of Sliding*, Journal of Tribology, 116(2), pp. 186–193.
7. Hamrock, B.J., Schmid, S.R., Jacobson, B.O., 2004, *Fundamentals of Fluid Film Lubrication*, Marcel Dekker, New York.
8. Prescott, J., 1946, *Applied Elasticity*, Dover Publications.
9. Thomas, H.R., Hoersch, V.A., 1930, *Stresses Due to the Pressure of One Elastic Solid Upon Another: A Report of an Investigation Conducted by the Engineering Experiment Station*, University of Illinois in Cooperation with the Utilities Research Commission.
10. Lundberg, G., 1939, *Elastische Berührung zweier Halbräume*, Forschung auf dem Gebiet des Ingenieurwesens A, 10(5), pp. 201–211.
11. Norden, B.N., 1973, *On the compression of a cylinder in contact with a plane surface*, National Bureau of Standards, Washington D.C.
12. Puttock, M.J., Thwaite, E.G., 1969, *Elastic Compression of Spheres and Cylinders at Point and Line Contact*, National Standards Laboratory.
13. Nakhatakyan, F.G., 2011, *Precise solution of Hertz contact problem for circular cylinders with parallel axes*, Russian Engineering Research, 31(3), pp. 193–196.
14. Kunz, J., de Maria, E., 2002, *Die Abplattung im Kontaktproblem paralleler Zylinder*, Forschung Im Ingenieurwesen, 67(4), pp. 146–156.
15. Thwaite, E.G., 1969, *A precise measurement of the compression of a cylinder in contact with a flat surface*, Journal of Physics E: Scientific Instruments, 2(1), pp. 79–82.
16. Glovnea, M., Diaconescu, E., 2004, *New Investigations of Finite Length Line Contact*, In ASME Proceedings, Special Symposia on Contact Mechanics, pp. 147–152.
17. Najjari, M., Guilbault, R., 2014, *Modeling the edge contact effect of finite contact lines on subsurface stresses*, Tribology International, 77, pp. 78–85.
18. Argatov, I., Heß, M., Pohrt, R., Popov, V.L., 2016, *The extension of the method of dimensionality reduction to non-compact and non-axisymmetric contacts*, ZAMM Journal of Applied Mathematics and Mechanics, 96(10), pp. 1144–1155.
19. Popov, V.L., Heß, M., 2015, *Method of Dimensionality Reduction in Contact Mechanics and Friction*, Springer, Berlin.
20. Popov, V.L., Pohrt, R., Heß, M., 2016, *General procedure for solution of contact problems under dynamic normal and tangential loading based on the known solution of normal contact problem*, The Journal of Strain Analysis for Engineering Design, 51(4), pp. 247–255.
21. Pohrt, R., Li, Q., 2014, *Complete Boundary Element Formulation for Normal and Tangential Contact Problems*, Physical Mesomechanics, 17(4), pp. 334–340.
22. Pohrt, R., Popov, V.L., 2015, *Adhesive contact simulation of elastic solids using local mesh-dependent detachment criterion in boundary elements method*, Facta Universitatis, Series: Mechanical Engineering, 13(1), pp. 3–10.
23. Li, Q., Popov, V.L., 2016, *Boundary element method for normal non-adhesive and adhesive contacts of power-law graded elastic materials*, arXiv:1612.08395.

Chapter 4

Applications of the Method of Dimensionality Reduction

THE INFLUENCE OF VISCOELASTICITY ON VELOCITY-DEPENDENT RESTITUTIONS IN THE OBLIQUE IMPACT OF SPHERES

UDC 539.3

Emanuel Willert¹, Stephan Kusche¹, Valentin L. Popov^{1,2,3}

¹Berlin University of Technology, Berlin, Germany

²National Research Tomsk State University, Tomsk, Russia

³National Research Tomsk Polytechnic University, Tomsk, Russia

Abstract. *We analyse the oblique impact of linear-viscoelastic spheres by numerical models based on the Method of Dimensionality Reduction and the Boundary Element Method. Thereby we assume quasi-stationarity, the validity of the half-space hypothesis, short impact times and Amontons-Coulomb friction with a constant coefficient for both static and kinetic friction. As under these assumptions both methods are equivalent, their results differ only within the margin of a numerical error. The solution of the impact problem written in proper dimensionless variables will only depend on the two parameters necessary to describe the elastic problem and a sufficient set of variables to describe the influence of viscoelastic material behaviour; in the case of a standard solid this corresponds to two additional variables. The full solution of the impact problem is finally determined by comprehensive parameter studies and partly approximated by simple analytic expressions.*

Key Words: *Oblique Impacts, Friction, Viscoelasticity, Standard Solid Model, Method of Dimensionality Reduction, Boundary Element Method*

1. INTRODUCTION

Collisions of macroscopic particles determine the dynamics of granular gases. As long as the particle density in the granular gas is small enough and hence the impact durations are small compared to the mean free time between two collisions, these will in general be binary. In many cases the difference of the particle velocities before and after the impact

Received April 20, 2017 / Accepted June 21, 2017

Corresponding author: Willert, Emanuel

Affiliation: Berlin University of Technology, Sekr. C8-4, Straße des 17. Juni 135, D-10623 Berlin

E-mail: e.willert@tu-berlin.de

© 2017 by University of Niš, Serbia | Creative Commons Licence: CC BY-NC-ND

can be described by two coefficients of restitution, one for each the normal and tangential direction of the impact. Due to friction, adhesion, viscoelasticity, plasticity or other effects those coefficients of restitution will in general exhibit strong and non-trivial dependencies not only of the geometric or material parameters but of the impact velocities themselves. Among the vast literature about granular media only few publication lines account for this velocity-dependence, which is mostly because of two reasons: on the one hand, the various analytical methods of statistical physics applied to deal with granular media are severely complicated by the fact that the restitution coefficients are actually velocity-dependent. On the other hand, the rigorous solution of the single contact-impact problem even in the simplest case of spherical colliding particles is a rather non-trivial task.

Lun and Savage [1] and Walton and Braun [2] were the first to study the effects of the described velocity-dependence on the granular dynamics using the granular-flow kinetic theory of Lun, Savage, Jeffrey and Chepurtnity. However, lacking rigorous solutions, they only used an ad-hoc model of a restitution coefficient in normal direction exponentially decreasing with the impact velocity, which can be realistic only in few cases. Besides, they did not account for inter-particle friction during the collisions and could hence achieve only rough agreement with their experimental data. Only ten years later a research group around Brilliantov and Pöschel started a series of publications to tackle this problem again. Brilliantov et al. [3] gave models for the collisions of spheres accounting for viscoelasticity and friction. However, their material model is equivalent to a Kelvin-Voigt body, which is only realistic if the time scale of interest is large compared to the relaxation time of the elastomer. As the impact times are short, this might be problematic. Moreover, their tribological friction model of broken welds and asperities leads to a stepwise linear dependence of the tangential force on the tangential displacement between the contacting bodies. For spherical profiles this cannot be true due to the profile shape. These collision models have been implemented in granular gas simulations by Schwager and Pöschel [4], Brilliantov and Pöschel [5] and Dubey et al. [6].

The history of rigorous impact solutions started with Hertz [7], who solved the frictionless and non-adhesive normal contact problem of two parabolic surfaces and the associated quasi-static impact problem. Hunter [8] studied the influence of the quasi-stationarity and found that the proportion of kinetic energy lost during the impact due to elastic wave propagation is negligible, if the impact velocities are small compared to the speed of sound in the elastic medium. Cattaneo [9] and Mindlin [10] solved the tangential contact problem of two elastically similar spheres in the case of a constant normal force and an increasing tangential force. The circular contact area will consist of an inner circular stick area and an annular region of local slip. The tangential traction distribution in the contact is a superposition of two Hertzian distributions. Their work has been extended by Mindlin and Deresiewicz [11] for various different and by Jäger [12] for arbitrary loading protocols. Based on the results of Mindlin and Deresiewicz, Maw et al. [13] and Barber [14] studied the oblique impact of elastic spheres without adhesion; they found out that the problem written in proper dimensionless variables only depends on two parameters, one describing the elastic and the other (containing a generalized angle of incidence and hence the impact velocities) the frictional properties. Moreover, the authors carried out experiments to validate their calculations. The oblique impact problem of elastic spheres with and without adhesion was also studied by Thornton and Yin [15]. A nice overview of elastic impact problems and several analytical solutions including torsional loading can be found in the paper by Jäger [16].

In a series of publications – see for example [17, 18] and the summarizing book [19] – Popov and his co-workers have shown that the generalized Hertz-Mindlin problem for any convex axisymmetric indenter and arbitrary loading histories can be exactly mapped onto a contact between a properly chosen plain profile and a one-dimensional foundation of independent linear springs in such a way that the solution of the obtained one-dimensional model will exactly coincide with the one of the original three-dimensional problem. Due to the enormous simplification and effort reduction of analytical or numerical calculations achieved by this so-called Method of Dimensionality Reduction (MDR) Lyashenko and Popov [20] were able to give a comprehensive solution for the problem studied earlier by Maw and his co-workers in the no-slip regime, i.e. an infinite coefficient of friction. Those results have later been generalized by Willert and Popov [21] for the partial slip regime, i.e. a finite friction coefficient.

The viscoelastic contact problem was first addressed by Lee and Radok [22-24]. From the close relationship between the fundamental equations of elasticity and viscosity the authors deduced a method of functional equations to obtain the solution of a viscoelastic problem if the solution of the associated elastic problem is known and the contact radius is a monotonically increasing function in time. This has been generalized to the case of any number of maxima and minima of the contact radius by Graham [25], [26] and Ting [27, 28]. An equivalent but somewhat easier formulation of Ting's solution was given by Greenwood [29]. However, with every maximum or minimum of the contact radius the analytic calculations get more and more cumbersome. The Hertz impact problem for viscoelastic media was treated by Pao [30] and Hunter [31]. They used arbitrary viscoelastic rheologies to formulate the problem but gave only few concrete solutions. Argatov [32] found analytical solutions for the respective flat punch problem in the case of Kelvin-Voigt-, Maxwell- or standard solid model.

The viscoelastic contact problem in the case of convex axisymmetric indenters and arbitrary loading protocols can also be exactly mapped within the framework of the MDR, which was proven by Kürschner and Filippov [33] and Argatov and Popov [34].

Hence, the aim of the present paper is to give a comprehensive solution of the viscoelastic oblique impact of spheres with and without slip based on the MDR. Very recently Kusche [35, 36] presented the no-slip solution of this impact problem using the Boundary Element Method (BEM). However, the BEM-calculations are numerically much more costly compared with the MDR. As the parameter space for the more general case with slip is larger by one dimension, the comprehensive solution based on BEM will be numerically very expensive. Nevertheless, the BEM-algorithm to solve the impact problem with slip has been implemented and can serve as a validation for the faster MDR-based model.

We will use a standard solid for modelling viscoelastic properties because it exhibits all characteristics of general elastomers. As a limiting case the Kelvin-Voigt solid is also studied at some point. Finally, we will focus on the velocity-dependence of the coefficients of restitution as this is the main point of interest for the implementation of the obtained solutions into simulation algorithms for granular media.

The paper is organized as follows: In Section 2 we will give a formulation of the studied problem. Section 3 is devoted to the description of the numerical model based on the MDR, the results of which are given in Section 5. Section 4 will present a BEM-based algorithm to solve the impact problem, which was used to validate the MDR model described before. Section 6 will give conclusions.

2. PROBLEM FORMULATION

The present paper is concerned with the oblique impact of two linear-viscoelastic spheres of similar materials. This problem is equivalent to the one of a rigid sphere impacting on a viscoelastic half-space, which is why we will restrict ourselves to the latter one. During contact the frictional interaction between the two surfaces shall be assumed to obey the Amontons-Coulomb's law with the static and the kinetic coefficients of friction being constant and equal to each other: $\mu_S = \mu_F \equiv \mu$. The sphere shall have initial velocities v_{x0} and v_{z0} , z pointing into the half-space, and initial angular velocity ω_0 . The mass, radius and moment of inertia of the sphere are m , R and J^S , respectively. The point on the sphere which first comes into contact shall be denoted as K .

The half-space shall possess a constant Poisson number ν and a creep function giving the response in shear. Actually a viscoelastic material may possess a second creep function for the response to hydrostatic stress, but this shall be neglected. As most elastomers can be considered incompressible (this will also fulfil the condition of elastic similarity) our assumption does not pose a considerable loss of generality. In this case we can introduce time-dependent shear modulus $G(t)$. For the standard solid model G reads:

$$G(t) = G_1 + G_2 \exp\left(-\frac{G_2 t}{\eta}\right). \quad (1)$$

The Kelvin-Voigt model can be recovered from this expression *via* the limit

$$G_{KV}(t) = \lim_{G_2 \rightarrow \infty} G(t) = G_1 + \eta \delta(t), \quad (2)$$

with the Dirac δ -distribution. A scheme of the impact with notations is shown in Fig. 1. We will make further following assumptions:

Quasi-stationarity: The impact velocities shall be much smaller than the speed of sound in the viscoelastic material. We therefore neglect all inertia effects like wave propagation.

Half-space hypothesis: The surface gradients shall be small. For an axisymmetric contact with parabolic indenter shapes in the vicinity of the contact point, this can be written as

$$d_{\max} \ll a_{\max} \ll R, \quad (3)$$

with the maximum values of indentation depth d and contact radius a .

Very short impact: The displacement of the contact point due to the change of position and the rotation of the sphere shall be small compared to the contact radius. This ensures that the contact configuration stays axisymmetric and the contact problem can be treated like a tangential one. Rolling will then be accounted for only kinematically. The displacement in vertical direction is of the order of magnitude of the maximum indentation depth. The displacement in tangential direction is of the order of magnitude

$$\Delta u_{x,K} \sim \frac{v_{x0} + R\omega_0}{v_{z0}} d_{\max}. \quad (4)$$

Hence, this assumption will be covered by the half space hypothesis if the ratio of tangential and vertical initial velocity of the contact point is of the order of 1 or smaller.

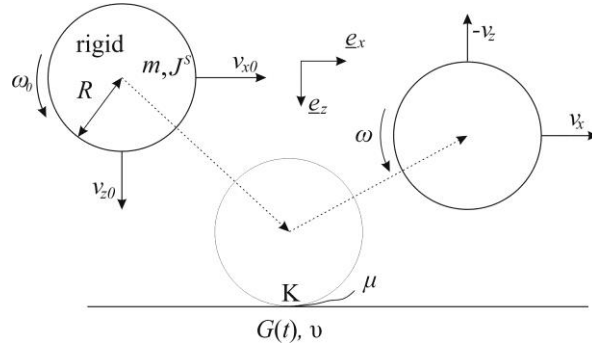


Fig. 1 Scheme of the analysed impact problem – a rigid sphere is impacting on a viscoelastic half-space

3. NUMERICAL MODEL BASED ON THE MDR

Under the assumptions made, the motion of point K fully determines the motion of the sphere. The normal and tangential displacements of this point shall be $u_{K,z}$ and $u_{K,x}$. The equations of motion for those displacements are elementary given by

$$\begin{aligned} \ddot{u}_{K,x} &= \frac{F_x}{m} \left(1 + \frac{mR^2}{J^s} \right), \\ \ddot{u}_{K,z} &= \frac{F_z}{m}, \end{aligned} \tag{5}$$

where F_x and F_z are the contact forces while the dots denote the time derivative. To determine these forces and thereby solve the axisymmetric problem described above within the framework of the MDR, two preliminary steps are necessary. First an equivalent plain profile $g(x)$ has to be obtained from axisymmetric indenter profile $f(r)$ via the Abel-like integral transform

$$g(x) = |x| \int_0^{|x|} \frac{df}{dr} \frac{dr}{\sqrt{x^2 - r^2}}. \tag{6}$$

A spherical indenter in the vicinity of the contact can be described by the parabolic profile

$$f(r) = \frac{r^2}{2R} \tag{7}$$

and the equivalent profile accordingly is given by the expression

$$g(x) = \frac{x^2}{R}. \tag{8}$$

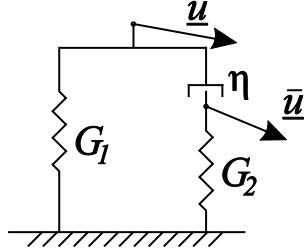


Fig. 2 Single element to model a standard solid

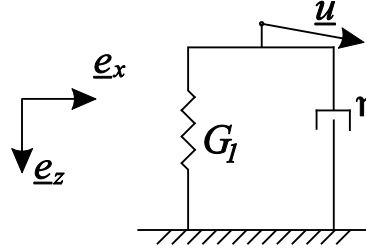


Fig. 3 Single element to model a Kelvin-Voigt solid

As the second step the viscoelastic properties of the half-space must be replaced by a one-dimensional foundation of independent, linear-viscoelastic elements. In case of a linear standard solid with the time-dependent shear modulus given in Eq. (1) those elements consist of a spring in series with a dashpot, the pair in parallel with a second spring (see Fig. 2). In case of a Kelvin-Voigt model (see Fig. 3) the spring in series with the dashpot is rigid. The elements are at a distance Δx of each other. This value is arbitrary if small enough. Let us first consider the standard solid and write down the necessary relations of the model and the numerical algorithm. All equations for the Kelvin-Voigt model can be derived afterwards by the limiting process.

The reaction force for a single element at position $x_i = i \Delta x$, with outer and inner displacement vectors \underline{u}_i and $\bar{\underline{u}}_i$ has the components

$$\begin{aligned} f_{i,x} &= \frac{4\Delta x}{2-\nu} \left[G_1 u_{i,x} + \eta (\dot{u}_{i,x} - \dot{\bar{u}}_{i,x}) \right], \\ f_{i,z} &= \frac{2\Delta x}{1-\nu} \left[G_1 u_{i,z} + \eta (\dot{u}_{i,z} - \dot{\bar{u}}_{i,z}) \right]. \end{aligned} \quad (9)$$

The inner point must fulfil the equilibrium conditions

$$\begin{aligned} G_2 \bar{u}_{i,x} + \eta (\dot{\bar{u}}_{i,x} - \dot{u}_{i,x}) &= 0, \\ G_2 \bar{u}_{i,z} + \eta (\dot{\bar{u}}_{i,z} - \dot{u}_{i,z}) &= 0. \end{aligned} \quad (10)$$

For the time integration we will use the least order explicit Euler integration scheme with constant time step Δt . The current time step number shall be denoted by an upper index j . In the beginning all displacements are set to zero. Then, in each time step, first the normal contact problem must be solved. For the elements in contact the normal displacement is enforced by the motion of K,

$$u_{i,z}^j = u_{i,z}^{j-1} + \dot{u}_{K,z}^j \Delta t, \quad \text{for contact.} \quad (11)$$

The elements not in contact are free of forces, i.e. the left side of Eqs. (9) is zero, and one obtains

$$u_{i,z}^j = \frac{\eta}{\eta + G_1(\tau + \Delta t)} (u_{i,z}^{j-1} - \bar{u}_{i,z}^{j-1}), \text{ for no contact,} \quad (12)$$

where we introduce relaxation time $\tau = \eta / G_2$. An element gets into contact if $u_{i,z}^j \leq u_{K,z}^j - g(x_i)$ and leaves contact if $f_{i,z}^j \leq 0$. To solve the tangential contact problem the tangential displacements must be calculated. The elements outside the contact area progress according to

$$u_{i,x}^j = \frac{\eta}{\eta + G_1(\tau + \Delta t)} (u_{i,x}^{j-1} - \bar{u}_{i,x}^{j-1}), \text{ for no contact.} \quad (13)$$

For the elements in contact one has to distinguish between sticking and slipping elements. For all the sticking elements, the displacement is enforced by the movement of K,

$$u_{i,x}^j = u_{i,x}^{j-1} + \dot{u}_{K,x}^j \Delta t, \text{ for sticking contact.} \quad (14)$$

An element in contact is able to stick if the resulting tangential force does not exceed the maximum value given by the Amontons-Coulomb law, i.e. if

$$|f_{i,x}^j| \leq \mu f_{i,z}^j, \text{ for sticking contact.} \quad (15)$$

Any element violating this condition will slip. In this case the tangential force is known to be

$$f_{i,x}^j = \mu f_{i,z}^j \text{sgn}(f_{i,x}^{j-1}), \text{ for slipping contact.} \quad (16)$$

After the total contact forces are calculated by summation over all elements,

$$\begin{aligned} F_x^j &= -\sum_i f_{i,x}^j, \\ F_z^j &= -\sum_i f_{i,z}^j \end{aligned} \quad (17)$$

the equations of motion (5) can be solved in each time step. Note that it is impossible that contact is re-established by the viscoelastic creep. For the Kelvin-Voigt model only τ and hence the inner displacements must be set to zero in the equations above.

The algorithm was implemented in MATLAB™. Only time steps j and $j-1$ have to be stored. That is why this algorithm requires only little memory space. Also all operations are elementary, which makes the algorithm very fast (this is also why we are able to use a least order explicit integration scheme without stability problems) and enables us to do comprehensive parameter studies on an ordinary desktop PC (the calculation of a single impact took around one or two seconds on a machine with an Intel i5 processor).

4. NUMERICAL INVESTIGATION USING BEM

The results acquired with the MDR have been validated using the Boundary Element Method (BEM). The BEM-solution of the described problem is numerically exact under the assumptions stated before: the half-space approximation, quasi-static conditions and elastic similarity between the contacting surfaces. Since the BEM does not rely on axis-symmetry, this assumption is only made to have results comparable with the MDR.

The application of the BEM consists of two steps. Firstly the problem of calculating the deflection field from a given pressure distribution and *vice versa* must be solved. This can be done by utilizing the fundamental solution for a point load acting on a viscoelastic half-space [37-39]. The material is assumed to be incompressible and components F_x , F_y , F_z of the point load are applied at time zero and are kept constant. The deflection of the surface can then be written as

$$\left. \begin{aligned} 4\pi u_x &= \frac{2}{r} \varphi_x + \left(\frac{x^2}{r^3} - \frac{1}{r} \right) \varphi_x + \frac{xy}{r^3} \varphi_y, & 4\pi u_z &= \frac{\varphi_z}{r}, \\ \varphi_i &= F_i J(t), & r &= \sqrt{x^2 + y^2} \end{aligned} \right\} \quad (18)$$

In difference to the MDR, the time-dependent creep function for shear $J(t)$ has been used. It is clear and known that $J(t)$ and $G(t)$ are not independent of each other. The creep function can be written by using the constants introduced in equation (1) in the following form:

$$J(t) = \frac{1}{G_1 + G_2} \left[1 + \frac{G_2}{G_1} \left(1 - \exp \left\{ -t \frac{G_1 G_2}{\eta(G_1 + G_2)} \right\} \right) \right]. \quad (19)$$

Since the geometric dependences in the viscoelastic and elastic cases are the same, the developed algorithm can be used with only small modifications. In elastic contact mechanics it is a standard procedure to integrate the fundamental solution over a rectangle, assuming constant pressure [40]. This analytic solution is used to find the deflection field for an arbitrary but piecewise constant pressure distribution [41]. This task can be performed very fast and efficiently by using convolution techniques on a parallel computing architecture [42-44]. The corresponding inverse problem, namely finding the pressure distribution to a given deflection field can be tackled by using the biconjugate gradient stabilized method [45].

The above described methods have been applied to the viscoelastic problem. Since the pressure distribution will change in time, a discretisation is necessary. If, for each time step, the pressure distribution is assumed to be constant, the overall solution in the deflection field can be obtained by adding two solutions in each time step: one to remove the prior load and one to add the current load. Based on the fact that the arising sum grows linearly in time, it is crucial to reduce the numerical effort. This can be achieved by applying the special form of the creep function (19) and by observing the following time step. Then an iterative algorithm can be developed:

$$\begin{aligned} u_{z,j} &= \frac{J_\infty}{J_0} f_n + \frac{1}{J_0 \eta} \underbrace{\sum_{i=0}^{j-1} (t_{i+1} - t_i)}_{a_j^z} f_i - \underbrace{\frac{J}{J_0} \sum_{i=0}^j (f_i - f_{i-1}) \exp \left(-\frac{t_j - t_i}{\lambda} \right)}_{b_j^z} \\ u_{z,j+1} &= \frac{J_\infty}{J_0} f_{j+1} + \underbrace{a_j^z}_{a_{j+1}^z} + \frac{\Delta t}{J_0 \eta} f_j - \underbrace{\exp \left(-\frac{\Delta t}{\lambda} \right) b_j^z}_{b_{j+1}^z} + (f_{j+1} - f_j) \frac{J}{J_0} \\ &= \underbrace{f_{j+1} + a_{j+1}^z - \exp \left(-\frac{h_j}{\lambda} \right) b_j^z}_{D^z} + f_j \frac{J}{J_0} \end{aligned} \quad (20)$$

Herein $u_{z,n}$ is the normal deflection of the surface, $J_\infty = J(t = \infty)$, $J_0 = J(t = 0)$, and f_j is the deflection due to a pressure distribution p_j – each at the time t_j . In the last line of Eq. (20)

it can be seen that an additional deformation D^z has to be taken into account to include viscoelastic behaviour (in the elastic case D^z is equal to zero). The unknown term in the last line of Eq. (20) is f_{j+1} , which means that the pressure distribution p_{j+1} is unknown. This can be calculated with the elastic algorithms mentioned before. It should be noted that this algorithm can handle only materials with a finite modulus of instant deformation, which excludes the Kelvin-Voigt solid.

The tangential contact can be solved very similarly to the normal contact so that the same scheme can be used [46]. Only the calculation of the deflection in tangential direction u_x , caused by shear stress has to be adopted. If a partial slip is involved, the calculation is modified in the following way: starting with a complete stick area, the deflection is given by the increment of displacement in one time step. If this leads to shear stress that is larger than the value allowed by the Coulomb's law, this part of the contact area will slip. In the slip areas the tangential stress is set to $|\tau| = \mu p$. Then the stress in the remaining stick area is calculated again, under the consideration of the deflection caused by the shear stress in the slip area. This is done until the stick area does not change anymore. In all performed simulations, the deformation perpendicular to the plane of the motion, u_y , is neglected. It turns out that this assumption, in the case of parabolic bodies, causes a negligible error [47]. At this point, the contact problem itself is solved. For the integration in time both an explicit Euler scheme and the velocity Verlet algorithm have been used. In comparison, they show no difference in the global error of the velocities at the end of the simulation and in the contact time itself. For an estimation of the step size Δt the MDR solution has been used. For the geometric discretization a matrix of 256×256 points has been chosen. The comparison with a finer discretization shows only a slight error reduction.

For implementation it has to be considered that the total deflection in normal direction within the contact area is known at every time step since the indentation depth of the sphere is known. Contrariwise in tangential direction: the points coming into contact have a pre-deformation through coupling to the points within the contact area from a previous time step. This can be handled by adding only the current increment of tangential movement at the boundary of the sphere in each time step.

The systematic investigation of the problem has been done with the MDR. The processing time for the BEM is much higher compared to the MDR. Therefore, only a few hundred parameter sets spreading over the full range covered by the investigation done with the MDR have been calculated with the BEM. It turns out that the relative differences in the coefficients of restitution have always been smaller than 0.5%. Therefore, it is reasonable that the MDR can be applied.

5. RESULTS OF THE NUMERICAL MODEL: THE RESTITUTION COEFFICIENTS

As a solution we are interested in the coefficients of restitution in normal and tangential direction

$$\begin{aligned} e_z &= -\frac{\dot{u}_{K,z}(t=t_e)}{\dot{u}_{K,z}(t=0)} = -\frac{v_z}{v_{z0}}, \\ e_x &= -\frac{\dot{u}_{K,x}(t=t_e)}{\dot{u}_{K,x}(t=0)} = -\frac{v_x + R\omega}{v_{x0} + R\omega_0}. \end{aligned} \quad (21)$$

Maw et al. [13] have shown that in an ideally elastic case (the coefficient in normal direction being obviously unity) the coefficient in tangential direction only depends on the two dimensionless parameters

$$\chi = \frac{1-\nu}{2-\nu} \left(1 + \frac{mR^2}{J^s} \right), \quad \psi = \frac{2-2\nu}{2-\nu} \frac{|v_{x0} + R\omega_0|}{\mu v_{z0}}. \quad (22)$$

In the case of a sphere impacting on a viscoelastic half space modelled as a linear standard solid, two more dimensionless parameters are of interest, describing the viscoelastic material properties, namely

$$\delta_1 = \eta \sqrt{\frac{a_{el,1}}{G_1 M (1-\nu)}}, \quad \gamma = \frac{G_1}{G_2}, \quad (23)$$

with the maximum contact radius for the impact with an elastic half space,

$$a_{el,i} = \left(\frac{15m v_{z0}^2 R^2 (1-\nu)}{32G_i} \right)^{1/5}, \quad i = 1, 2 \quad (24)$$

Of course, any combinations of those two additional parameters would also be possible to choose as governing variables. For example, in the previous publication on the no-slip impact Kusche [35] used the parameters

$$\delta_1 = \eta \sqrt{\frac{a_{el,1}}{G_1 M (1-\nu)}}, \quad \delta_2 = \eta \sqrt{\frac{a_{el,2}}{G_2 M (1-\nu)}} = \delta_1 \gamma^{3/5} \quad (25)$$

to capture the influence of the material behaviour. However, as we are interested mainly in the velocity-dependence of the coefficients of restitution, it seems convenient to select δ_1 and γ , because the latter one is velocity-independent and therefore the velocity-dependence due to viscoelasticity can be fully covered by parameter δ_1 . Moreover, the Kelvin-Voigt model can be recovered as the limiting case $\gamma = 0$. Also limit $\gamma \rightarrow \infty$ corresponds to the elastic result. To reduce the number of governing parameters, we restrict ourselves mostly to $\chi = 7/6$, which, amongst other cases, corresponds to the case of incompressible, homogenous spheres. To prove that actually

$$e_z = e_z(\delta_1, \gamma) \quad \text{and} \quad e_x = e_x(\chi, \psi, \delta_1, \gamma) \quad (26)$$

we made comprehensive numerical studies, the results of which are shown in the upcoming figures. Thereby we first focus on the limiting case of a Kelvin-Voigt solid and afterwards look at the more general standard solid.

In Fig. 4 the coefficient of restitution in normal direction is shown for a Kelvin-Voigt solid as a function of δ_1 . All free input parameters for the simulations, i.e. velocities, measures of inertia and so on, have been generated randomly. Nevertheless, the points create continuous curves and hence our hypothesis is proven for the normal direction. It is easy to interpret the results, as the coefficient of normal restitution shows the often-used quasi-exponentially decreasing behaviour. This, however, only remains true for this material model of a Kelvin-Voigt solid, which corresponds to an infinitely fast relaxation within

the elastomer. It was already pointed out that this is problematic as the impact times are considered to be small and the relaxation time has to be accounted for in some way. We will see the effects later in the results for the standard solid.

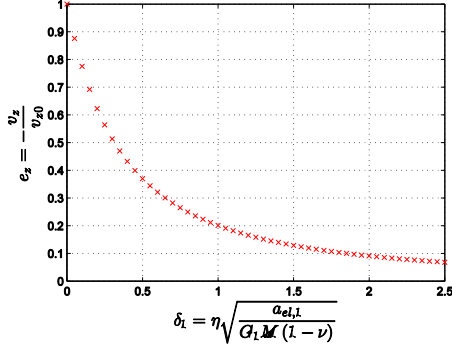


Fig. 4 Coefficient of restitution in normal direction for the impact on a Kelvin-Voigt solid as a function of δ_1

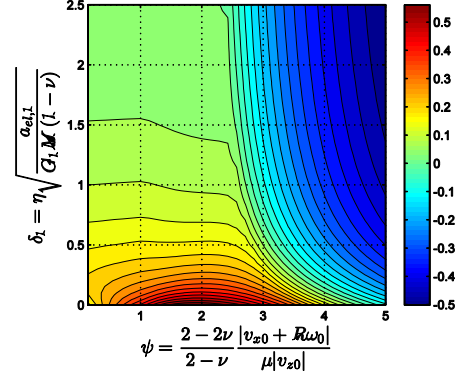


Fig. 5 Coefficient of restitution in tangential direction as a function of δ_1 and ψ with $\chi = 7/6$. Online version in colour

Fig. 5 gives the tangential coefficient of restitution e_x as a function of δ_1 and ψ for the impact on a Kelvin-Voigt half-space. The value of χ was fixed at $7/6$, all other input parameters for the impact problem have been generated randomly and yet the solutions create continuous, smooth curves. The tangential restitution has a global maximum for an impact without viscosity around $\psi = 2$. On the right side of the contour plot the behaviour gets quite simple and can be explained the following way: for any material model configurations are possible for which the contact will completely slip during the whole impact. In this case the total tangential force is known due to the Coulomb's law and hence the tangential restitution coefficient for full slip (and any material model) is given by the relation

$$e_x^{fs} = (1 + e_z) \frac{2\chi}{\psi} - 1. \quad (27)$$

Let us now look into the results for the standard solid. We restrict ourselves again to the case $\chi = 7/6$ to spare the generally least important parameter.

Fig. 6 gives the results for the normal restitution coefficient as a function of δ_1 . Several logarithmically-equally-distributed values for γ have been chosen and all other input parameters for the impact problem, as always, have been generated randomly. Nevertheless, the solutions create continuous curves and it is easy to observe the influence of γ on the velocity-dependent restitution: as said before $\gamma \rightarrow \infty$ corresponds to the trivial elastic case and $\gamma = 0$ to the monotonically decreasing Kelvin-Voigt solution. For intermediate values of γ the coefficient of restitution has a global minimum. After that it increases again with increasing δ_1 , i.e. increasing normal inbound velocities. This distinguishes the general standard solid from its limiting case with infinitely fast relaxation and has, for example, a very interesting consequence for a (driven) granular gas of viscoelastic particles: as on the increasing part of the restitution curve, the coefficient

of restitution is larger for *larger* inbound velocities, a region of locally higher internal energy of the granular gas, i.e. higher velocities of the particles, might dissipate less energy than regions of lower energy, which might result in unstable states of the granular gas.

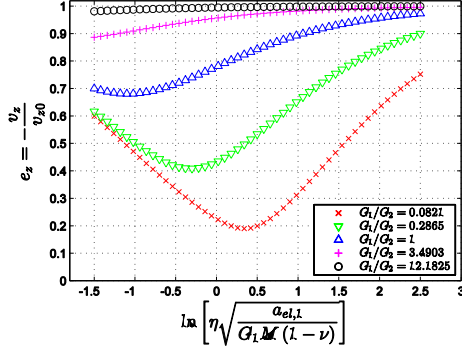


Fig. 6 Coefficient of restitution in normal direction as a function of δ_1 (logarithmic) and different values of γ for the impact with a standard solid

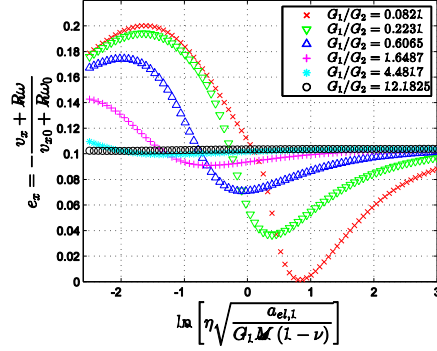


Fig. 7 Coefficient of restitution in tangential direction without slip ($\psi = 0$) as a function of δ_1 (logarithmic) and different values of γ for the impact with a standard solid; $\chi = 7/6$

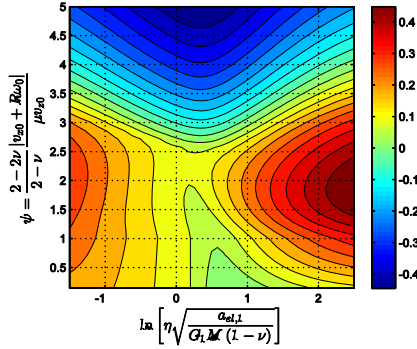


Fig. 8 Coefficient of restitution in tangential direction as a function of δ_1 (logarithmic) and ψ for the impact with a standard solid; $\chi = 7/6$ and $\gamma = 0.0825$

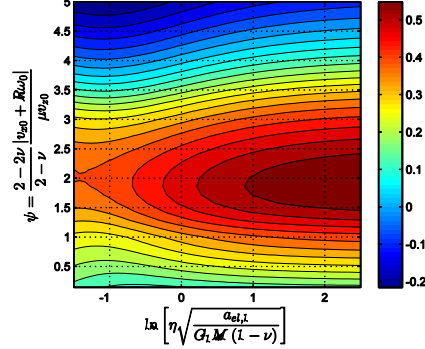


Fig. 9 Coefficient of restitution in tangential direction as a function of δ_1 (logarithmic) and ψ for the impact with a standard solid; $\chi = 7/6$ and $\gamma = 1$

Fig. 7 presents the results for the tangential restitution in the case of no slip, which have been reported by Kusche [35] with a slightly different set of governing dimensionless parameters. In Fig. 8 and 9 the results are shown for the behaviour with slip. For increasing values of γ a bulb with $e_x \approx 0.5$ around $\psi \approx 2$ is stretching to the left, i.e. the area with less viscosity. The other areas are less affected by the material properties.

Finally, we come back to the full slip solution and the different regimes for parameter ψ .

In the elastic case Maw et al. [13] distinguish three different regimes: for $\psi < 1$ the impact will start in a completely sticking contact and remain like this during the whole compression phase; for $\psi > 4\chi - 1$ the contact will fully slip during the whole impact; the intermediate values correspond to a mixed regime. Now, in the viscoelastic case, the time derivatives of the contact forces in the MDR-model in the very first moment of contact are given by

$$\begin{aligned}\dot{F}_z(t=0) &= \frac{2\Delta x}{1-\nu} G(t=0) \dot{u}_{K,z}(t=0) \\ \dot{F}_x(t=0) &= \frac{4\Delta x}{2-\nu} G(t=0) \dot{u}_{K,x}(t=0)\end{aligned}\quad (28)$$

Hence, for a finite instantaneous stiffness (this excludes the Kelvin-Voigt body), the impact will begin with sticking contact, if

$$|\dot{F}_x(t=0)| \leq \mu \dot{F}_z(t=0) \quad \Leftrightarrow \psi \leq 1. \quad (29)$$

In case of the Kelvin-Voigt body the contact forces in the first moment of contact are nonzero and the no-slip condition will be

$$|F_x(t=0)| \leq \mu F_z(t=0) \quad \Leftrightarrow \psi \leq 1. \quad (30)$$

Hence, this lower transition value for ψ is unaffected by viscoelasticity.

For any standard solid characterised by the two parameters δ_1 and γ – and probably any material behaviour – there also exists a value ψ_c , for which the contact will completely slip during the whole impact if $\psi > \psi_c$. For complete slip the tangential coefficient of restitution is given by Eq. (27).

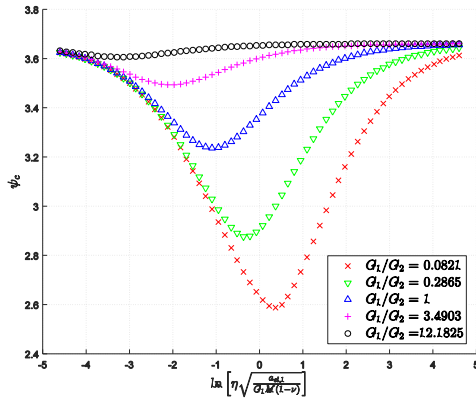


Fig. 10 Critical value ψ_c , for which the contact will completely slip during the whole impact if $\psi > \psi_c$ for the impact with a standard solid

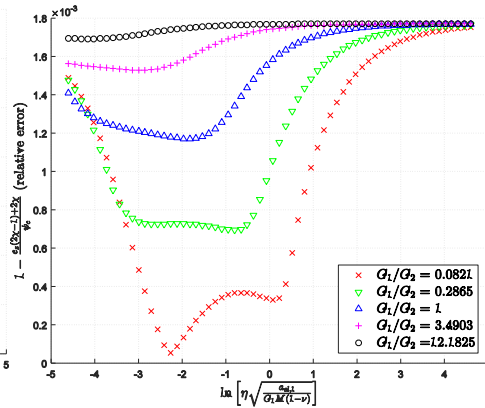


Fig. 11 Relative error between the numerical result for ψ_c and the analytic approximation (31)

In Fig. 10 the value of ψ_c is shown for different materials. Obviously this transition value strongly correlates with the normal restitution coefficient. The global maximum is elastic case

$\psi_c = 11/3$, and a very good approximation (with a relative error always smaller than 0.2%, see Fig. 11) is given by the expression

$$\psi_c \approx -e_z + 2\chi(1 + e_z). \quad (31)$$

6. CONCLUSIONS

Based on the numerical models we investigated the oblique impact of linear-viscoelastic spheres under the assumptions of quasi-stationarity, the validity of the half-space hypothesis, Amontons-Coulomb friction and short impact times. Numerical models based on both the Method of Dimensionality Reduction (MDR) and the Boundary Element Method (BEM) have been implemented. As expected both methods in their results only differ within the margin of a numerical error. Due to the enormous reduction of mathematical and computational effort achieved by the MDR we were able to perform comprehensive parameter studies for the examined impact problem. It is found that the problem solution, i.e. the coefficients of normal and tangential restitution, written in proper dimensionless variables will depend on exactly four different values, at least two of which contain explicit dependencies on the inbound velocities. By accounting for the finite relaxation time within the elastomer it is possible to increase the normal restitution coefficient with increasing inbound velocities. This is in contrast with most viscoelastic collision models used in the literature about granular media and may have interesting applications in granular chains or gases.

As in the elastic case, three different regimes are possible depending on the inbound velocities: the contact may fully slip during the whole impact, completely stick during the compression phase or be in a mixed regime. Viscoelasticity reduces the angle of incidence necessary to ensure complete slip but does not affect the transition between the two other regimes. The transition to full slip strongly correlates with the coefficient of normal restitution.

Of course, in practice the here-given assumptions pose severe restrictions, especially the half-space hypothesis, the assumed short impact time and the assumption of perfectly linear material behaviour. Nevertheless, the proposed model and its solution to the best our knowledge are the first – from a contact-mechanical point of view – rigorous and self-consistent approach to the topic despite the extensive existing literature dealing with it.

The proposed methods can without problems be applied to more general forms of the time-dependent shear modulus, for example represented in a Prony series.

REFERENCES

1. Lun, C.K.K., Savage, S.B., 1986, *The Effects of an Impact Velocity Dependent Coefficient of Restitution on Stresses Developed by Sheared Granular Materials*, Acta Mechanica, 63(1), pp. 15–44.
2. Walton, O.R., Braun, R.L., 1986, *Stress Calculations for Assemblies of Inelastic Spheres in Uniform Shear*, Acta Mechanica, 63(1), pp. 73–86.
3. Brilliantov, N.V., Spahn, F., Hertzsch, J.M., Pöschel, T., 1996, *Model for Collisions in Granular Gases*, Physical Review E, 53(5), pp. 5382–5392.
4. Schwager, T., Pöschel, T., 1998, *Coefficient of Normal Restitution of Viscous Particles and Cooling Rate of Granular Gases*, Physical Review E, 57(1), pp. 650–654.
5. Brilliantov, N.V., Pöschel, T., 2000, *Velocity Distribution in Granular Gases of Viscoelastic Particles*, Physical Review E, 61(5B), pp. 5573–5587.

6. Dubey, A.K., Brodova, A., Puri, S., Brilliantov, N.V., 2013, *Velocity Distribution Function and Effective Restitution Coefficient for a Granular Gas of Viscoelastic Particles*, Physical Review E, 87, 062202.
7. Hertz, H., 1882, *Über die Berührung fester elastischer Körper*, Journal für die reine und angewandte Mathematik, 92, pp. 156–171.
8. Hunter, S.C., 1957, *Energy Absorbed by Elastic Waves during Impact*, Journal of the Mechanics and Physics of Solids, 5(3), pp. 162–171.
9. Cattaneo, C., 1938, *Sul Contato di Due Corpo Elastici*, Accademia dei Lincei, Rendiconti, Series 6, 27, pp. 342–348, 434–436 and 474–478.
10. Mindlin, R.D., 1949, *Compliance of Elastic Bodies in Contact*, Journal of Applied Mechanics, 16, pp. 259–268.
11. Mindlin, R.D., Deresiewicz, H., 1953, *Elastic Spheres in Contact under Varying Oblique Forces*, Journal of Applied Mechanics, 20, pp. 327–344.
12. Jäger, J., 1993, *Elastic contact of Equal Spheres under Oblique Forces*, Archive of Applied Mechanics, 63(6), pp. 402–412.
13. Maw, N., Barber, J.R., Fawcett, J.N., 1976, *The Oblique Impact of Elastic Spheres*, Wear, 38(1), pp. 101–114.
14. Barber, J.R., 1979, *Adhesive Contact during the Oblique Impact of Elastic Spheres*, Journal of Applied Mathematics and Physics (ZAMP), 30, pp. 468–476.
15. Thornton, C., Yin, K.K., 1991, *Impact of Elastic Spheres with and without Adhesion*, Powder Technology, 65(1–3), pp. 153–166.
16. Jäger, J., 1994, *Analytical Solutions of Contact Impact Problems*, Applied Mechanics Review, 47(2), pp. 35–54.
17. Popov, V.L., Heß, M., 2014, *Method of Dimensionality Reduction in Contact Mechanics and Friction: A Users Handbook. I. Axially Symmetric Contacts*, Facta Universitatis, Series Mechanical Engineering, 12(1), pp. 1–14.
18. Popov, V.L., Pohrt, R., Heß, M., 2016, *General Procedure for Solution of Contact Problems under Dynamic Normal and Tangential Loading Based on the Known Solution of Normal Contact Problem*, Journal of Strain Analysis for Engineering Design, 51(4), pp. 247–255.
19. Popov, V.L., Heß, M., 2015, *Method of Dimensionality Reduction in Contact Mechanics and Friction*, Springer, Heidelberg, ISBN 978-3-642-53875-9.
20. Lyashenko, I.A., Popov, V.L., 2015, *Impact of an Elastic Sphere with an Elastic Half Space Revisited: Numerical Analysis based on the Method of Dimensionality Reduction*, Scientific Reports, 5, 8479.
21. Willert, E., Popov, V.L., 2016, *Impact of an Elastic Sphere with an Elastic Half Space with a Constant Coefficient of Friction: Numerical Analysis Based on the Method of Dimensionality Reduction*, ZAMM Zeitschrift für Angewandte Mathematik und Mechanik, 96(9), pp. 1089–1095.
22. Lee, E.H., 1955, *Stress Analysis in Visco-Elastic Bodies*, Quarterly Applied Mathematics, 13(2), pp. 183–190.
23. Radok, J.R.M., 1957, *Visco-Elastic Stress Analysis*, Quarterly Applied Mathematics, 15(2), pp. 198–202.
24. Lee, E.H., Radok, J.R.M., 1960, *The Contact Problem for Viscoelastic Bodies*, Journal of Applied Mechanics, 27(3), pp. 438–444.
25. Graham, G.A.C., 1965, *The Contact Problem in the Linear Theory of Viscoelasticity*, International Journal of Engineering Science, 3(1), pp. 27–46.
26. Graham, G.A.C., 1967, *The Contact Problem in the Linear Theory of Viscoelasticity When the Time-Dependent Contact Area Has any Number of Maxima and Minima*, International Journal of Engineering Science, 5(6), pp. 495–514.
27. Ting, T.C.T., 1966, *The Contact Stresses between a Rigid Indenter and a Viscoelastic Half Space*, Journal of Applied Mechanics, 33(4), pp. 845–854.
28. Ting, T.C.T., 1968, *Contact Problems in the Linear Theory of Viscoelasticity*, Journal of Applied Mechanics, 35(2), pp. 248–254.
29. Greenwood, J.A., 2010, *Contact between an Axisymmetric Indenter and a Viscoelastic Half Space*, International Journal of Mechanical Sciences, 52(6), pp. 829–835.
30. Pao, Y.H., 1955, *Extension of the Hertz Theory of Impact to the Viscoelastic Case*, Journal of Applied Physics, 26(9), pp. 1083–1088.
31. Hunter, S.C., 1960, *The Hertz Problem for a Rigid Spherical Indenter and a Viscoelastic Half Space*, Journal of the Mechanics and Physics of Solids, 8(4), pp. 219–234.
32. Argatov, I.I., 2013, *Mathematical Modeling of Linear Viscoelastic Impact: Application to Drop Impact Testing of Articular Cartilage*, Tribology International, 63, pp. 213–225.
33. Kürschner, S., Filippov, A.E., 2012, *Normal Contact between a Rigid Surface and a Viscous Body: Verification of the Method of Reduction of Dimensionality for Viscous Media*, Physical Mesomechanics, 15(4), pp. 25–30.
34. Argatov, I.I., Popov, V.L., 2015, *Rebound Indentation Problem for a Viscoelastic Half-Space and Axisymmetric Indenter – Solution by the Method of Dimensionality Reduction*, ZAMM Zeitschrift für Angewandte Mathematik und Mechanik, 96(8), pp. 956–967.

35. Kusche, S., 2016, *The Boundary Element Method for Visco-elastic Material Applied to the Oblique Impact of Spheres*, Facta Universitatis, Series Mechanical Engineering, 14(3), pp. 293–300.
36. Kusche, S., 2016, *Simulation von Kontaktproblemen bei linearem viskoelastischem Materialverhalten*, Doctoral Dissertation, Technische Universität Berlin
37. Talybly, L., 2010, *Boussinesq's viscoelastic problem on normal concentrated force on a half-space surface*, Mechanics of Time-Dependent Materials, 14(3), pp. 253–259.
38. Gasanova, L., Gasanova, P., Talybly, L., 2011, *Solution of a viscoelastic boundary-value problem on the action of a concentrated force in an infinite plane*, Mechanics of Solids, 46(5), pp. 772–778.
39. Peng, Y., Zhou, D., 2012, *Stress Distributions Due to a Concentrated Force on Viscoelastic Half-Space*, Journal of Computation & Modeling, 2(4), pp. 51–74.
40. Johnson, K. L., 1985, *Contact Mechanics*, Cambridge University Press, Cambridge.
41. Pohrt, R., Li, Q., 2014, *Complete Boundary Element Formulation for Normal and Tangential Contact Problems*, Physical Mesomechanics, 17(4), pp. 334–340.
42. Cho, Y. J., Koo, Y. P., Kim, T. W., 2000, *A new FFT technique for the analysis of contact pressure and subsurface stress in a semi-infinite solid*, KSME International Journal, 14(3), pp. 331–337.
43. Liu, S., Wang, Q., Liu, G., 2000, *A versatile method of discrete convolution and FFT DC-FFT for contact analyses*, Wear, 243(1-2), pp. 101–111.
44. Wang, W.Z., Wang, H., Liu, Y.C., Hu, Y.Z., Zhu, D., 2003, *A comparative study of the methods for calculation of surface elastic deformation*, Proceedings of the Institution of Mechanical Engineers, Part J: Journal of Engineering Tribology, 217, pp. 145–154.
45. van der Vorst, H.A., 1992, *BI-CGSTAB: A Fast and Smoothly Converging Variant of BI-CG for the Solution of Nonsymmetric Linear Systems*, SIAM Journal of Scientific and Statistical Computing, 13(2), pp. 631–644.
46. Kusche, S., 2016, *Frictional force between a rotationally symmetric indenter and a viscoelastic half-space*, ZAMM Zeitschrift für Angewandte Mathematik und Mechanik, DOI: 10.1002/zamm.201500169.
47. Munisamy, R.L., Hills, D.A., Nowell, D., 1994, *Static axisymmetric Hertzian contacts subject to shearing forces*, Journal of Applied Mechanics, 61(2), pp. 278–283.

DUGDALE-MAUGIS ADHESIVE NORMAL CONTACT OF AXISYMMETRIC POWER-LAW GRADED ELASTIC BODIES

UDC 539.3

Emanuel Willert

Berlin University of Technology, Berlin, Germany

Abstract. *A closed-form general analytic solution is presented for the adhesive normal contact of convex axisymmetric power-law graded elastic bodies using a Dugdale-Maugis model for the adhesive stress. The case of spherical contacting bodies is studied in detail. The known JKR- and DMT-limits can be derived from the general solution, whereas the transition between both can be captured introducing a generalized Tabor parameter depending on the material grading. The influence of the Tabor parameter and the material grading is studied.*

Key Words: *Adhesive Contact, Power-Law Elastic Grading, Dugdale-Maugis Model, Axial Symmetry, Method of Dimensionality Reduction*

1. INTRODUCTION

Propelled by the technological demand for versatile high-performance materials and the study of biological materials and contact solutions, living nature developed in several circumstances, Functionally Graded Materials (FGM), i.e. media with continuously inhomogeneous mechanical properties, have encountered a lot of scientific interest and research in the past years. The use of FGM is proven to be possibly beneficial in physical [1] and biological [2] applications. Whereas rigorous solutions for non-adhesive contact problems of FGM, at least for some special forms of inhomogeneity, have been available for quite a long time [3-5], the adhesive contact of FGM is still in the focus of current research [6-9]. These latter studies, nonetheless, only concern the limiting case of a negligible range of the adhesive interaction, established by Johnson, Kendall and Roberts (JKR, [10]) in 1971. After Derjaguin, Muller and Toporov (DMT, [11]) a few years later presented a different theory of long-range adhesive interactions giving a different result

Received November 21, 2017 / Accepted January 11, 2018

Corresponding author: Emanuel Willert

Technische Universität Berlin, Sekr. C8-4, Straße des 17. Juni 135, D-10623 Berlin

E-mail: e.willert@tu-berlin.de

© 2018 by University of Niš, Serbia | Creative Commons Licence: CC BY-NC-ND

for the critical pull-off force in a parabolic contact, a discussion started, which was only finally resolved by Maugis [12], who – based on a model of the adhesive stress first introduced by Dugdale [13] – was able to show the transition between what was proven by Tabor [14] to be correct descriptions of limiting cases. The present paper generalizes Maugis’ solution for the adhesive contact of homogeneous spheres to arbitrary axisymmetric bodies with elastic-grading in form of a power-law. As the contact problem of interest can be ascribed to the frictionless, non-adhesive normal contact of power-law graded elastic materials a solution procedure based on the Method of Dimensionality Reduction (MDR) can be applied.

2. GENERAL AXISYMMETRIC SOLUTION

We consider elastic grading of the Young modulus E with depth z in form of a power-law:

$$E(z) = E_0 \left(\frac{z}{z_0} \right)^k, \quad -1 < k < 1. \quad (1)$$

Thereby constants E_0 and z_0 as well as Poisson ratio ν may be different for the contacting bodies. Exponent k , however, needs to be the same for both of them. As the exponent may take positive or negative values, both soft surfaces with a hard core and hard surfaces with a soft core can be studied.

It has been shown that the frictionless normal contact of axisymmetric power-law graded elastic bodies can be exactly mapped onto a plain contact of a rigid profile g with a one-dimensional foundation of independent linear springs, each in distant Δx from each other [15,16]. Thereby the equivalent plain profile $g = g(x)$ within this mapping procedure called Method of Dimensionality Reduction (MDR) can be calculated from the axisymmetric gap $f = f(r)$ between the non-deformed three-dimensional bodies by the integral transform:

$$g(x) = |x|^{1-k} \int_0^{|x|} \frac{f'(r)}{\sqrt{(x^2 - r^2)^{1-k}}} dr. \quad (2)$$

Stiffness Δk_z of a single spring at position x is given by the expression:

$$\Delta k_z(x) = c_N \left(\frac{|x|}{z_0} \right)^k \Delta x, \quad (3)$$

with:

$$c_N := \left(\frac{1 - \nu_1^2}{H(k, \nu_1) E_{01}} + \frac{1 - \nu_2^2}{H(k, \nu_2) E_{02}} \right)^{-1}. \quad (4)$$

Dimensionless auxiliary function H can be determined from exponent k and Poisson’s ratio according to:

$$H(k, \nu) := \frac{2(1+k) \cos(k\pi/2) \Gamma(1+k/2)}{\sqrt{\pi} C(k, \nu) \beta(k, \nu) \sin[\beta(k, \nu)\pi/2] \Gamma[(1+k)/2]}, \quad (5)$$

with:

$$C(k, \nu) := \frac{2^{1+k} \Gamma[(3+k+\beta(k, \nu))/2] \Gamma[(3+k-\beta(k, \nu))/2]}{\pi \Gamma(2+k)} \quad (6)$$

and

$$\beta(k, \nu) := \sqrt{(1+k) \left(1 - \frac{k\nu}{1-\nu}\right)} \quad (7)$$

and Gamma function Γ .

Note that the spatial distribution of the spring stiffness in Eq. (3) obeys the same power-law as the elastic grading. If equivalent profile g is pressed into the foundation of springs by an indentation depth d the vertical spring displacement $w_{1D}(x)$ in the area of direct contact is elementarily given by:

$$w_{1D}(x) = d - g(x), \quad |x| \leq a, \quad (8)$$

with contact radius a . Normal force F_N as well as the local distributions of pressure p and relative displacement w in the original three-dimensional system can be calculated from $w_{1D}(x)$ according to:

$$\begin{aligned} F_N &= \frac{c_N}{z_0^k} \int_{-\infty}^{\infty} w_{1D}(x) |x|^k dx, \\ p^*(r) &= -\frac{c_N}{\pi z_0^k} \int_r^{\infty} \frac{w'_{1D}(x) dx}{\sqrt{(x^2 - r^2)^{1-k}}}, \\ w(r) &= \frac{2 \cos(k\pi/2)}{\pi} \int_0^r \frac{x^k w_{1D}(x) dx}{\sqrt{(r^2 - x^2)^{1+k}}}. \end{aligned} \quad (9)$$

The second of these latter Eqs. (9) can be inverted to give:

$$w_{1D}(x) = \frac{2 z_0^k \cos(k\pi/2)}{c_N} \int_x^{\infty} \frac{rp(r) dr}{\sqrt{(r^2 - x^2)^{1+k}}}. \quad (10)$$

If we now assume a Dugdale model of a constant adhesive stress σ_0 within the adhesive zone with radius b :

$$p_{\text{adh}}(r) = -\sigma_0, \quad r \leq b, \quad (11)$$

the corresponding displacements in the MDR model are due to Eq. (10) given by:

$$w_{1D, \text{adh}}(x) = -\frac{2 z_0^k \cos(k\pi/2) \sigma_0}{c_N (1-k)} \sqrt{(b^2 - x^2)^{1-k}}, \quad |x| \leq b. \quad (12)$$

Hence, the one-dimensional displacements in the Dugdale-Maugis adhesive contact are:

$$w_{1D}(x) = \begin{cases} d - g(x), & |x| \leq a, \\ -\frac{2z_0^k \cos(k\pi/2)\sigma_0}{c_N(1-k)} \sqrt{(b^2 - x^2)^{1-k}}, & a < |x| \leq b. \end{cases} \quad (13)$$

For the three-dimensional stresses to be finite at the edge of direct contact these displacements must be continuous at $x = a$, which results in:

$$d = g(a) - \frac{2z_0^k \cos(k\pi/2)\sigma_0}{c_N(1-k)} \sqrt{(b^2 - a^2)^{1-k}}. \quad (14)$$

The total external normal force is due to the first of Eqs. (9) given by:

$$F_N = \frac{2c_N}{z_0^k} \int_0^a [d - g(x)] x^k dx - F_{adh}, \quad (15)$$

$$F_{adh} := \sigma_0 b^2 \left[\pi - \frac{4 \cos(k\pi/2)}{1-k^2} \left(\frac{a}{b}\right)^{1+k} {}_2F_1\left(\frac{k-1}{2}, \frac{1+k}{2}; \frac{3+k}{2}; \frac{a^2}{b^2}\right) \right],$$

with the hypergeometric function:

$${}_2F_1(a, b; c; z) := \sum_{n=0}^{\infty} \frac{(a)_n (b)_n}{(c)_n} \frac{z^n}{n!}, \quad |z| < 1, \quad (16)$$

$$(x)_n := \frac{\Gamma(x+n)}{\Gamma(x)}.$$

Radius b of the adhesive zone is not known *a priori* but can be determined from the condition that the gap between the deformed surfaces at $r = b$ has to equal the range h of the adhesive stresses. As the gap between the deformed surfaces can be easily calculated from three-dimensional relative displacement w , indentation depth d and axisymmetric non-deformed gap f , we obtain the additional relation

$$h = w(r=b) - d + f(r=b). \quad (17)$$

to close the equation system. Evaluating Eq. (17) with the help of the third of Eqs. (9) and using the identity:

$$\frac{2 \cos(k\pi/2)}{\pi} \int_0^b \frac{x^k [d - g(x)] dx}{\sqrt{(b^2 - x^2)^{1+k}}} = d - f(b) \quad (18)$$

one obtains:

$$h = -\frac{2 \cos(k\pi/2)}{\pi} \int_a^b \frac{x^k [d - g(x)] dx}{\sqrt{(b^2 - x^2)^{1+k}}} - \frac{4}{\pi} \frac{\cos^2\left(\frac{k\pi}{2}\right)}{1-k^2} \frac{\sigma_0 z_0^k b^{1-k}}{c_N} \left[\frac{\Gamma(1-k)\Gamma\left(\frac{3+k}{2}\right)}{\Gamma\left(\frac{3-k}{2}\right)} - \left(\frac{a}{b}\right)^{1+k} {}_2F_1\left(k, \frac{1+k}{2}; \frac{3+k}{2}; \frac{a^2}{b^2}\right) \right]. \quad (19)$$

Equations (14), (15) and (19) completely solve the given contact problem. In the homogeneous case $k = 0$ they are reduced to the axisymmetric generalization of Maugis' results given very recently by Popov et al. [17]. The stresses in the area of direct contact could theoretically be calculated inserting Eq. (13) into the second of Eqs. (9).

3. THE JKR LIMIT

It is of course possible to retrieve the known solution in the JKR limit of adhesion from the relations derived in the previous section. For this purpose we study the limit of negligible adhesion range $h \rightarrow 0$, whereas the surface energy per unit area, $\Delta\gamma = \sigma_0 h$, is kept constant. In this case the radius of the adhesive zone can be written in the form:

$$b = a(1 + \varepsilon), \quad (20)$$

with a small parameter ε . Using the linearization:

$$g(a + \Delta x) \approx g(a) + g'(a)\Delta x, \quad (21)$$

performing the integration and neglecting all terms of higher than first order in ε leads to:

$$\begin{aligned} d &\approx g(a) - \frac{2 \cos(k\pi/2) \sigma_0 z_0^k a^{1-k}}{1-k} \frac{1}{c_N} \sqrt{(2\varepsilon)^{1-k}}, \\ h &\approx -\frac{2}{\pi} \cos\left(\frac{k\pi}{2}\right) \left[\frac{d - g(a)}{1-k} \sqrt{(2\varepsilon)^{1-k}} \right] - \frac{2 \cos^2(k\pi/2) \sigma_0 z_0^k a^{1-k}}{\pi (1-k)^2} \frac{1}{c_N} (2\varepsilon)^{1-k}. \end{aligned} \quad (22)$$

Hence,

$$h = \frac{\Delta\gamma}{\sigma_0} \approx \frac{2 \cos^2(k\pi/2) \sigma_0 z_0^k a^{1-k}}{\pi (1-k)^2} \frac{1}{c_N} (2\varepsilon)^{1-k} \quad (23)$$

and therefore:

$$d \approx g(a) - \sqrt{\frac{2\pi\Delta\gamma z_0^k}{c_N} a^{1-k}}, \quad (24)$$

which perfectly coincides with the known solution in the JKR limit [8]. The normal force *via* the same mechanism is also reduced to the known relation:

$$F_N \approx \frac{2c_N}{z_0^k} \int_0^a [d - g(x)] x^k dx. \quad (25)$$

Note that Eq. (23) is actually independent of the profiles of the contacting bodies.

4. PARABOLIC CONTACT

Let us now consider the specific case of parabolic contact with the radius of curvature R , i.e.:

$$f(r) = \frac{r^2}{2R}. \quad (26)$$

The equivalent profile is accordingly:

$$g(x) = \frac{x^2}{R(1+k)}. \quad (27)$$

Thus, evaluating the general solution derived above, the solution of the Dugdale-Maugis adhesive normal contact problem in case of power-law elastic grading is given by:

$$\begin{aligned} d &= \frac{a^2}{R(1+k)} - \frac{2z_0^k \cos(k\pi/2)\sigma_0}{c_N(1-k)} \sqrt{(b^2 - a^2)^{1-k}}, \\ F_N &= \frac{4c_N}{Rz_0^k} \frac{a^{3+k}}{(1+k)^2(3+k)} - \sigma_0 b^2 \left[\pi + \frac{4\cos(k\pi/2)}{1-k^2} \left(\frac{a}{b}\right)^{1+k} \right. \\ &\quad \left. \cdot \left\{ \sqrt{\left(1 - \frac{a^2}{b^2}\right)^{1-k}} - {}_2F_1\left(\frac{k-1}{2}, \frac{1+k}{2}; \frac{3+k}{2}; \frac{a^2}{b^2}\right) \right\} \right]. \end{aligned} \quad (28)$$

Radius b of the adhesive zone can be determined from the condition:

$$\begin{aligned} h &= d \left[\frac{2}{\pi} \frac{\cos(k\pi/2)}{1+k} \left(\frac{a}{b}\right)^{1+k} {}_2F_1\left(\frac{1+k}{2}, \frac{1+k}{2}; \frac{3+k}{2}; \frac{a^2}{b^2}\right) - 1 \right] - \\ &\quad - \frac{b^2}{2R} \left[\frac{4}{\pi} \frac{\cos(k\pi/2)}{(1+k)(3+k)} \left(\frac{a}{b}\right)^{3+k} {}_2F_1\left(\frac{1+k}{2}, \frac{3+k}{2}; \frac{5+k}{2}; \frac{a^2}{b^2}\right) - 1 \right] - \\ &\quad - \frac{4}{\pi} \frac{\cos^2\left(\frac{k\pi}{2}\right)}{1-k^2} \frac{\sigma_0 z_0^k b^{1-k}}{c_N} \left[\frac{\Gamma(1-k)\Gamma\left(\frac{3+k}{2}\right)}{\Gamma\left(\frac{3-k}{2}\right)} - \left(\frac{a}{b}\right)^{1+k} {}_2F_1\left(k, \frac{1+k}{2}; \frac{3+k}{2}; \frac{a^2}{b^2}\right) \right]. \end{aligned} \quad (29)$$

Introducing the normalized variables

$$\tilde{d} := \frac{d}{|d_c|}, \quad \tilde{a} := \frac{a}{a_c}, \quad \tilde{F}_c := \frac{F_N}{|F_c|}, \quad m := \frac{b}{a}, \quad (30)$$

with the critical values in the JKR limit under force-controlled boundary conditions [6]:

$$\begin{aligned} d_c &= \frac{k-1}{(1+k)(3+k)R} \left[\frac{\pi(1+k)^2(3+k)^2 R^2 \Delta\gamma z_0^k}{8c_N} \right]^{\frac{2}{3+k}}, \\ a_c &= \left[\frac{\pi(1+k)^2(3+k)^2 R^2 \Delta\gamma z_0^k}{8c_N} \right]^{\frac{1}{3+k}}, \\ F_c &= -\frac{3+k}{2} \pi \Delta\gamma R, \end{aligned} \quad (31)$$

and the generalized Tabor parameter for power-law elastic grading, i.e. the ratio of the characteristic height of the adhesive neck and the adhesion range:

$$\Lambda := \frac{|d_c|}{h}, \quad (32)$$

Equations (28) can be written in the form:

$$\begin{aligned} \tilde{d} &= \frac{3+k}{1-k} \tilde{a}^2 - \frac{16 \cos(k\pi/2)}{\pi(1-k)^3} \Lambda \tilde{a}^{1-k} \sqrt{(m^2-1)^{1-k}}, \\ \tilde{F} &= \tilde{a}^{3+k} - \frac{2}{\pi} \frac{1+k}{1-k} \Lambda (m\tilde{a})^2 \left[\pi + \frac{4 \cos(k\pi/2)}{1-k^2} \frac{1}{m^{1+k}} \right. \\ &\quad \left. \cdot \left\{ \sqrt{\left(1 - \frac{1}{m^2}\right)^{1-k}} - {}_2F_1\left(\frac{k-1}{2}, \frac{1+k}{2}; \frac{3+k}{2}; \frac{1}{m^2}\right) \right\} \right]. \end{aligned} \quad (33)$$

The compatibility condition (29) in dimensionless variables reads:

$$\begin{aligned} \frac{1}{\Lambda} &= \tilde{d} \left[\frac{2 \cos(k\pi/2)}{\pi} \frac{1}{1+k} \frac{1}{m^{1+k}} {}_2F_1\left(\frac{1+k}{2}, \frac{1+k}{2}; \frac{3+k}{2}; \frac{1}{m^2}\right) - 1 \right] - \\ &\quad - \frac{(m\tilde{a})^2}{2(1-k)} \left[\frac{4}{\pi} \cos\left(\frac{k\pi}{2}\right) \frac{1}{m^{3+k}} {}_2F_1\left(\frac{1+k}{2}, \frac{3+k}{2}; \frac{5+k}{2}; \frac{1}{m^2}\right) - (1+k)(3+k) \right] - \\ &\quad - \frac{32}{\pi^2} \frac{\cos^2\left(\frac{k\pi}{2}\right) \Lambda (m\tilde{a})^{1-k}}{(1-k)^3(1+k)} \left[\frac{\Gamma(1-k)\Gamma\left(\frac{3+k}{2}\right)}{\Gamma\left(\frac{3-k}{2}\right)} - \frac{1}{m^{1+k}} {}_2F_1\left(k, \frac{1+k}{2}; \frac{3+k}{2}; \frac{1}{m^2}\right) \right], \end{aligned} \quad (34)$$

which in the homogeneous case coincides with Maugis' solution [12] (Maugis uses a slightly different scaling for normalization). The JKR limit is given by the known relations [17]:

$$\begin{aligned} \tilde{d}^{\text{JKR}} &= \frac{3+k}{1-k} \tilde{a}^2 - \frac{4}{1-k} \tilde{a}^{\frac{1-k}{2}}, \\ \tilde{F}^{\text{JKR}} &= \tilde{a}^{3+k} - 2\tilde{a}^{\frac{3+k}{2}}. \end{aligned} \quad (35)$$

As the adhesive force in the DMT limit,

$$F_{\text{adh}}^{\text{DMT}} = 2\pi\Delta\gamma R, \quad (36)$$

is independent of the elastic contact properties (it is actually the force for the adhesive contact of rigid spheres derived by Bradley [18]), the DMT limit of Eqs. (33) reads:

$$\begin{aligned}\tilde{a}^{\text{DMT}} &= \frac{3+k}{1-k} \tilde{a}^2, \\ \tilde{F}^{\text{DMT}} &= \tilde{a}^{3+k} - \frac{4}{k+3}.\end{aligned}\quad (37)$$

To illustrate above findings and the influence of material grading Figs. 1 and 2 show the implicitly defined force-indentation relations as well as the respective JKR- and DMT limits for two different values of the power-law exponent k .

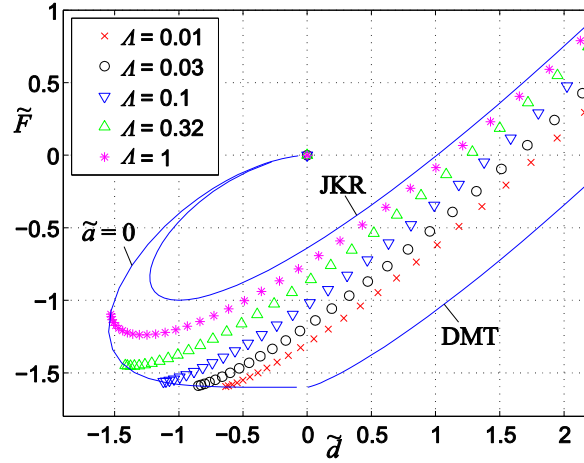


Fig. 1 Force-indentation-curves for the Dugdale-Maugis adhesive normal contact of power-law graded elastic spheres for $k = -0.5$ and several values of the Tabor parameter \mathcal{A}

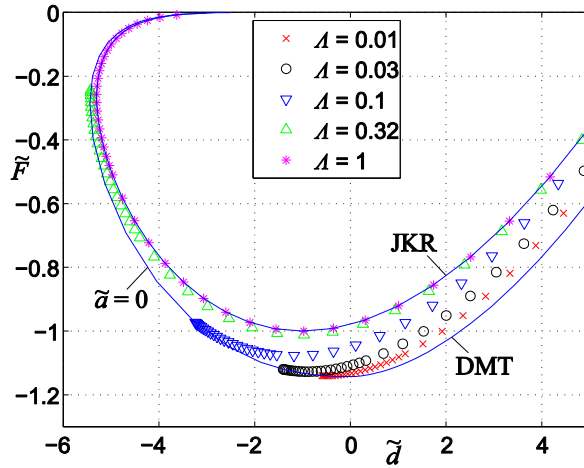


Fig. 2 Force-indentation-curves for the Dugdale-Maugis adhesive normal contact of power-law graded elastic spheres for $k = 0.5$ and several values of the Tabor parameter \mathcal{A}

Note that the DMT limit is only well-defined for positive indentation depths although the branch without direct contact (and therefore negative indentation depths) can be seen as its “natural” continuation. To denote this slight distinction a small gap is left between the DMT limit and the curve without direct contact in Fig. 1. Obviously the convergence for higher values of the Tabor parameter towards the JKR limit is much faster for larger values of k . For $k = 0.5$ there is already no noticeable difference between the solution for $\lambda = 1$ and the JKR limit. Also the normalized indentation depths are getting much higher for larger values of k . Interestingly, the critical pull-off forces in the JKR- and DMT limit are the same for $k \rightarrow 1$ (as it was pointed out already in [6]). In this case the left branch of the JKR curve and the curve without direct contact will be practically indistinguishable.

5. CONCLUSIONS

Based on the MDR a closed-form analytic solution has been obtained for the Dugdale-Maugis adhesive normal contact of arbitrary convex axisymmetric, power-law graded elastic bodies. As the most common and probably most relevant special case the contact of spherical or parabolic bodies has been studied in detail. The common limits for very large (JKR) or very small (DMT) values of the Tabor parameter are derived from the general solution. In dimensionless variables the relations between indentation depth, contact radii and normal force only depend on the Tabor parameter and exponent k of the elastic grading. Thereby the convergence for larger values of the Tabor parameter towards the JKR limit is faster for higher values of k .

The presented solution is of course based on strong contact-mechanical assumptions (half-space hypothesis, absence of friction or roughness) and quantitatively problematic physical models (power-law grading with either infinitely stiff or infinitely soft surfaces, Dugdale model for the adhesive stress); it is, however, to the author’s best knowledge, the only tool, to rigorously study the influence of both material grading and adhesion range in a closed form, for example in micro- or nano-applications, for which the range of the (adhesive) molecular forces becomes relevant. And although other models might seem physically more appropriate, they will probably neither allow for analytic treatment nor show a qualitatively different behavior.

For future work it would be interesting to compare the obtained analytical results with numerical or experimental findings.

REFERENCES

1. Suresh, S., 2001, *Graded Materials for Resistance to Contact Deformation and Damage*, Science, 292, pp. 2447-2451.
2. Scherge, M., Gorb, S., 2001, *Biological Micro- and Nano-Tribology – Nature’s Solutions*, Springer, Berlin Heidelberg.
3. Booker, J.R., Balaam, N.P., Davis, E.H., 1985, *The Behaviour of an Elastic Non-Homogeneous Half-Space. Part I—Line and Point Loads*, International Journal for Numerical and Analytical Methods in Geomechanics, 9(4), pp. 353-367.
4. Giannakopoulos, A.E., Suresh, S., 1997, *Indentation of Solids with Gradients in Elastic Properties: Part I. Point Forces*, International Journal of Solids and Structures, 34(19), pp. 2357-2392.
5. Giannakopoulos, A.E., Suresh, S., 1997, *Indentation of Solids with Gradients in Elastic Properties: Part II. Axisymmetric Indentors*, International Journal of Solids and Structures, 34(19), pp. 2393-2428.

6. Chen, S., Yan, C., Zhang, P., Gao, H., 2009, *Mechanics of adhesive contact on a power-law graded elastic half-space*, Journal of the Mechanics and Physics of Solids, 57(9), pp. 1437-1448.
7. Guo, X., Jin, F., Gao, H., 2011, *Mechanics of non-slipping adhesive contact on a power-law graded elastic half-space*. International Journal of Solids and Structures, 48(18), pp. 2565-2575.
8. Jin, F., Guo, X., Zhang, W., 2013, *A Unified Treatment of Axisymmetric Adhesive Contact on a Power-Law Graded Elastic Half-Space*. Journal of Applied Mechanics, 80(6), 061024.
9. Liu, Z., Meyers, M.A., Zhang, Z., Ritchie, R.O., 2017, *Functional gradients and heterogeneities in biological materials: Design principles, functions, and bioinspired applications*, Progress in Materials Science, 88, pp. 467-498.
10. Johnson, K.L., Kendall, K., Roberts, A.D., 1971, *Surface Energy and the Contact of Elastic Solids*. Proceedings of the Royal Society of London, Series A, 324, pp. 301-313.
11. Derjaguin, B.V., Muller, V.M., Toporov, Y.P., 1975, *Effect of contact deformations on the adhesion of particle*, Journal of Colloid and Interface Science, 53(2), pp. 314-326.
12. Maugis, D., 1992, *Adhesion of spheres: The JKR-DMT-transition using a Dugdale model*. Journal of Colloid and Interface Science, 150(1), pp. 243-269.
13. Dugdale, D.S., 1960, *Yielding of steel sheets containing slits*, Journal of the Mechanics and Physics of Solids, 8(2), pp. 100-104.
14. Tabor, D., 1977, *Surface forces and surface interactions*, Journal of Colloid and Interface Science, 58(1), pp. 2-13.
15. Heß, M., 2016, *A simple method for solving adhesive and non-adhesive axisymmetric contact problems of elastically graded materials*, International Journal of Engineering Science, 104, pp. 20-33.
16. Heß, M., Popov, V.L., 2016, *Method of Dimensionality Reduction in Contact Mechanics and Friction: A User's Handbook. II. Power-Law Graded Materials*, Facta Universitatis-Series Mechanical Engineering, 14(3), pp. 251-268.
17. Popov, V.L., Heß, M., Willert, E., 2018, *Handbuch der Kontaktmechanik – Exakte Lösungen axialsymmetrischer Kontaktprobleme*, Springer, Berlin Heidelberg.
18. Bradley, M.A., 1932, *The cohesive force between solid surfaces and the surface energy of solids*, The London, Edinburgh, and Dublin Philosophical Magazine and Journal of Science, 13(86), pp. 853-862.

Original scientific paper

LIMITING PROFILE OF AXISYMMETRIC INDENTER DUE TO THE INITIALLY DISPLACED DUAL-MOTION FRETTING WEAR

UDC 539.3

Qiang Li

Berlin Institute of Technology, Department of Dynamics and Tribology, Germany

Abstract. *Recently the final worn shape of elastic indenters due to fretting wear was analytically solved using the method of dimensionality reduction. In this paper we extend this model to dual-motion fretting wear and take into account that the indenter is initially pressed with constant indentation depth and moved horizontally with constant displacement. Two key parameters, the maximal indentation depth during oscillation and the stick area radius in the final state as well as the limiting shape of indenter are analytically calculated. It is shown that the oscillation amplitudes and the initially indented or moved displacements have an influence on the final shaking-down shape.*

Key Words: *Fretting Wear, Dual-motion, Tangential Force, Oscillation*

1. INTRODUCTION

Fretting wear is a surface destruction process in the frictional contacts subjected to oscillating load with small amplitude [1]. This phenomenon occurs very often in the vibrating connections of mechanical elements, such as clamping devices, interference fit joints, gear or bearing contacts and electrical connectors, etc. [2-4]. Fretting leads to material loss, crack formation as well as fatigue failure [5]. In the last few decades many experimental and theoretical investigations have been intensively carried out to understand this process, for example, by using the finite element method or that of the boundary element [6, 7]. However, there are still some unsolved basic problems, especially under complicated loading [8]. Recently, a new method known as that of dimensionality reduction (MDR) was applied to analyzing the process of fretting wear as well as its final ‘shake down’ state for arbitrary axisymmetric shape of elastic or viscoelastic indenter [9-11]. In

Received January 4, 2016 / Accepted March 1, 2016

Corresponding author: Qiang Li

Technical University of Berlin, 10623 Berlin, Germany

E-mail: qiang.li@tu-berlin.de

paper [9] a general theoretical solution of the limiting profile due to fretting wear was given for an arbitrary axisymmetric indenter. For the case of an elastic indenter under the tangential oscillation [10], a rapid numerical procedure based on the MDR was later developed to simulate the wear process, and its results for the final state of wear also verified the solution in [9]. Furthermore, a similar MDR-based procedure was suggested for a gross-slip wear problem and the results are exactly same to the solution obtained by the full FEM formulation, and it is for several orders of magnitude faster than the FEM [12]. Fretting wear of viscoelastic indenters was analyzed in papers [13] and [14], where the analytical solution of limiting profile due to dual-motion oscillation was presented in [13], and the numerical simulation of fretting wear under the tangential oscillation was carried out in [14]. These final worn shapes for spherical indenters under multiple-mode fretting conditions have been validated by experimental investigation [15]. Till now most work focuses on fretting wear only under the tangential oscillation and less on dual-mode fretting. In this paper, we consider the fretting wear of elastic indenter oscillating in both tangential and normal directions, and take into account the factor that the indenter has initially constant displacements in both normal and tangential direction.

2. WEAR CRITERION IN FRETTING CONTACT

This paper is an extension of the solutions in [9]; therefore, firstly we give a very brief discussion of wear condition in [9]. We consider a contact between a rigid axis-symmetrical body and an elastic half space. Under the normal load the indenter is pressed into the half space and then oscillates tangentially. It is known that, if the oscillation amplitude is small enough, there will be an annular slip-zone generated at the boundary of contact area and a circular stick-zone at the inner area, as illustrated in Fig.1.

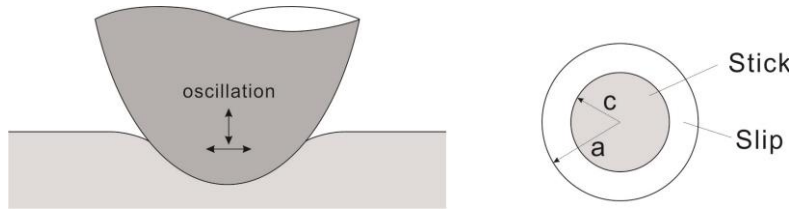


Fig. 1 Schematic representation of the stick-slip area in fretting contact

The stick and slip condition can be determined by the classic Amontons' law: if tangential stress τ is smaller than normal pressure p multiplied by a constant coefficient of friction μ , $\tau < \mu p$, the surfaces of contact bodies stick together, and in the slip region the tangential stress remains constant and equal to product μp :

$$\begin{cases} \tau < \mu p, & \text{in stick area} \\ \tau = \mu p, & \text{in slip area} \end{cases} \quad (1)$$

According to the Reye-Archard-Khrushchov wear law [16, 17], the wear volume is proportional to the normal force (or pressure), the relative tangential displacement and of contacting bodies and reversely proportional to the hardness. From this law, the wear in the

local contact area vanishes when the normal pressure becomes zero or there is no relative displacement between two bodies. As described in [9], this no-wear condition can be written as:

$$\text{No wear condition: } \begin{cases} \text{either} & p = 0 \\ \text{or} & \Delta u_x = 0 \end{cases} \quad (2)$$

In the process of fretting wear, the surfaces in the stick area have no relative displacement, so that no wear occurs in this contact area during the whole process. Due to slip at the boundary wear occurs in this area, but the normal pressure will reduce to zero finally; therefore, there is no wear any more in this local contact area in the final state. In this paper we analyze this limiting profile of indenter.

3. SOLUTION FOR PRE-STRESSED DUAL-MOTION PROBLEM

The analytical solution of limiting profile in [9] was obtained based on the method of dimensionality reduction (MDR). Using this method the three-dimensional normal and tangential contact problems for axis-symmetric bodies can be mapped into one-dimensional contact with a properly defined foundation [18-21]. According to the rules of the MDR, three-dimensional pressure distribution $p(r)$ can be calculated from the profile of one-dimensional indenter $g(x)$:

$$p(r) = \frac{E^*}{\pi} \int_r^\infty \frac{g'(x)}{\sqrt{x^2 - r^2}} dx. \quad (3)$$

From no-wear conditions, Eq. (2), it follows that there are two parts in the contact areas in the final state: in the inner contact area with radius c no wear occurs because of no relative displacement $\Delta u_x=0$, so that the final profile keeps its initial form $g_\infty(x) = g_0(x)$ for $r < c$; at boundary $r > c$ the pressure in the final state reduces to zero, $p(r) = 0$. From Eq. (3), $p(r) = 0$ means that $g'(x) = 0$ and $g(x) = \text{const}$ for $c < x < a$ and the value of const is equal to maximum indentation depth d_{\max} achieved during the whole oscillation process. Thus, the one-dimensional MDR-transformed profile in the final shakedown state has the form

$$g_\infty(x) = \begin{cases} g_0(x), & \text{for } 0 < x < c \\ d_{\max}, & \text{for } c < x < a \end{cases} \quad (4)$$

According to the reverse transformation in the MDR, the three-dimensional limiting shape can be calculated as [9]

$$f_\infty(r) = \begin{cases} f_0(r), & \text{for } 0 < r < c \\ \frac{2}{\pi} \int_0^c \frac{g_0(x)}{\sqrt{r^2 - x^2}} dx + \frac{2}{\pi} d_{\max} \int_c^r \frac{1}{\sqrt{r^2 - x^2}} dx, & \text{for } c < r < a \end{cases} \quad (5)$$

Eq. (5) gives the solution for limiting shake-down-state shape of the indenter. Given an initial three-dimensional profile of indenter, its limiting shape can be determined if the two parameters are known: radius c of the stick area in the limiting state and maximum indentation depth d_{\max} . In the following we discuss how these two governing parameters can be determined in our pre-stressed dual-motion problem.

Such a contact is taken into consideration. The indenter is pressed into an elastic half-space with an indentation depth d_0 , and moved horizontally with a distance x_0 , then oscillates harmonically according to

$$d = d_0 + u_z = d_0 + u_z^{(0)} \sin(\omega_z t + \phi) \quad (6)$$

in vertical direction and

$$u_x = x_0 + u_x^{(0)} \sin(\omega_x t) \quad (7)$$

in horizontal direction. ϕ is phase shift between normal and tangential oscillations. This movement is illustrated in Fig. 2. Here we consider small amplitude of oscillations under the assumption that $u_z^{(0)} < d_0$ and $u_x^{(0)} < x_0$, and all these four parameters are positive. Now we calculate the two important parameters.

(1) *The maximum indentation depth.* This one can be easily obtained by Eq. (6):

$$d_{\max} = \max_{(t)} \{d_0 + u_z^{(0)} \sin(\omega_z t + \phi)\} = d_0 + u_z^{(0)}. \quad (8)$$

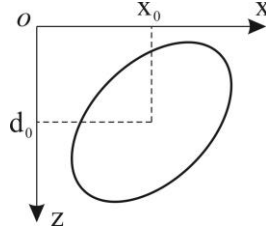


Fig. 2 Illustration of dual-motion of the indenter

(2) *Radius c of the stick area.* According to Eq.(1), radius c can be determined by the condition that tangential force $k_x u_x(c)$ of springs at each time moment is smaller than or equal to coefficient of friction μ multiplied by normal force $k_z u_z(x)$:

$$\left| G^* \Delta x \cdot (x_0 + u_x^{(0)} \sin(\omega_x t)) \right| \leq \mu E^* \Delta x \cdot (d_0 + u_z^{(0)} \sin(\omega_z t + \phi) - g(c)) \quad (9)$$

Solving this inequality with respect to $g(c)$ gives

$$g(c) < d_0 + u_z^{(0)} \sin(\omega_z t + \phi) - \frac{G^*}{\mu E^*} (x_0 + u_x^{(0)} \sin(\omega_x t)) \quad (10)$$

or

$$g(c) = \min_{(t)} \left\{ d_0 + u_z^{(0)} \sin(\omega_z t + \phi) - \frac{G^*}{\mu E^*} (x_0 + u_x^{(0)} \sin(\omega_x t)) \right\} \quad (11)$$

From Eq.(11), it can be seen that the value of $g(c)$ is dependent on phase shift ϕ . If it is not fixed, that means phase shift ϕ is not constant but changes all the time, then $g(c)$ has a very simple and general form

$$g(c) = d_0 - u_z^{(0)} - \frac{G^*}{\mu E^*} (x_0 + u_x^{(0)}). \quad (12)$$

However, if the phase shift is constant, the solution of Eq. (11) is not easy to calculate. Here we consider only a special case of same oscillation frequencies: $\omega_x = \omega_z = \omega$. Solving the Eq. (11) gives

$$g(c)_{\min} = d_0 - \frac{G^*}{\mu E^*} x_0 - \sqrt{u_z^{(0)2} - 2u_z^{(0)}u_x^{(0)} \frac{G^*}{\mu E^*} \cos \phi + \left(\frac{G^*}{\mu E^*} u_x^{(0)} \right)^2}. \quad (13)$$

Now the two parameters, radius c of the stick area in the limiting state and maximum indentation depth d_{\max} are obtained. Substitute Eqs. (8) and (13) to the limiting profile Eq. (5), then the three-dimensional limiting shape of the indenter can be calculated. It is seen that the two parameters as well as the limiting shape depend on oscillation amplitudes $u_z^{(0)}$ and $u_x^{(0)}$, phase shift ϕ between normal and tangential movements, and also the initial pre-indentation and -displaced distance d_0 and x_0 .

Radius c of the stick area is briefly discussed here. From Eq.(13), the smallest stick radius is given when phase shift $\phi = \pi$, and the value are the same to (12) in the case of no-fixed phase. The maximum stick radius (minimum wear volume) is realized at $\phi = 0$:

$$g(c) = d_0 - \frac{G^*}{\mu E^*} x_0 - \left| u_z^{(0)} - \frac{G^*}{\mu E^*} u_x^{(0)} \right|. \quad (14)$$

If the phase $\phi = \pm\pi/2$, the stick area is given by

$$g(c) = d_0 - \frac{G^*}{\mu E^*} x_0 - \sqrt{u_z^{(0)2} + \left(\frac{G^*}{\mu E^*} \right)^2 u_x^{(0)2}}. \quad (15)$$

It is noted that these results of the stick area as well as the related limiting profile are independent of the frequencies of normal and tangential oscillations.

With an example of parabolic indenter we show how the limiting profile can be calculated in the case of pre-displaced dual-motion. The one-dimensional profile of spherical indenter with radius R is given by $g(x) = x^2/R$ [18]. From Eq. (8) the maximal indentation depth is equal to $d_{\max} = d_0 + u_z^{(0)}$. If the phase shift between normal and tangential oscillations is $\phi = \pi$, then the stick radius is calculated by Eq. (12) as $c^2/R = d_0 - u_z^{(0)} - (x_0 + u_x^{(0)})G^*/(\mu E^*)$. Substituting these two parameters d_{\max} and c into basic solution, Eq. (5), the final profile in this case is then obtained. An example of this final shape is shown in Fig. 3. The worn shape of the indenter can be clearly seen, that is, this part lies in the slip area and the strongest wear is almost in the middle of the slip region.

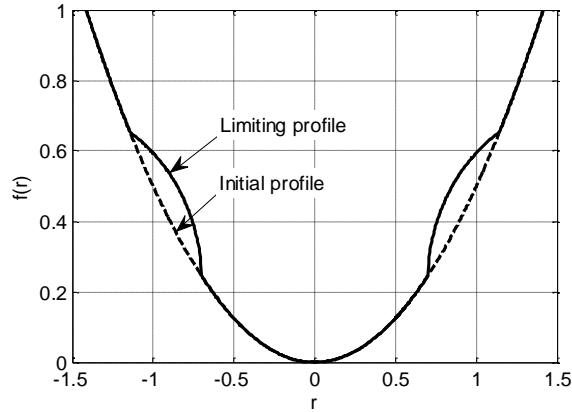


Fig. 3 An example of limiting shape of parabolic indenter

4. CONCLUSION

We extended the basic solution of limiting shape of axis-symmetric profiles due to fretting wear in paper [9] to the case of pre-stressed dual-motion fretting wear. It means that the indenter is pressed into the half space with initial indentation depth and initial tangential displacement; it oscillates in both vertical and horizontal directions. The emphasis of the analysis is placed on two parameters – the maximum indentation depth during the oscillation process and the radius of the stick area in the final state, which determine the limiting shape of worn profile according to basic analytical solution in [9]. For the particular case in this paper we derived and obtained the relation of these two parameters, and it is shown that they depend on the oscillation amplitudes, the phase shift between normal and tangential movements, as well as on the initially indented and displaced distance. Especially the different phase shift between normal and tangential oscillations for the same frequency will result in a different size of the stick area as well as a different limiting profile. With an example of parabolic indenter oscillating on a half space, we present its final worn shape. The worn area is clearly observed and the volume of material loss can be further calculated by comparison with the initial shape of profile.

Acknowledgements: *The author thanks V.L. Popov for valuable discussions.*

REFERENCES

1. Kennedy, P., Peterson, M.B., Stallings, L., 1982, *An Evaluation of Fretting at Small Slip Amplitudes*. In: *Materials Evaluation under Fretting Conditions*, ASTM Spec. Tech. Publ., 780, pp. 30–48.
2. Zhang, H., Brown, L.T., Blunt, L.A., Jiang, X., Barrans, S.M., 2009, *Understanding initiation and propagation of fretting wear on the femoral stem in total hip replacement*, *Wear*, 266, pp. 566–569.
3. Zheng, J. F. et al., 2010, *Fretting wear behaviors of a railway axle steel*, *Tribol. Int.* 43, pp. 906–911.
4. Antler, M., 1985, *Electrical effects of fretting connector contact materials: A review*, *Wear*, 106, pp. 5–33.
5. Szolwinski, M.P., Farris, T.N., 1996, *Mechanics of fretting fatigue crack formation*, *Wear*, 198, pp. 93–107.
6. Fisher, N.J., Chow, A.B., Weckwerth, M.K., 1995, *Experimental Fretting Wear Studies of Steam Generator Materials*, *J. Press. Vessel Technol.*, 117, pp. 312–320.
7. Liu, J., Shen, H.M., Yang, Y.R., 2014, *Finite element implementation of a varied friction model applied to torsional fretting wear*, *Wear*, 314, pp. 220–227.
8. Ciavarella, M., Demelio, G., 2001, *A review of analytical aspects of fretting fatigue, with extension to damage parameters, and application to dovetail joints*, *Int. J. Solids Struct.*, 38, pp. 1791–1811.
9. Popov, V.L., 2014, *Analytic solution for the limiting shape of profiles due to fretting wear*, *Sci. Rep.*, 4, 3749.
10. Dimaki, A.V., Dmitriev, A.I., Chai, Y.S., Popov V.L., 2014, *Rapid simulation procedure for fretting wear on the basis of the method of dimensionality reduction*, *Int. J. Solids Struct.*, 51, pp. 4215–4220.
11. Li, Q., Filippov, A.E., Dimaki, A.V., Chai, Y.S., Popov, V.L., 2014, *Simplified simulation of fretting wear using the method of dimensionality reduction*, *Phys. Mesomech.*, 17, pp. 236–241.
12. Dimaki, A.V., Dmitriev, A.I., Menga, N., Papangelo, A., Ciavarella, M., Popov, V.L., 2016, *Fast High-Resolution Simulation of the Gross Slip Wear of Axially Symmetric Contacts*, *Tribol. Trans.*, 59, pp. 189–194.
13. Mao, X.Y., Liu, W., Ni, Y.Z., Popov, V.L., 2015, *Limiting shape of profile due to dual-mode fretting wear in a contact with an elastomer*, *J. Mech. Eng. Sci.*, 203–210, pp. 1989–1996.
14. Dimaki, A.V., Popov, V.L., 2015, *A model of fretting wear in the contact of an axisymmetric indenter and a visco-elastic half-space*, *AIP Conf. Proc.*, 1683, 020040.
15. Dmitriev, A.I., Voll, L.B., Psakhie, S.G., Popov, V.L., 2016, *Universal limiting shape of worn profile under multiple-mode fretting conditions: theory and experimental evidence*, *Sci. Rep.*, 6, 23231.
16. Reye, T., 1860, *Zur Theorie der Zapfenreibung*, *Der Civil.*, 4, pp. 235–255.

17. Popov, V.L., 2010, *Contact mechanics and friction*, Springer, Berlin.
18. Popov, V.L., 2013, *Method of reduction of dimensionality in contact and friction mechanics: A linkage between micro and macro scales*, *Friction*, 1, pp. 41–62.
19. Popov, V.L., Heß, M., 2015, *Method of dimensionality reduction in contact mechanics and friction*, Springer, Berlin.
20. Heß, M., 2011, *Über die Abbildung ausgewählter dreidimensionaler Kontakte auf Systeme mit niedrigerer räumlicher Dimension*, Cuvillier-Verlag, Göttingen.
21. Heß, M., 2012, *On the reduction method of dimensionality: The exact mapping of axisymmetric contact problems with and without adhesion*, *Phys. Mesomech.*, 15, pp. 264–269.

Chapter 5

Further Generalizations of the Method of Dimensionality Reduction

APPLICATION OF THE METHOD OF DIMENSIONALITY REDUCTION TO CONTACTS UNDER NORMAL AND TORSIONAL LOADING

UDC 539.3

Emanuel Willert¹, Markus Hess¹, Valentin L. Popov^{1,2}

¹Berlin University of Technology, Germany

²National Research Tomsk State University, Russia

Abstract. *Recently the method of dimensionality reduction (MDR) has been introduced to solve axisymmetric contact problems easily and exactly. The list of tasks that this method can deal with comprises normal, tangential, adhesive and rolling contacts with simply connected contact areas between elastic or viscoelastic bodies. Due to its simplicity and easy applicability the MDR provides the possibility of fast and comprehensive studies of contact problems in technological or biological systems, for example bearings, artificial hip joints, wheel-rail systems or others. Within the complicated three-dimensional contact theory those studies, in most cases, cannot be done without a tremendous mathematical or numerical effort.*

In view of all this, the torsional contact problems have been disregarded until now, although it is known that torsion is a major reason of wear and possible failure of system components. Therefore, in the present paper, we extend the MDR to contacts of axisymmetric profiles under superimposed normal and torsional loading.

Key Words: *Contact Mechanics, Method of Dimensionality Reduction, Torsion, Friction, Stick, Slip*

1. INTRODUCTION

Pure torsional contacts or normal and torsional contacts coupled by friction were not given much attention in the past, although torsional loading is known to be a major reason of wear and fatigue.

In [1] Lubkin gave the shear stress distribution for the torsional contact between two elastic spheres with partial slip. Hetényi and McDonald Jr. calculated the stresses and displacements for the full-sliding contact between an elastic sphere and an elastic halfspace using Hankel transforms [2]. Also based on Hankel transforms, i.e. Bessel functions, Kartal

Received: May 29, 2015

Corresponding author: Emanuel Willert

Technische Universität Berlin, Institut für Mechanik, Str. des 17. Juni 135, 10623 Berlin, Germany

E-mail: e.willert@tu-berlin.de

et al. analyzed the torsional contact with partial slip between flat-ended elastic cylinders [3]. Jäger determined the stress distributions in the form of Abel transforms for the torsional contact with partial slip between axisymmetric bodies of arbitrary profile shape [4]. He thereby used a superposition of flat-punch-solutions to solve the contact problem of arbitrarily shaped bodies. In the experimental work [5] Trejo et al. investigated the friction between an elastomer and a randomly rough surface using a torsional contact configuration.

In a series of recent papers, Popov and collaborators have introduced the so-called method of dimensionality reduction (MDR), which allows solving normal contact problems of axisymmetric elastic and viscoelastic bodies as well as tangential contact problems with a constant coefficient of friction for arbitrary loading histories [6, 7]. In the monographs [8] and [9], the MDR has been summarized and many applications have been provided. Moreover, an introduction into its usage in the form of a user's handbook can be found in [10].

In the present paper, we are showing that the contact with torsion (rotation around the normal axis to the contact plane) can also be described with the MDR as long as there is no slip in the contact or the thickness of the slip annulus at the edge of the contact is small compared to the contact radius.

The paper is organized as follows: In the Section 2 we reproduce, for convenience of the reader, the derivation of the MDR equations for the normal contact following [9]. In the Section 3 the application of the MDR to contacts with torsion without slip is discussed. In the Section 4 the torsional contact with a narrow slip region is considered. Section 5 closes the paper.

2. METHOD OF DIMENSIONALITY REDUCTION FOR THE NORMAL CONTACT

In this section, the equations of the MDR for the normal contact of axisymmetric profiles $f(r)$ with a compact area of contact are deduced. Thereby we follow the idea of Jäger [11] to derive the solution of an axisymmetric contact problem by summation of differential flat punch solutions.

A flat punch of radius a , indenting an elastic half space with effective elastic modulus E^* by indentation depth d , produces displacement u_z

$$u_z = \begin{cases} d, & r < a \\ \frac{2}{\pi} d \cdot \arcsin(a/r), & r > a \end{cases} \quad (1)$$

The resulting pressure distribution will be

$$p(r) = \begin{cases} \frac{1}{\pi} \frac{E^* d}{\sqrt{a^2 - r^2}}, & r < a \\ 0, & r > a \end{cases} \quad (2)$$

and the total normal force

$$F_N = 2E^* a d. \quad (3)$$

Hence, contact stiffness k_z is

$$k_z(a) = \frac{dF_N}{dd} = 2E^* a. \quad (4)$$

Note that this equation is valid for any profile shape, if a is understood as the current contact radius.

Let us assume a contact between a rigid indenter of shape $z = f(r)$ and an elastic half space. The indentation depth due to normal force F_N will be d and contact radius a . For any given profile shape any of those three parameters will unambiguously define the other two. Especially, the indentation depth is a definite function of the contact radius, which we will denote by

$$d = g(a). \quad (5)$$

Firstly we show that the complete solution of the normal contact problem will be unambiguously determined by function $d = g(a)$.

Analyzing the complete process of indentation from its very first moment until the final indentation, the current values of the normal force, indentation depth and contact radius are given by \tilde{F}_N , \tilde{d} and \tilde{a} . During the indentation process, the indentation depth changes from $\tilde{d} = 0$ to $\tilde{d} = d$, the contact radius accordingly from $\tilde{a} = 0$ to $\tilde{a} = a$ and the normal force from $\tilde{F}_N = 0$ to $\tilde{F}_N = F_N$. The final normal force can be written as

$$F_N = \int_0^{F_N} d\tilde{F}_N = \int_0^a \frac{d\tilde{F}_N}{d\tilde{d}} \frac{d\tilde{d}}{d\tilde{a}} d\tilde{a}. \quad (6)$$

If we take into account that the differential contact stiffness of an area with radius \tilde{a} is given by (4) and the indentation depth by (5), we get

$$F_N = 2E^* \int_0^a \tilde{a} \frac{dg(\tilde{a})}{d\tilde{a}} d\tilde{a}, \quad (7)$$

which gives after partial integration

$$F_N = 2E^* \left[a \cdot g(a) - \int_0^a g(\tilde{a}) d\tilde{a} \right] = 2E^* \left[\int_0^a (d - g(\tilde{a})) d\tilde{a} \right]. \quad (8)$$

Let us calculate the pressure distribution within the contact area. An infinitesimal indentation $d\tilde{d}$ of an area with radius \tilde{a} will, due to (2), produce the pressure

$$dp(r) = \frac{1}{\pi} \frac{E^*}{\sqrt{\tilde{a}^2 - r^2}} d\tilde{d}. \quad (9)$$

The pressure distribution at the end of the indentation process is given by the sum of all infinitesimal pressure components,

$$p(r) = \int_{d(r)}^d \frac{1}{\pi} \frac{E^*}{\sqrt{\tilde{a}^2 - r^2}} d\tilde{d} = \int_r^a \frac{1}{\pi} \frac{E^*}{\sqrt{\tilde{a}^2 - r^2}} \frac{dg(\tilde{a})}{d\tilde{a}} d\tilde{a}. \quad (10)$$

Hence, function $d = g(a)$ unambiguously defines the pressure distribution and therefore the total normal force as well. That is why the solution of the contact problem is reduced to the determination of this function.

This can be done as follows: Infinitesimal indentation $d\tilde{d}$ mentioned above will, due to (1), produce surface displacement at $r = a > \tilde{a}$

$$du_z(a) = \frac{2}{\pi} \arcsin\left(\frac{\tilde{a}}{a}\right) d\tilde{d}. \quad (11)$$

Again, the total displacement can be understood as a sum of all infinitesimal indentations:

$$u_z(a) = \frac{2}{\pi} \int_0^a \arcsin\left(\frac{\tilde{a}}{a}\right) d\tilde{a} = \frac{2}{\pi} \int_0^a \arcsin\left(\frac{\tilde{a}}{a}\right) \frac{dg(\tilde{a})}{d\tilde{a}} d\tilde{a} \quad (12)$$

On the other hand, this displacement is given by $u_z(a) = d - f(a)$:

$$d - f(a) = \frac{2}{\pi} \int_0^a \arcsin\left(\frac{\tilde{a}}{a}\right) \frac{dg(\tilde{a})}{d\tilde{a}} d\tilde{a}, \quad (13)$$

which gives after partial integration

$$f(a) = \frac{2}{\pi} \int_0^a \frac{g(\tilde{a})}{\sqrt{a^2 - \tilde{a}^2}} d\tilde{a}. \quad (14)$$

This is an Abel integration equation, which can be inverted [12]:

$$g(a) = a \int_0^a \frac{f'(\tilde{a})}{\sqrt{a^2 - \tilde{a}^2}} d\tilde{a}. \quad (15)$$

The MDR is mainly an interpretation of the equations (5), (8), (10) and (15), which, on the one hand, can be interpreted as just a mnemonic rule. However, in many ways it has a deeper physical meaning.

Let us assume an elastic foundation of independent equal springs, each at distance Δx from each other and with stiffness $\Delta k_z = E^* \Delta x$, as shown in Fig. 1.

Also, we define a one-dimensional profile $g(x)$ as a formal transformation of the three-dimensional axisymmetric profile $z = f(r)$ according to

$$g(x) = |x| \int_0^{|x|} \frac{f'(r)}{\sqrt{x^2 - r^2}} dr. \quad (16)$$

This transformation is illustrated in Fig. 2.

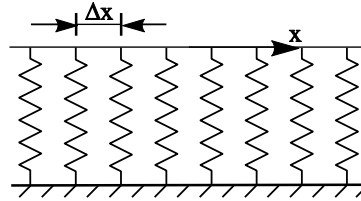


Fig. 1 Equivalent elastic foundation

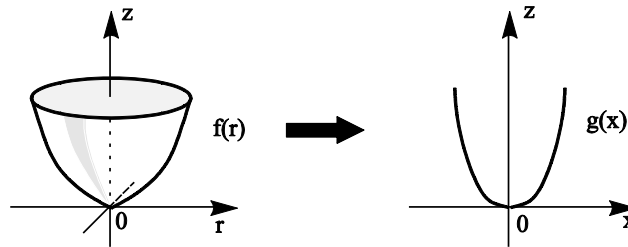


Fig. 2 Axisymmetric three-dimensional profile and one-dimensional analogue within the framework of the MDR (see Eq. (16))

The transformed profile is now pressed into the elastic foundation described above. This is shown in Fig. 3. The surface displacement in normal direction at any point x will be given by the difference of indentation depth d and profile shape $g(x)$:

$$u_z^{1D}(x) = d - g(x) . \quad (17)$$

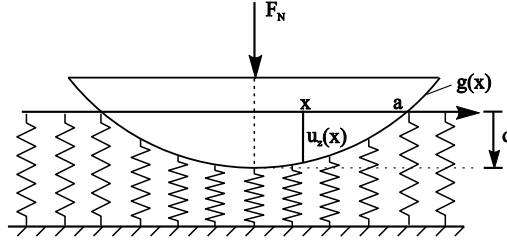


Fig. 3 MDR-model for the normal contact

For contacts without adhesion the displacement vanishes at the edge of the contact:

$$u_z^{1D}(a) = d - g(a) = 0 . \quad (18)$$

The normal force in a single spring is given by

$$\Delta F_N(x) = \Delta k_z (d - g(x)) = E^* (d - g(x)) \Delta x , \quad (19)$$

from which the total normal force in the equilibrium state can be calculated by summation over all springs. In limiting case $\Delta x \rightarrow 0$ the sum will be the integral

$$F_N = E^* \int_{-a}^a u_z^{1D}(x) dx = 2E^* \int_0^a (d - g(x)) dx . \quad (20)$$

It can be seen easily that the equations (18), (20) and (16) reproduce (5), (8) and (15). Hence, transformed profile $g(x)$ is the geometrical interpretation of dependence $d = g(a)$ for the given three-dimensional profile shape. By the equivalence of the equations presented above it is also shown that, instead of analyzing the three-dimensional contact problem, the described equivalent one-dimensional problem can be solved, obtaining the correct and exact results for the original contact.

In the next paragraph we are going to show how this can be done, by the same method, for torsional contact as well.

3. DESCRIPTION OF THE TORSIONAL CONTACT WITH THE METHOD OF DIMENSIONALITY REDUCTION

Again, we start with the known solution for the torsional contact of a rigid flat cylinder. If a rigid flat-ended punch is pressed on an elastic half space and rotated around the axis of the cylinder by angle φ , the produced torsional moment, surface displacement and stress distribution will be given by equations [13]

$$M_z = \frac{16}{3} G a^3 \varphi , \quad (21)$$

$$u_\varphi(r) = \begin{cases} \varphi r, & r < a \\ \frac{2}{\pi} \varphi \left\{ r \arcsin\left(\frac{a}{r}\right) - a \sqrt{1 - \frac{a^2}{r^2}} \right\}, & r > a \end{cases}, \quad (22)$$

$$\tau(r) = \begin{cases} \frac{4G\varphi}{\pi} \frac{r}{\sqrt{a^2 - r^2}}, & r < a \\ 0, & r > a \end{cases}, \quad (23)$$

where G is the shear modulus. In the case of rotational symmetry and of no slip, the torsional contact problem completely decouples from the normal contact problem.

We analyze the torsional contact problem that is analogical to the normal contact problem described in the previous section, i.e. we imprint rotational surface displacement $u_\varphi(r) = r(\varphi - \psi(r))$ into an elastic half space and want to determine the shear stresses due to this displacement. $\psi(r)$ is the deviation of the torsional angle from the pure constant rotation with φ . This displacement is understood as a sum of infinitesimal torsional loadings of flat punches [4]. In analogy to (5) we introduce the function

$$\varphi = \Phi(a). \quad (24)$$

The complete torsional moment after the process of torque loading can be calculated as

$$M_z = \int_0^M d\tilde{M}_z = \int_0^a \frac{d\tilde{M}_z}{d\tilde{\varphi}} \frac{d\Phi(\tilde{a})}{d\tilde{a}} d\tilde{a} = \frac{16}{3} G \int_0^a \tilde{a}^3 \frac{d\Phi(\tilde{a})}{d\tilde{a}} d\tilde{a}. \quad (25)$$

We introduce variable $u_y(x)$ in the following differential way:

$$du_y(x) = \begin{cases} x d\varphi, & 0 < x < a \\ 0, & x > a \end{cases}. \quad (26)$$

At the end of the described process of infinitesimal torsional loadings this field will be

$$u_y(x) = \int_{\varphi(x)}^{\varphi} x d\tilde{\varphi} = \int_x^a x \frac{d\Phi(\tilde{a})}{d\tilde{a}} d\tilde{a}. \quad (27)$$

Dividing (27) by x and differentiating with respect to x we get

$$\frac{d}{dx} \left(\frac{u_y(x)}{x} \right) = - \frac{d\Phi(x)}{dx} - \frac{u_y(a)}{a} \delta(x-a). \quad (28)$$

Equation (25) can then be written in the following way:

$$M_z = - \frac{16}{3} G \int_0^a \tilde{a}^3 \left[\frac{d}{d\tilde{a}} \left(\frac{u_y(\tilde{a})}{\tilde{a}} \right) + \frac{u_y(a)}{a} \delta(\tilde{a}-a) \right] d\tilde{a}, \quad (29)$$

which gives after partial integration

$$M_z = 16G \int_0^a \tilde{a} \cdot u_y(\tilde{a}) d\tilde{a}. \quad (30)$$

It is obvious that this equation can also be interpreted within a one-dimensional model.

Let us assume an elastic foundation with tangential stiffness

$$\Delta k_y = 8G\Delta x. \quad (31)$$

The force of a single spring is given by

$$\Delta F_y = \Delta k_y u_y(x) \quad (32)$$

and the resulting torsional moment by

$$\Delta M_z = 8Gxu_y(x)\Delta x. \quad (33)$$

The total moment can be calculated again by integration and will be

$$M_z = 8G \int_{-a}^a x \cdot u_y(x) dx = 16G \int_0^a x \cdot u_y(x) dx, \quad (34)$$

which coincides with (30).

To complete the solution of the described torsional contact problem, let us calculate function $\Phi(a)$ and the stress distribution. According to (23) the stress distribution can – analogically to the previous section – be calculated from function $\Phi(a)$:

$$\tau(r) = \frac{4G}{\pi} \int_r^a \frac{r}{\sqrt{\tilde{a}^2 - r^2}} \frac{d\Phi(\tilde{a})}{d\tilde{a}} d\tilde{a}, \quad (35)$$

or with equation (28)

$$\tau(r) = -\frac{4G}{\pi} \int_r^a \frac{r}{\sqrt{\tilde{a}^2 - r^2}} \left[\frac{d}{d\tilde{a}} \left(\frac{u_y(\tilde{a})}{\tilde{a}} \right) + \frac{u_y(a)}{a} \delta(\tilde{a} - a) \right] d\tilde{a}, \quad (36)$$

which is equivalent to

$$\tau(r) = -\frac{4G}{\pi} \left[\int_r^a \frac{r}{\sqrt{\tilde{a}^2 - r^2}} \frac{d}{d\tilde{a}} \left(\frac{u_y(\tilde{a})}{\tilde{a}} \right) d\tilde{a} + \frac{u_y(a)}{a} \frac{r}{\sqrt{a^2 - r^2}} \right]. \quad (37)$$

The displacement at the edge of the contact, i.e. at $r = a > \tilde{a}$, will be, according to (22),

$$u_\varphi(a) = a(\varphi - \psi(a)) = \frac{2}{\pi} \int_0^a \frac{d\Phi(\tilde{a})}{d\tilde{a}} \left\{ a \arcsin \left(\frac{\tilde{a}}{a} \right) - \tilde{a} \sqrt{1 - \frac{\tilde{a}^2}{a^2}} \right\} d\tilde{a}. \quad (38)$$

In the next section we will analyze the case of slip in the contact area. This will inevitably lead to requirement $\tau(a) = 0$. This given, (27) can be written as

$$u_y(x) = x(\varphi - \Phi(x)) \quad (39)$$

and partial integration of (38) will give

$$\psi(a) = \frac{4}{\pi a^2} \int_0^a \Phi(\tilde{a}) \frac{\tilde{a}^2}{\sqrt{a^2 - \tilde{a}^2}} d\tilde{a}. \quad (40)$$

This is again an Abel integration equation, which can be inverted [12]:

$$\Phi(a) = \frac{1}{2a} \int_0^a \frac{d}{dr} (r^2 \psi(r)) \frac{dr}{\sqrt{a^2 - r^2}}. \quad (41)$$

4. TORSIONAL CONTACT WITH A NARROW SLIP REGION

The boundary conditions at the surface of the half space in the presence of slip can generally be written in the form

$$\begin{aligned} \psi(r) &= 0, & \text{for } r < c, \\ \tau(r) &= \mu p(r), & \text{for } c < r < a, \end{aligned} \quad (42)$$

with the radius of stick domain c and coefficient of friction μ . From (41) it is obvious that

$$\Phi(x) = 0, \quad \text{for } x < c. \quad (43)$$

Hence, the shear stresses within the contact area will be

$$\tau(r) = \begin{cases} \frac{4G}{\pi} \int_c^a \frac{r}{\sqrt{\tilde{a}^2 - r^2}} \frac{d\Phi(\tilde{a})}{d\tilde{a}} d\tilde{a}, & \text{for } r < c \\ \frac{4G}{\pi} \int_r^a \frac{r}{\sqrt{\tilde{a}^2 - r^2}} \frac{d\Phi(\tilde{a})}{d\tilde{a}} d\tilde{a}, & \text{for } c < r < a \end{cases}. \quad (44)$$

Note, that (44) can always be written in the form

$$\tau(r) = \begin{cases} \mu(p_a(r) - p_c(r)), & \text{for } r < c \\ \mu p_a(r), & \text{for } c < r < a \end{cases}. \quad (45)$$

Here $p_a(r)$ and $p_c(r)$ denote known pressure distribution $p(r)$ with respective contact radii a and c . Thus the shear stress distribution in the whole contact area is known. The contact problem will be solved completely, if the integral equation

$$\frac{4G}{\pi} \int_r^a \frac{r}{\sqrt{\tilde{a}^2 - r^2}} \frac{d\Phi(\tilde{a})}{d\tilde{a}} d\tilde{a} = \mu p_a(r) = \frac{\mu E^*}{\pi} \int_r^a \frac{1}{\sqrt{\tilde{a}^2 - r^2}} \frac{dg(\tilde{a})}{d\tilde{a}} d\tilde{a} \quad (46)$$

can be solved for function $\Phi(\tilde{a})$.

In case of a very small area of the slip domain, i.e. if $a - c \ll a$, this solution is elementary, because $r \approx a$ and therefore

$$d\Phi = \lambda dg, \quad \text{for } c < x < a \quad (47)$$

with $\lambda = \frac{\mu E^*}{4Ga}$.

Geometrically, (47) together with (43) describes the following indentation process: First the indenter is pressed into the half space in a pure normal direction until the radius of stick domain c is reached. After that any infinitesimal indentation is a superposition of normal and torque loading, bound by (47). The solution of (47) with the boundary conditions (24) and (5) is given by

$$\Phi(x) = \varphi + \lambda(g(x) - d), \quad \text{for } c < x < a. \quad (48)$$

Hence,

$$u_y(x) = x \begin{cases} \varphi, & \text{for } x < c \\ \lambda u_z(x), & \text{for } c < x < a \end{cases} . \quad (49)$$

Again, as we assumed $a - c \ll a$, it is $x \approx a$ in the slip domain and therefore

$$u_y(x) = \begin{cases} x\varphi, & \text{for } x < c \\ \frac{\mu E^*}{4G} u_z(x), & \text{for } c < x < a \end{cases} \quad (50)$$

If we choose $\mu^* = 2\mu$ as the equivalent coefficient of friction in the MDR-model for torsion, (50) can be written in the form

$$u_y(x) = \begin{cases} x\varphi, & \text{for } x < c \\ \frac{\mu^* \Delta k_z}{\Delta k_y} u_z(x), & \text{for } c < x < a \end{cases} . \quad (51)$$

The radius of the stick domain is given by

$$8G\varphi c = 2\mu E^* (g(a) - g(c)) = \mu^* E^* (g(a) - g(c)) , \quad (52)$$

which agrees with the condition of no slip for the springs at the edge of the stick domain in the MDR-model. That is why this torsional contact problem with a finite coefficient of friction can be described by the MDR.

We emphasize again that the derivation starting with (47) is only valid for $a - c \ll a$.

In the case of general partial slip the solution for $\Phi(\tilde{a})$ in the slip domain is given by the inverse Abel transform of (46) [12]:

$$\Phi(a) - \Phi(x) = \frac{\mu}{2G} \int_x^a \frac{p(r)dr}{\sqrt{r^2 - x^2}}, \quad \text{for } c < x < a \quad (53)$$

However, the resulting necessary spring displacement of the MDR-model

$$u_y(x) = x(\Phi(a) - \Phi(x)) = \frac{\mu x}{2G} \int_x^a \frac{p(r)dr}{\sqrt{r^2 - x^2}}, \quad \text{for } c < x < a \quad (54)$$

cannot be interpreted as easily as in the case described above in (47) - (51).

5. CONCLUSION

In the present paper, we have extended the method of dimensionality reduction to contacts subjected to a superimposed normal and tangential loading. For the case of the simultaneous normal and torsional loading we have shown that the consideration of the original three-dimensional contact problem can be replaced by a contact with a one-dimensional elastic foundation with a properly defined coefficient of friction and normal and tangential stiffness if the slip annulus is small compared to the contact radius.

Acknowledgements: *This work was supported in parts by the German Research Society and the Tomsk State University Academic D.I. Mendeleev Fund Program.*

REFERENCES

1. Lubkin J.L., 1951, *The torsion of elastic spheres in contact*, Journal of Applied Mechanics, 18, pp. 183-187.
2. Hetényi M., McDonald Jr. P.H., 1958, *Contact Stresses Under Combined Pressure and Twist*, Journal of Applied Mechanics, 25, pp. 396-401.
3. Kartal M.E., Hills D.A., Nowell D., Barber J.R., 2010, *Torsional contact between elastically similar flat-ended cylinders*, International Journal of Solids and Structures, 47, pp. 1375-1380.
4. Jaeger J., 1995, *Axi-symmetric bodies of equal material in contact under torsion or shift*, Archive of Applied Mechanics, 65, pp. 478-487.
5. Trejo M., Fretigny C., Chateauminois A., 2013, *Friction of viscoelastic elastomers with rough surfaces under torsional contact conditions*, Physical Review, E88, 052401.
6. Popov V.L., Psakhie S.G., 2007, *Numerical simulation methods in tribology*, Tribology International, 40, pp. 916-923.
7. Hess M., 2011, *Über die exakte Abbildung ausgewählter dreidimensionaler Kontakte auf Systeme mit niedrigerer räumlicher Dimension*, Cullier Verlag, Berlin.
8. Popov V.L., Hess M., 2015, *Method of dimensionality reduction in contact mechanics and friction*, Springer.
9. Popov V.L., 2015, *Kontaktmechanik und Reibung*, 3. überarbeitete Auflage, Springer.
10. Popov V.L., Hess M., 2014, *Method of dimensionality reduction in contact mechanics and friction: A users handbook. I. Axially symmetric contacts*, Facta Universitatis, Mechanical Engineering, 12(1), pp. 1-14.
11. Jaeger J., 2005, *New Solutions in Contact Mechanics*, WIT Press.
12. Bracewell R., 1965, *The Fourier Transform and Its Applications*, McGraw-Hill Book Company.
13. Johnson K.L., 2001, *Contact mechanics*, Cambridge University Press.

Chapter 6

Approximate Solutions using the Method of Dimensionality Reduction

SIMULATION OF FRICTIONAL DISSIPATION UNDER BIAXIAL TANGENTIAL LOADING WITH THE METHOD OF DIMENSIONALITY REDUCTION

UDC 531.4

Andrey V. Dimaki¹, Roman Pohrt², Valentin L. Popov^{2,3,4}

¹Institute of Strength Physics and Materials Science SB RAS, Tomsk, Russia

²Berlin University of Technology, Germany

³National Research Tomsk Polytechnic University, Russia

⁴National research Tomsk State University, Russia

Abstract. *The paper is concerned with the contact between the elastic bodies subjected to a constant normal load and a varying tangential loading in two directions of the contact plane. For uni-axial in-plane loading, the Cattaneo-Mindlin superposition principle can be applied even if the normal load is not constant but varies as well. However, this is generally not the case if the contact is periodically loaded in two perpendicular in-plane directions. The applicability of the Cattaneo-Mindlin superposition principle guarantees the applicability of the method of dimensionality reduction (MDR) which in the case of a uni-axial in-plane loading has the same accuracy as the Cattaneo-Mindlin theory. In the present paper we investigate whether it is possible to generalize the procedure used in the MDR for bi-axial in-plane loading. By comparison of the MDR-results with a complete three-dimensional numeric solution, we arrive at the conclusion that the exact mapping is not possible. However, the inaccuracy of the MDR solution is on the same order of magnitude as the inaccuracy of the Cattaneo-Mindlin theory itself. This means that the MDR can be also used as a good approximation for bi-axial in-plane loading.*

Key Words: *Friction, Dissipation, Tangential Contact, Biaxial In-plane Loading, Circular Loading, Cattaneo, Mindlin, MDR*

1. INTRODUCTION

Friction is a dissipative process transforming mechanical energy into heat and material changes of the contacting partners. The energy dissipation may be connected with material dissipation (wear) [1] or utilized for structural damping [2]. Studying both wear and

Received May 03, 2017 / Accepted June 20, 2017

Corresponding author: Andrey V. Dimaki

Institute of Strength Physics and Materials Science SB RAS, Akademicheskii av. 2/4, 634055 Tomsk, Russia

E-mail: dav@ispms.tsc.ru

damping requires the solution of a tangential contact problem. The simplest case of a tangential loading is an increasing uni-axial tangential loading at a constant normal force. This problem has been solved first by Cattaneo [3] and later independently by Mindlin [4]. They have shown that a tangential stress distribution can be represented as a superposition of two solutions for the normal contact problem of the same geometry, only multiplied with the coefficient of friction. This reduction to the normal contact problem is exactly the feature which allows the application of the method of dimensionality reduction (MDR) [5], (see also Chapter 5 devoted to tangential contact in [6]). However, Cattaneo and Mindlin have not noticed a small inconsistency in their solution. In their theory, it is assumed that the frictional stresses in the slip domain are all directed in the direction of the applied tangential force. With the exception of the unrealistic case where both the contacting materials have Poisson ratio zero, this assumption violates the condition that at every position in the slip domain, the slip is directed in the direction opposing the tangential stresses. The reason for this is the presence of an additional slip motion perpendicular to the direction of the applied force. This was first pointed out by Johnson [7] who showed that the maximum inclination of slip angle is on the order of magnitude $v/(4-v)$ which is equal to 0.09 for $v=1/3$ and 0.14 for $v=1/2$. He concluded that the error is not large and that the Cattaneo-Mindlin solution is a good approximation. Later comparisons with numerical solutions have shown that the above mentioned inconsistency may have an important influence on the distribution of wear but has almost no impact on the macroscopic force-displacement relations [8]. A detailed analysis can be found also in [9].

In the present paper we consider a more complicated problem of bi-axial oscillating loading (superimposed loading in two in-plane directions). The aim of the paper is twofold: on one hand, we are interested in a better understanding of the energy dissipation in bi-axially loaded contacts; on the other hand, we would like to check the applicability of the dimensionality reduction method to this class of problems. At present, there are only a few numerical studies providing the dependencies of dissipated friction energy on the parameters of loading [10]. The applicability of the MDR would provide a simple tool for simulating arbitrary loading histories with applications in the dynamics of structures with frictional contacts.

2. ENERGY DISSIPATION IN A SINGLE-POINT CONTACT FOR CIRCULAR MOVEMENT

Let us start by considering a single isotropic linearly elastic massless element which can deform in normal direction as well as in two tangential directions. We will call this element a “spring”. The spring should have out-of-plane stiffness k_z and isotropic in-plane stiffness $k_x=k_y$. It is first pressed against a rigid half-plane with a normal force F_z and then moved in the direction of the x -axis. We will assume that at the immediate contact point between the spring and the substrate, there is friction characterized by a constant coefficient of friction μ . When the free end of the spring is moved horizontally, it first deforms elastically until the in-plane displacement achieves the critical value

$$l_0 = \mu F_z / k_x . \quad (1)$$

After this, the lower contact point starts sliding and the force remains constant.

If the spring is moved on a circle with radius $R < l_0$, then it remains in the stick state at any time. However, if the radius of movement exceeds critical value, $R \geq l_0$, the contact

point will slip. In the stationary state, it will move in a circle with a smaller radius r_c , while the in-plane displacement of the spring remains constant and equal to l_0 . The frictional force is assumed to be opposite to the elastic force and at the same time it has to be directed opposite to the velocity vector. Therefore, the contact point between the spring and the half-plane will move in the direction of the elastic displacement. On the other hand, this velocity will be directed tangentially to the inner circle with radius r_c , which means that the elastic displacement of the spring is directed tangentially to this circle, as shown in Fig. 1. The dissipation power is then obviously given by the equation

$$\dot{W} = v_{\text{macro}} \cdot \mu F_z \cdot \cos \theta = v_{\text{macro}} \mu F_z \sqrt{1 - (l_0 / R)^2}, \quad (2)$$

where v_{macro} is the absolute velocity of the spring motion. For one cycle of motion with radius $R > l_0$ the value of the dissipated energy is

$$W = \dot{W} \Delta t_{\text{cycle}} = 2\pi R \mu F_z \sqrt{1 - (l_0 / R)^2}, \quad (3)$$

where Δt_{cycle} is the time needed to perform one cycle of circular motion. If the initial position of the spring does not correspond to the stationary one, it moves on a spiral asymptotically approaching the circle with radius r_c as shown in Fig. 1b.

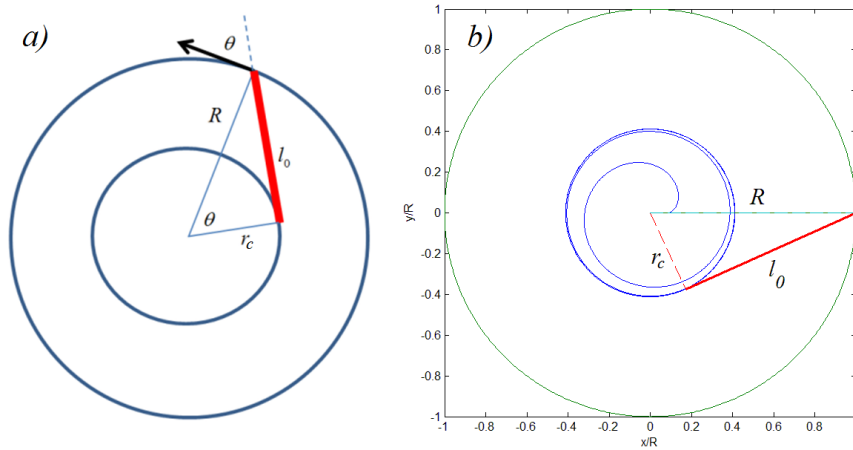


Fig. 1 a) The scheme of a circular motion of a single spring; b) The results of the numerical simulation: the evolution of the trajectory of a single spring during a circular motion

3. ENERGY DISSIPATION IN A CURVED CONTACT FOR CIRCULAR MOVEMENT

Generally, a non-conforming contact between elastic solids cannot be modeled with a single spring. In the case of uni-axial in-plane loading, the contact problem can be reduced to a contact of a rigid plane profile with a series of independent springs. This method is known as the method of dimensionality reduction [5, 6, 11]. It replaces a contact between two continuum bodies with an ensemble of independent one-spring problems and thus reduces the general contact problem to the above one-spring problem (see Fig. 2).

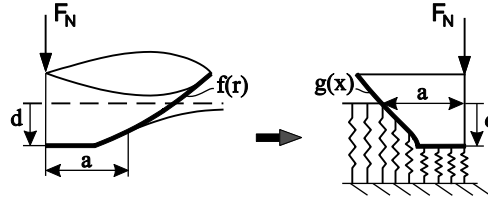


Fig. 2 Mapping of a three-dimensional contact into one-dimensional one

If the MDR-procedure was applicable to the bi-axial in-plane loading, then we could compute the energy dissipation rate just by summing Eq. (2) over all effective springs of the MDR-model. Let us *assume* at this point that this is indeed possible and calculate the dissipation in a circularly moving and curved contact. Later we will check and discuss the accuracy of this procedure.

We consider the movement of a parabolic indenter having the shape $z=f(r)=r^2/(2r_0)$. According to the MDR-rules [5, 6], in the equivalent MDR model it is to be replaced by the plane profile

$$g(x) = |x| \int_0^{|x|} \frac{f'(r) dr}{\sqrt{x^2 - r^2}} = \frac{x^2}{r_0}. \quad (4)$$

This profile is brought into contact with an elastic foundation consisting of independent springs, each spring having normal stiffness Δk_z and equal tangential stiffnesses Δk_x and Δk_y for the displacements along the x -axis and y -axis (not shown in Fig. 2) which are defined according to the rules

$$\Delta k_z = E^* \Delta x, \quad \Delta k_x = \Delta k_y = G^* \Delta x, \quad (5)$$

where

$$\frac{1}{E^*} = \frac{1-\nu_1^2}{E_1} + \frac{1-\nu_2^2}{E_2} \quad \text{and} \quad \frac{1}{G^*} = \frac{(2-\nu_1)}{4G_1} + \frac{(2-\nu_2)}{4G_2}, \quad (6)$$

with E_1 and E_2 being the Young's moduli, G_1 and G_2 the shear moduli and ν_1 and ν_2 the Poisson's ratios of the contacting bodies. Further, throughout the paper, we assume that the contacting materials satisfy the condition of "elastic similarity"

$$\frac{1-2\nu_1}{G_1} = \frac{1-2\nu_2}{G_2}, \quad (7)$$

which guarantees the decoupling of normal and tangential contact problems [12].

If the indentation depth is d , then the vertical displacement of an individual spring at position x is given by

$$u_{z,1D}(x) = d - g(x) \quad (8)$$

and the normal force of a single spring equals to

$$\Delta F_z(x) = \Delta k_z (d - g(x)) = E^* \Delta x (d - g(x)). \quad (9)$$

The dissipation power in one spring at the position x is given by Eq. (2) which we rewrite here as

$$\Delta \dot{W} = \mu \Delta F_z \sqrt{1 - \left(\mu \frac{\Delta F_z}{R \Delta k_x} \right)^2} = v_{\text{macro}} \mu E^* \Delta x (d - g(x)) \sqrt{1 - \left(\mu \frac{E^* (d - g(x))}{G} \right)^2}. \quad (10)$$

Let us assume that we have a situation with partial slip. Radius c of the stick region is determined by the condition

$$d - g(c) = \frac{1}{\mu} R \frac{G^*}{E^*} \quad (11)$$

whence

$$\frac{c^2}{r_0} = d - \frac{1}{\mu} R \frac{G^*}{E^*}. \quad (12)$$

The whole dissipation power is thus equal to

$$\dot{W} = \frac{2v_{\text{macro}} \mu E^*}{r_0} \int_c^a (a^2 - x^2) \sqrt{1 - \left(\frac{a^2 - x^2}{a^2 - c^2} \right)^2} dx, \quad (13)$$

where $a = \sqrt{r_0 d}$ is the contact radius. Evaluation of the integral yields

$$\dot{W} = \frac{3}{2} v_{\text{macro}} \mu F_z \Phi(\tilde{c}), \quad (14)$$

where

$$\Phi(\tilde{c}) = \int_{\tilde{c}}^1 (1 - \xi^2) \sqrt{1 - \left(\frac{1 - \xi^2}{1 - \tilde{c}^2} \right)^2} d\xi \quad (15)$$

with $\tilde{c} = c/a$. Function $\Phi(\tilde{c})$ is shown in Fig. 3. From (14) we see that the energy dissipation power is given by the formally calculated "nominal power" $v_{\text{macro}} \mu F_z$ multiplied with function $\frac{3}{2} \Phi(\tilde{c})$, which only depends on the reduced radius of the stick area.

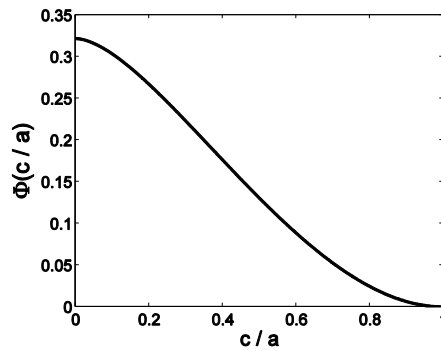


Fig. 3 Dependence $\Phi(\tilde{c})$

4. CALCULATION OF STRESSES IN THE FRAMEWORK OF MDR

The above MDR-solution is based on the Coulomb criterion for sticking and sliding for the springs of the effective one-dimensional elastic foundation. This MDR model gives the correct solution to the three-dimensional problem only if the conditions for sticking and sliding are fulfilled also for in-plane stresses in relation with normal stresses in the initial (truly three-dimensional) problem. We thus begin our analysis by checking the fulfillment of the sticking conditions and go later to an additional validation by comparison with results of direct 3D simulation given in [10].

According to the MDR rules, the distribution of normal pressure p in the three-dimensional problem may be calculated using the following integral transformation [11]:

$$p(r) = -\frac{1}{\pi} \int_r^\infty \frac{q'_z(x)}{\sqrt{x^2 - r^2}} dx, \quad (16)$$

where $q_z(x) = \Delta F_z(x) / \Delta x$ is a linear density of the normal force. A similar transformation is valid for the tangential stress:

$$\tau_x(r) = -\frac{1}{\pi} \int_r^\infty \frac{q'_x(x)}{\sqrt{x^2 - r^2}} dx, \quad (17)$$

where $q_x(x) = \Delta F_x(x) / \Delta x$ is a linear density of the tangential reaction force, respectively. The proof for these rules can be found in Appendix D of Ref. [5]. This proof can be easily generalized to an arbitrary two in-plane dimensions and shows that the transformation (17) can be applied separately to each component of tangential stress, so we can obtain tangential stresses in y-direction similar to Eq. (17):

$$\tau_y(r) = -\frac{1}{\pi} \int_r^\infty \frac{q'_y(x)}{\sqrt{x^2 - r^2}} dx. \quad (18)$$

Thus, for calculating the stress component we have to determine first the linear force densities $q_x(x) = \Delta F_x(x) / \Delta x$ and $q_y(x) = \Delta F_y(x) / \Delta x$.

Let us denote the coordinates of a spring tip as $(u_{x,tip}, u_{y,tip})$ and the coordinates of the upper point of the spring as (u_x, u_y) . Assume that in an iteration step the coordinates of the spring u_x and u_y , are changed by δu_x and δu_y , so that

$$\begin{cases} \tilde{u}_x = u_x + \delta u_x \\ \tilde{u}_y = u_y + \delta u_y \end{cases}. \quad (19)$$

If new coordinates \tilde{u}_x and/or \tilde{u}_y now lie outside a circle having a central point $(u_{x,tip}, u_{y,tip})$ and a radius $l_0(x)$:

$$l_0(x) = \mu \Delta F_z(x) / \Delta k_x, \quad (20)$$

then the spring tip will start to slide in the direction of the tangential reaction force (see Fig. 4) until it reaches the point $(\tilde{u}_{x,tip}, \tilde{u}_{y,tip})$:

$$\sqrt{(\tilde{u}_x - \tilde{u}_{x,tip})^2 + (\tilde{u}_y - \tilde{u}_{y,tip})^2} = l_0(x). \quad (21)$$

In other words, the new equilibrium point lays on the straight line connecting the points $(u_{x,tip}, u_{y,tip})$ and $(\tilde{u}_x, \tilde{u}_y)$, at distance $l_0(x)$ from $(\tilde{u}_x, \tilde{u}_y)$ (see Fig. 4).

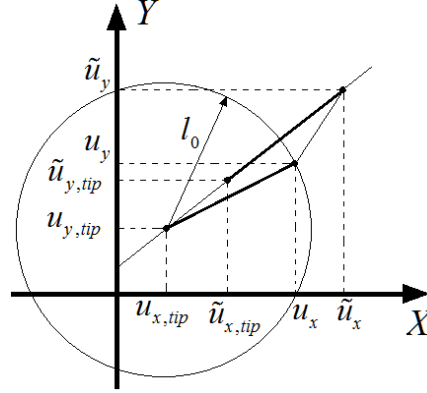


Fig. 4 The slip displacement of a single spring in XY plane under lateral motion

The components of the tangential reaction force of the spring can be found as follows:

$$\begin{cases} \Delta F_x(x) = \Delta k_x (u_x - u_{x,tip}) \\ \Delta F_y(x) = \Delta k_y (u_y - u_{y,tip}) \end{cases} \quad (22)$$

We have studied the frictional energy dissipation for the parabolic indenter with the following fictive parameters: $r_0=1$ m, $E^*=1$ GPa, $d=0.001$ m, $\nu=0.28$, $\mu=0.3$. The indenter was initially moved to the point $(U_{x0}, 0)$ and then subjected to an in-plane harmonic displacement

$$\begin{cases} U_x(t) = U_{x0} \cos(\omega t) \\ U_y(t) = U_{y0} \sin(\omega t) \end{cases} \quad (23)$$

Controlling the tangential reaction forces in Ox and Oy directions, it is possible to introduce the force-dependent governing parameters, following the paper of Ciavarella [10]:

$$Q / \mu F_z \text{ and } R_M = Q_x / Q_y, \quad (24)$$

where

$$Q_x = \max |F_x(t)|, \quad Q_y = \max |F_y(t)|, \quad Q = \sqrt{Q_x^2 + Q_y^2}. \quad (25)$$

Note that the value of Q , defined in Eq. (25), does not correspond to any real tangential force acting on the indenter, but it serves only as a governing parameter in the parametric study of the problem under consideration.

With Eq. (22) we determine linear force densities $q_x(x)=\Delta F_x(x)/\Delta x$ and $q_y(x)=\Delta F_y(x)/\Delta x$. We then calculate the tangential stress components given by Eqs. (17) and (18) and finally the absolute value of the tangential stress:

$$\tau_{MDR}(r) = \sqrt{\tau_x^2(r) + \tau_y^2(r)} \quad (26)$$

The corresponding dependencies are presented in Fig. 5 together with the normal stress distribution multiplied with the coefficient of friction and the formal Mindlin solution with the same radius of stick region (dashed lines in Fig. 5). One can see that the obtained stress distributions do not exactly fulfill the conditions for stick and slip. In most ranges of radii smaller than the stick radius, the tangential stress is smaller than the normal stress multiplied with the coefficient of friction; there is only a small region inside the stick radius with τ too high. Thus the stick condition is fulfilled not exactly but in good approximation. However, for radii moderately larger the stick radius, the tangential stress is higher than the normal stress times the coefficient of friction, which means that the sliding condition is not fulfilled. At even larger radii, the condition that in the sliding region the tangential stress must be equal to normal stress times the coefficient of friction is fulfilled with good accuracy. Thus, the tangential stress distribution has a qualitatively correct shape but it does not exactly match the stick and slip conditions.

The mentioned discrepancy is observed only in a relatively narrow interval of radii. Thus, the integral influence of this error may be moderate. This situation can be compared with the solution by Cattaneo and Mindlin which also has a local error, but the global error in the force-displacement relations is moderate and is generally tolerated.

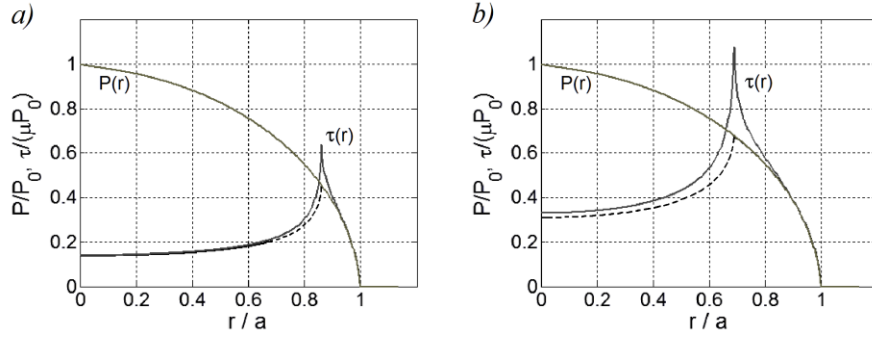


Fig. 5 The distributions of normal pressure and the absolute value of tangential stress. P_0 is the pressure under the axis of the indenter. The dashed line indicates the formal Mindlin solution with the same radius of stick region. $R_M = 1$. a) $Q/\mu F_z = 0.5$; b) $Q/\mu F_z = 0.9$

In order to estimate the possible global error, let us determine the integral discrepancy between the obtained stress distribution and the Cattaneo-Mindlin distribution [3] (which fulfils the stick and slip conditions):

$$\Delta = 100\% \cdot \left| \frac{2\pi \int_0^a \tau_{\text{MDR}}(r) r dr - 2\pi \int_0^a \tau_{\text{CM}}(r) r dr}{2\pi \int_0^a \tau_{\text{CM}}(r) r dr} \right|, \quad (27)$$

where $\tau_{\text{CM}}(r)$ corresponds to the Cattaneo-Mindlin solution. This discrepancy is shown in Fig. 6. The integral difference between tangential stresses, predicted by the theory of Cattaneo-Mindlin, and the MDR results, is about two percent for low values of $Q/\mu F_z$ and R_M . This means that the above MDR theory has a good accuracy at least for oscillations with small amplitude comparable to the full slip displacement.

Further, let us compare the results of MDR simulation with the full three-dimensional calculations. The tangential stresses are calculated using MDR as described above for the following set of parameters: $R_M = 1$, $Q = 0.9$, which correspond to the same values as used in Ref. [10]. Comparison of the MDR results with results of full three-dimensional simulations is presented in Fig. 7.

In Fig. 7, on the left hand side, the stress-field simulated by the MDR is presented and so is, on the right hand side, the stress field from the three-dimensional simulation [10]. While both results are in a good qualitative agreement, one can also see some differences. Firstly, the stick radius in the MDR results does not decrease after the start of the in-plane rotation, which can be connected to the application of the tangential displacement instead of tangential forces in 3D simulation. Secondly, the tangential stresses in the stick area in the MDR solution are higher than those in the full 3D calculation. However, the mentioned discrepancies between the MDR results and full 3D calculations are moderate. We can conclude that the MDR can be also used with “engineering accuracy” for contact problems with bi-axial in-plane loading.

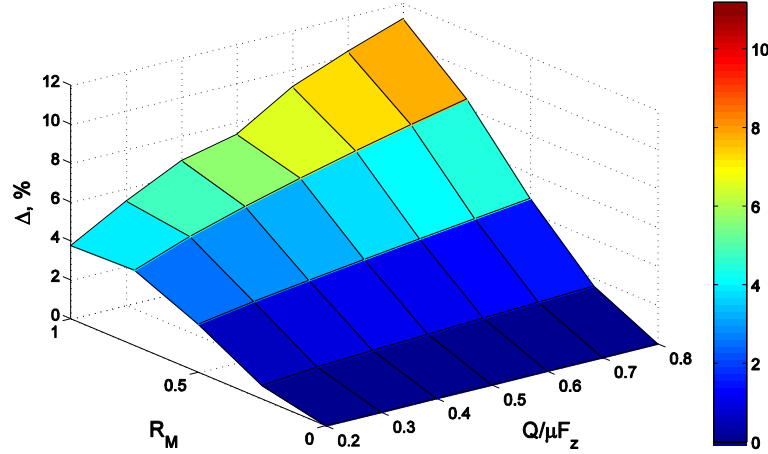


Fig. 6 The integral difference (27) between tangential stresses, predicted by the Cattaneo-Mindlin theory, and the MDR results

5. NUMERICAL SIMULATION OF DISSIPATION UNDER NON-CIRCULAR MOTION

In this paragraph we apply the MDR within its range of accuracy for studying energy dissipation in a contact subject to biaxial tangential loading with different oscillation amplitudes in two perpendicular directions. In order to normalize values of dissipated energy we use the solution of Mindlin [3] for friction energy dissipation during one cycle of a uniaxial tangential loading:

$$W_C = W_{R_M=0} = \frac{9\mu^2 F_z^2}{10a} \frac{2}{G^*} \left\{ 1 - \left(1 - \frac{Q}{\mu F_z} \right)^{5/3} - \frac{5Q}{6\mu F_z} \left[1 + \left(1 - \frac{Q}{\mu F_z} \right)^{2/3} \right] \right\}. \quad (28)$$

In the performed calculations we have varied the governing parameters (24) in a wide range of values. The results of simulation, accompanied with the corresponding results of the full 3D simulations, given in Ref. [10], are shown in Fig. 8a. It can be seen that the MDR results are in a good agreement with the results of the full 3D simulations, except for the curve for $R_M = 1$ which also is in a qualitative agreement but shows distinctive quantitative differences.

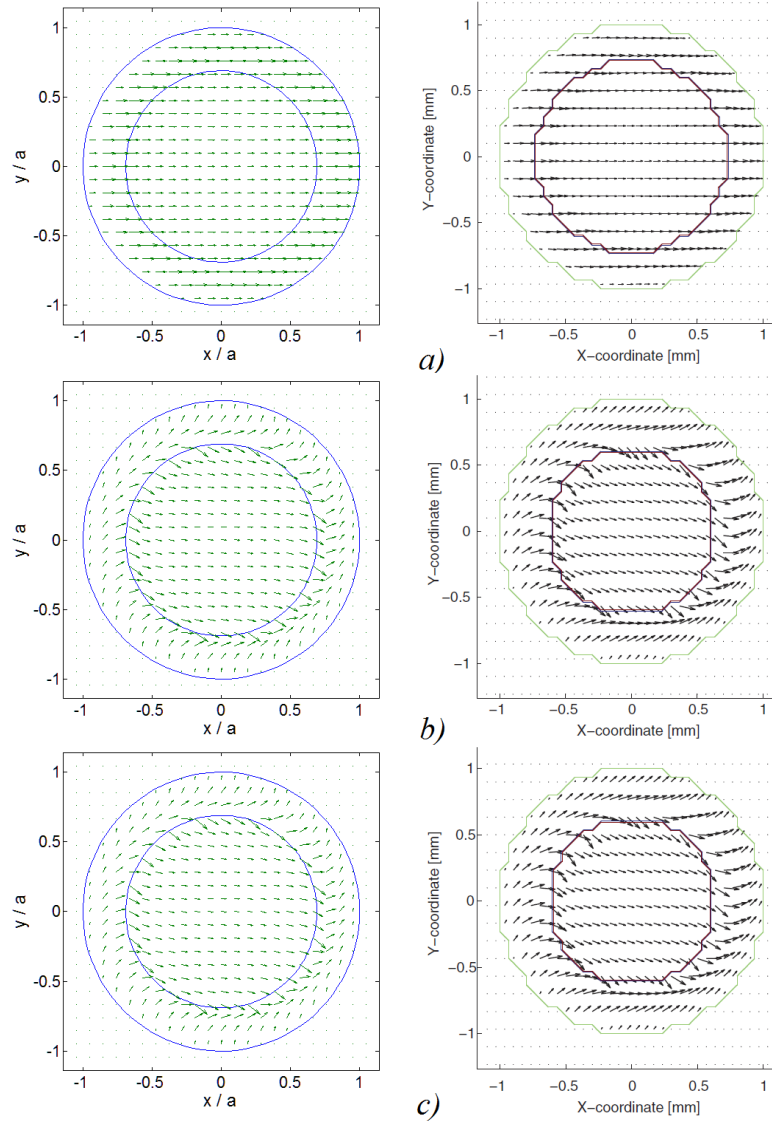


Fig.7 The distributions of tangential stresses in the contact area - the results of the MDR simulation in the left column, the results of the full 3D simulation, from Ref. [10], in the right column: a) after the initial displacement; b) after one revolution; c) after two revolutions; $R_M=1$, $Q=0.9$. The inner circle indicates the stick area

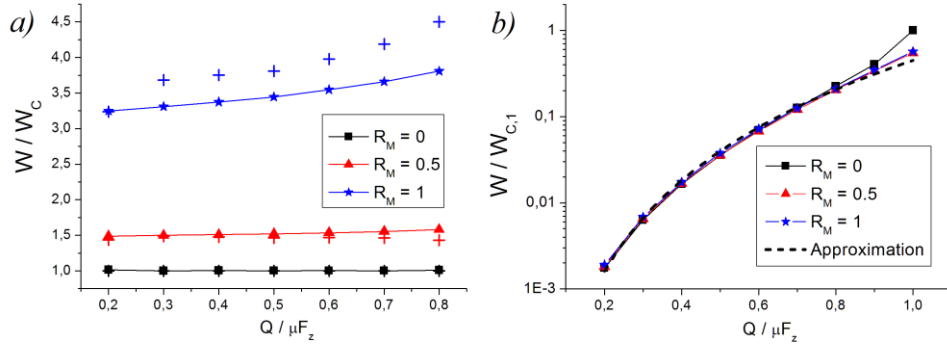


Fig. 8 a) The normalized dependencies of the energy, dissipated during one cycle of the circular motion, compared with the data from Ref. [10] (indicated by the crosses); b) The normalized dependencies of the energy, dissipated during one cycle of the circular motion, reduced into the universal curve. The normalizing factor $W_{1,C}$ is given by Eq. (29)

We have found that for various values of R_M , the dependencies of W on $Q/\mu F_z$ can be reduced to a universal curve (Fig. 8b). The results are normalized to the value of the energy $W_{1,C}$ dissipated during one cycle of uniaxial loading with $Q/\mu F_z=1$:

$$W_{1,C} = W_{R_M=0, Q=\mu F_z} = \frac{3\mu^2 F_z^2}{10aG^*}. \quad (29)$$

The universality of the given curve holds for relatively small amplitudes of oscillations. When the amplitude of oscillations becomes comparable with the value of amplitude needed for gross slip transition, the deviations from the universal curve appear (see Fig. 8b). We suggest a power-law approximation of the data shown in Fig. 8b as follows:

$$W = 0.45W_{1,C}(Q/\mu F_z)^{3.5}, \quad (30)$$

which fits the results of numerical simulations well for $Q/\mu F_z < 0.7$. Note that in Fig. 8b the curve for $R_M = 0$ coincides with the results of Cattaneo and Mindlin.

6. CONCLUSIONS

By analyzing the stick and slip conditions and comparing with three-dimensional calculations we have explored the question whether the MDR is applicable for the simulation of bi-axial in-plane loadings. We have found that the corresponding mapping is not exact (there are local violations of stick and slip conditions) but has an acceptable accuracy comparable with the accuracy of the Cattaneo and Mindlin solution for tangential contact. Comparison with three-dimensional simulations shows a good qualitative agreement but some quantitative deviations. We have found that the dependencies of the dissipated energy on the amplitude of loading, obtained for various values of R_M , fit into one universal curve. This curve may be approximated by a power law in the range of small values of $Q/\mu F_z < 0.7$. The obtained results may be helpful for a better understanding of the mechanics of tangential contacts under bi-axial loading.

Acknowledgements: *A.V. Dimaki is thankful for the funding of the Fundamental Research Program of the State Academies of Sciences for 2013–2020. R. Pohrt and V.L. Popov thank V. Aleshin for helpful discussions.*

REFERENCES

1. Dimaki, A.V., Dmitriev, A.I., Chai, Y.S., Popov, V.L., 2014, *Rapid simulation procedure for fretting wear on the basis of the method of dimensionality reduction*, Int. J. Solids and Struct., 51, pp. 4215-4220.
2. Ginsberg, J.H., 2001, *Mechanical and Structural Vibrations: Theory and Applications*. Wiley, 704 p.
3. Cattaneo C., 1938, *Sul contatto di due corpi elastici: distribuzione locale degli sforzi*, Rendiconti dell'Accademia nazionale dei Lincei, 27, 342-348, 434-436, 474-478.
4. Mindlin, R.D., Mason, W.P., Osmer, T.F., Deresiewicz, H., 1951, *Effects of an oscillating tangential force on the contact surfaces of elastic spheres*, Proc. First US National Congress of Appl. Mech., pp. 203–208.
5. Popov, V.L., Heß, M., 2015, *Method of Dimensionality Reduction in Contact Mechanics and Friction*, Berlin, Heidelberg: Springer, 265 p.
6. Popov, V.L., 2017, *Contact Mechanics and Friction. Physical Principles and Applications*, 2nd Edition, Berlin, Heidelberg: Springer, 391 p.
7. Johnson, K.L., 1955, *Surface interaction between elastically loaded bodies under tangential forces*, Proceedings of the Royal Society, A230, p. 531-548.
8. Munisamy, R.L., Hills D.A., Nowell D., 1994, *Static Axisymmetric Hertzian Contacts Subject to Shearing Forces*, ASME Journal of Applied Mechanics, 61, pp. 278-283.
9. Gallego, L., Nelias, D., and Deyber, S., 2010, *A fast and efficient contact algorithm for fretting problems applied to fretting modes I, II and III*, Wear, 268.1, pp. 208-222.
10. Ciavarella, M., 2013, *Frictional energy dissipation in Hertzian contact under biaxial tangential harmonically varying loads*, J. Strain Analysis, 49(1), pp. 27–32.
11. Popov, V.L., Hess, M., 2014, *Method of dimensionality reduction in contact mechanics and friction: a user's handbook. I. Axially-symmetric contacts*, Facta Univ. Mech. Engng. 12, pp. 1-14.
12. Johnson, K.L., 1985, *Contact mechanics*, Cambridge: Cambridge University Press, 452 p.

ANALYSIS OF IMPACT ON COMPOSITE STRUCTURES WITH THE METHOD OF DIMENSIONALITY REDUCTION

UDC 539.3

Valentin L. Popov

Berlin University of Technology, Germany
National Research Tomsk State University, Russia

Abstract. *In the present paper, we discuss the impact of rigid profiles on continua with non-local criteria for plastic yield. For the important case of media whose hardness is inversely proportional to the indentation radius, we suggest a rigorous treatment based on the method of dimensionality reduction (MDR) and study the example of indentation by a conical profile.*

Key Words: *Contact Mechanics, Impact, Plasticity, Non-local Constitutive Relations, Roughness, Reduction of Dimensionality*

1. INTRODUCTION

Constitutive relations for materials are mostly formulated in terms of stresses and deformations. Correspondingly, the critical behavior of materials is generally described by parameters having the dimension of stress such as yield stress, fracture stress or hardness. Further, the constitutive relations are in most cases assumed to be local relations. However, it is well known that the processes of plastic deformation, damage and fracture, independently of the detailed mechanism, are always non-local processes. For dislocation plasticity, this immediately follows from the mechanism of deformation by formation of shear zones [1]. Each elementary event of plastic deformation is a non-local process [2, 3]. The same is valid for fracture processes: both the initial concept of Griffith [4] and its later microscopic [5] and macroscopic [6] generalizations are intrinsically non-local. In the past, there was much effort to address the non-locality in the frame of gradient generalizations of both theory of elasticity and plasticity [7, 8, 9, 10]. Practitioners often take the non-locality into account by introducing critical stresses

Received: January 02, 2015

Corresponding author: Valentin Popov

Berlin University of Technology, 10623 Berlin, Germany; National Research Tomsk State University, 634050 Tomsk, Russia

E-mail: v.popov@tu-berlin.de

depending on the size of the system or the size (or depth) of indentation. Thus, in [12], it is shown that the strength of micro contacts of Au-Au and Au-Pt is proportional to the contact radius for the contact radiuses between 10 and 100 nm, meaning that the “fracture stress” is inversely proportional to the contact radius. While for metals this size dependence is observed only at a sufficiently small scale, for composites it can be valid already at the macroscopic scale. The same is valid for plastic yielding: the nonlocal nature of plastic deformation leads to the size dependence of the “yield stress”. In [11], it is shown that the indentation hardness of polydimethylsiloxan (PDMS) is inversely proportional to the indentation depth over three decimal orders of magnitude. Similar dependencies are observed by nanoindentation of Au [13]. Such dependence of the characteristic parameters on the size of the system shows of course an inconsistency in the theory and should be replaced by an appropriate non-local formulation.

In the following we confine ourselves to the processes of plastic deformation and damage prior to the complete fracture of a structure. The whole spectrum of non-local yield criteria and thus the dependence of the hardness on the size of an indenter can be very roughly divided into three classes:

- (a) Constant hardness σ_c ,
- (b) Hardness, which is inversely proportional to indentation radius a : $\sigma_c = q_c / a$,
- (c) Hardness, which is inversely proportional to indentation area: $\sigma_c = f_c / a^2$.

In the cases (b) and (c), the hardness is in reality not a proper material parameter. It is rather quantity q_c having the dimension of surface energy density in the case (b) and quantity f_c having the dimension of the force in the cases (c), which now characterize unambiguously the plastic properties.

From the point of view of mechanisms of plasticity, the cases (a), (b) and (c) correspond to the situations where the plastic flow is governed by:

- (a) Volume processes, the characteristic critical quantity having the dimension of energy per volume or stress,
- (b) Surface processes, the characteristic critical property having the dimension of energy per area,
- (c) Line processes, the characteristic critical property having the dimension of energy per unit length.

All known criteria for plastic yielding either coincide with one of these classes or can be considered as their combinations.

In the present paper, we concentrate our attention only on the “intermediate” class of constitutive relations (b) and describe how the impact on materials with such non-local plastic criteria can be described using the *method of dimensionality reduction* (MDR) [14, 15, 16, 17].

2. METHOD OF DIMENSIONALITY REDUCTION

At the first glance, the non-local plasticity criterion (b) seems to be more complicated than the local criterion (a). However, the non-locality in three-dimensional systems can sometimes lead to a much simpler theoretical description than in the case of local relations. In a series of publications by Popov, Hess and co-authors (see e.g. [20, 14, 15, 16]), it is shown that the mechanical properties which in a three-dimensional system are

proportional to the contact diameter, can be easily mapped onto a contact with a one-dimensional elastic foundation. For example, this is the case for the contact stiffness of an arbitrary contact with an elastic half-space. The contact stiffness is proportional to the diameter of the contact and thus can be described naturally by a one-dimensional model. The same property is present in contact conductivity (both electrical and thermal) which thus can be described in the framework of MDR [21]. In the publications [14] and [22], it is shown that the mapping of the contact properties from 3D to 1D is exact for arbitrary bodies of revolution provided some rules are considered for recalculation of the material properties and profiles of the contacting bodies. In the case of plastic deformation with the indentation hardness inversely proportional to the contact radius (and thus the indentation force proportional to the radius), we again have a property, which is directly proportional to the contact radius. It is therefore logically to assume that the indentation with such a yield criterion will be correctly described within a one-dimensional model.

In the following, we shortly recapitulate the basics of the method of dimensionality reduction and then formulate its extension to the description of plasticity. If applied to a contact of a body with an elastic or viscoelastic half-space, the MDR consists of two main independent steps:

I. First, a viscoelastic half-space is replaced by a one-dimensional series of parallel springs with stiffness Δk_z and dash pots with damping constant $\Delta\gamma$ (Fig. 1):

$$\Delta k_z = E^* \Delta x, \quad \Delta\gamma = 4\eta\Delta x, \quad (1)$$

where E^* is the effective elastic modulus

$$\frac{1}{E^*} = \frac{1-\nu_1^2}{E_1} + \frac{1-\nu_2^2}{E_2}, \quad (2)$$

E_1 and E_2 are the Young's moduli of contacting bodies, ν_1 and ν_2 , their Poisson-ratios, and η the dynamic viscosity of the medium.

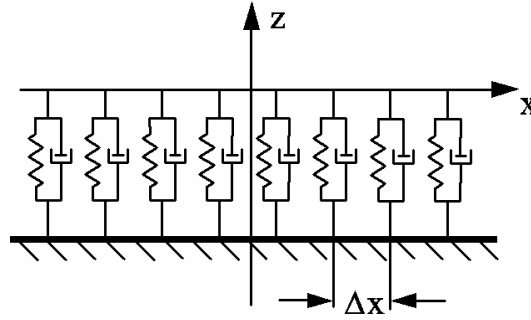


Fig. 1 Equivalent one-dimensional visco-elastic foundation

II. Secondly, the form of the indenter must be recalculated according to the following *rule of Hess*: If a body of revolution is described by equation $z = z(r)$, then the equivalent one-dimensional profile is defined as

$$z_{1D}(x) = |x| \int_0^{|x|} \frac{z'(r)}{\sqrt{x^2 - r^2}} dr. \quad (3)$$

It is proven in [14] and [22] that the contact of the modified 1D profile will provide *exactly* the same relations between the normal force, the indentation depth, and the contact radius as in the initial full three-dimensional problem. If the three-dimensional profile is described by a power-function with an arbitrary positive power n

$$z(r) = c_n r^n, \quad (4)$$

the equivalent one-dimensional profile is a power-function with the same power, but a modified coefficient:

$$z_{1D}(x) = c_n |x| \int_0^{|x|} \frac{nr^{n-1}}{\sqrt{x^2 - r^2}} dr = \tilde{c}_n |x|^n, \quad (5)$$

where

$$\tilde{c}_n = \kappa_n c_n \quad (6)$$

and

$$\kappa_n = \frac{\sqrt{\pi}}{2} \frac{n\Gamma(\frac{n}{2})}{\Gamma(\frac{n}{2} + \frac{1}{2})}. \quad (7)$$

$\Gamma(n)$ is the Gamma-function

$$\Gamma(n) = \int_0^{\infty} t^{n-1} e^{-t} dt. \quad (8)$$

In particular, for a cone ($n = 1$) we get $\kappa_1 = \pi/2$ and for a parabolic profile ($n = 2$) $\kappa_2 = 2$. This last case is known as the *rule of Popov* [14] (Fig. 2).

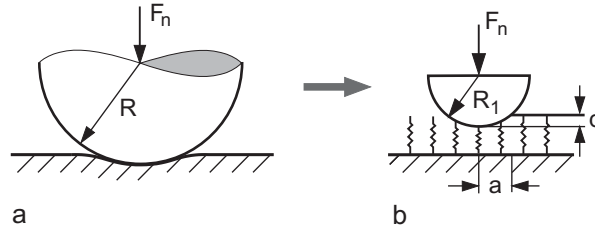


Fig. 2 (a) A three-dimensional contact and
(b) its one-dimensional representation in the MDR

The solution of the one-dimensional problem provides not only correct relations between the global properties (total force, indentation depth and contact radius), but allows to determine the exact three-dimensional distributions of stress. In the elastic foundation, normal forces $f(x)$ of separate springs are immediately determined for any contact configuration. We can define linear force density $q(x)$ by dividing these forces with spacing Δx :

$$q(x) = \frac{f(x)}{\Delta x}. \quad (9)$$

In [14], it is shown, that normal stress $\sigma_{zz}(r)$ in the contact area can be obtained from linear force density $q(x)$ by the following integral transformation:

$$\sigma_{zz}(r) = \frac{1}{\pi} \int_r^\infty \frac{q'(x)}{\sqrt{x^2 - r^2}} dx. \quad (10)$$

3. PLASTICITY CRITERION IN THE METHOD OF DIMENSIONALITY REDUCTION

As stated above, basically all properties which in three dimensions are proportional to the contact radius, can be easily mapped to an appropriate one-dimensional system. For plasticity, this is the case if the indentation force is proportional to the indentation radius:

$$F_N = \pi \sigma_c a^2 = \pi q_c a. \quad (11)$$

It is easily seen that we reproduce this behavior by introduction of the following criterion for plastic yielding of the one-dimensional model described in the previous Section:

$$f_c = \frac{\pi}{2} q_c \Delta x. \quad (12)$$

Note that while the three-dimensional criterion is a non-local one, the corresponding criterion in the equivalent one-dimensional model occurs to be local. Further numerical investigation of the model could lead to another coefficient of proportionality in Eq. (12), but they cannot change the functional form of this relation.

With criterion (12), the complete problem of an indentation in a “visco-elastic, non-locally plastic” medium is reduced completely to a contact problem with a one dimensional elastoplastic foundation with independent elements.

4. IMPACT OF CONICAL PROFILES ON THE MATERIAL WITH A NON-LOCAL YIELD CRITERION

As an illustration, let us consider an impact of a conical profile of the form

$$z = \tan \theta \cdot r \quad (13)$$

with an elastoplastic medium with the non-local yield criterion (11). According to the rule of Hess, the equivalent one-dimensional profile is given by

$$z = \frac{\pi}{2} \tan \theta \cdot |x|. \quad (14)$$

For indentation depth d , the displacement of a spring having coordinate x will be

$$u_z = d - \frac{\pi}{2} \tan \theta \cdot |x|. \quad (15)$$

The contact radius is obtained from condition $u_z(a) = d$, hence,

$$a = \frac{2}{\pi} \frac{d}{\tan \theta}. \quad (16)$$

The spring forces which are still in the elastic state are equal to

$$f(x) = E^* \Delta x \left(d - \frac{\pi}{2} \tan \theta \cdot |x| \right), \quad \text{for } f < \frac{\pi}{2} q_c \Delta x \quad (17)$$

After achieving the critical value, the spring force remains constant and equal to

$$f(x) = \frac{\pi}{2} q_c \Delta x. \quad (18)$$

Up to the indentation depth

$$d_c = \frac{\pi q_c}{2 E^*}, \quad (19)$$

there will be no plastic yielding of any spring. Thus, there exists a critical indentation force F_c for starting the plastic yielding:

$$F_c = 2E^* \int_0^{a_c} u_z(x) dx = 2E^* \int_0^{a_c} (d_c - (\pi/2) \tan \theta \cdot x) dx = \frac{\pi q_c^2}{2E^*} \frac{1}{\tan \theta}. \quad (20)$$

After exceeding the critical force, the inner part of the contact will be in the state of plastic yield. Radius c of the plastically deformed area is given by the condition $f(c) = \pi q_c \Delta x / 2$, hence

$$c = \frac{1}{\tan \theta} \left(\frac{2}{\pi} d - \frac{q_c}{E^*} \right), \quad a - c = \frac{q_c}{E^* \tan \theta} \quad (21)$$

The normal force is given by

$$F_N = 2E^* \int_c^a u_z(x) dx + \pi c q_c = F_c + \pi c q_c = F_c + \frac{2q_c}{\tan \theta} (d - d_c). \quad (22)$$

After achieving the critical state, the normal force increases linearly with the indentation depth.

We do not consider at this point the complete dynamic problem of an impact, which generally can also depend on the structure stiffness. We limit ourselves to the case of a very rapid impact, when the indentation depth is much larger than the critical one. In this case we can write $F_N \approx 2q_c d / \tan \theta$. The work of plastic deformation up to the maximum indentation will be

$$W \approx \int_0^{d_{\max}} \frac{2q_c}{\tan \theta} dd(d) = \frac{q_c d_{\max}^2}{\tan \theta}. \quad (23)$$

The area of contact will be equal to $A_{\max} = \pi a_{\max}^2 = \frac{4}{\pi \tan^2 \theta} d_{\max}^2$.

Thus, the damaged area will be proportional to the impact energy:

$$A_{\max} \approx \frac{4}{\pi q_c \tan \theta} W. \quad (24)$$

This differs from the result for the media with the local plastic criterion, where the impact energy is proportional to the expelled volume [18, 19].

5. CONCLUSION

In the present paper, we considered an indentation of a rigid profile into an elasto-plastic medium with a non-local yield criterion. We considered only the case where the non-locality leads to the inverse proportionality of the indentation hardness to the indentation radius. For such media, we have suggested a generalization of the method of dimensionality reduction and analyzed the case of indentation of a rigid conical indenter. As the method of dimensionality reduction is also valid for tangential contacts [23], the proposed method can be easily generalized for the case of impacts with a tangential component of impact velocity.

Acknowledgements: *Many valuable discussions with S. Psakhie, M. Ciavarella, S. Dubinsky and A. Ushakov are gratefully acknowledged. This work is supported in part by Tomsk State University Academic D.I. Mendeleev Fund Program.*

REFERENCES

1. Popov L. E., Kobayev V. S., Kovalevskaya T. A., 1982, *Concepts of strengthening and dynamic recovery in the theory of plastic deformation*, Russian Physics Journal, 25, pp. 520-541.
2. Popov L. E., Slobodskoi M. I., Kolupaeva S. N., 2005, *Simulation of single slip in FCC metals*, Russian Physics Journal, 49, pp. 62-73.
3. L. E. Popov, Kolupaeva S.N., Vihor N.A., Puspesheva S.I., 2000, *Dislocation dynamics of elementary crystallographic shear*, Computational materials science, 19(1), pp. 267-274.
4. Griffith A.A., 1921, *The phenomena of rupture and flow in solids*, Philos. Trans. R. Soc. Lond. Ser. A, 221, pp.163–198.
5. Prandtl L., 1933, *Ein Gedankenmodell für den Zerreivorgang spröder Körper*, ZAMM, J. Appl. Math. Mech., 13, pp. 129–133.
6. Rice J.R., 1968, *A Path Independent Integral and the Approximate Analysis of Strain Concentration by Notches and Cracks*, Journal of Applied Mechanics, 35, pp. 379–386.
7. Aifantis E.C., 1999, *Strain gradient interpretation of size effects*, Int. J. Fracture, 95, pp. 299–314.
8. Nix W.D., Gao H., 1998, *Indentation size effects in crystalline materials: a law for strain gradient plasticity*, Journal of the Mechanics and Physics of Solids, 46(3), pp. 411-425.
9. Gao H., Huang Y., Nix W.D., Hutchinson J.W., 1999, *Mechanism-based strain gradient plasticity—I. Theory*, Journal of the Mechanics and Physics of Solids, 47(6), pp.239-1263.
10. Popov V.L., 1992, *Gauge theory of plastically incompressible medium without dissipation. 1. Dispersion relations and propagation of perturbations without dissipation*, International Journal of Engineering Science, 30, pp. 329-334.
11. Wrucke A.J., Han C.-S., Majumdar P., 2013, *Indentation size effects of multiple orders of magnitude in Polydimethylsiloxane*, J. Appl. Polym. Sci., 128, pp. 258–264.

12. Budakian R., Putterman S.J., 2002, *Time scales for cold welding and the origins of stick-slip friction*, Phys. Rev. B, 65, pp. 235429.
13. Corcoran S.G., Colton J., 1997, *Anomalous plastic deformation at surfaces: nanoindentation of gold single crystals*, Phys. Rev. B, 55 pp. R16057.
14. Hess M., 2012, *On the reduction method of dimensionality: The exact mapping of axisymmetric contact problems with and without adhesion*, Phys. Mesomech., 15(5-6), pp. 264-269.
15. Popov V.L., Hess M., 2013, *Methode der Dimensionsreduktion in Kontaktmechanik und Reibung – Eine Berechnungsmethode im Mikro- und Makrobereich*, Springer-Verlag.
16. Popov V.L., 2013, *Method of reduction of dimensionality in contact and friction mechanics: A linkage between micro and macro scales*, Friction, 1(1), pp. 41-62.
17. Popov V.L., Hess M., 2014, *Method of dimensionality reduction in contact mechanics and friction*, Springer.
18. Popov V.L., 2010, *Contact Mechanics and Friction. Physical Principles and Applications*, Springer-Verlag, 362 pp.
19. Kleis I., Kulu P., 2008, *Solid Particle Erosion, Occurrence, prediction and control*, Springer, 206 pp.
20. Popov V.L., Psakhie S.G., 2007, *Numerical simulation methods in tribology*, Tribology International, 40, pp. 916–923.
21. Hess M. and Popov V.L., 2013, *Wärmeleitung und Wärmeerzeugung*, In: Popov, V.L. and Hess, M., *Methode der Dimensionsreduktion*, Springer, pp. 115-131.
22. Hess M. and Popov V.L., 2013, *Exakte Lösungen in drei Dimensionen für den Normalkontakt rotationsymmetrischer Körper*, In: Popov V.L. and Hess M., *Methode der Dimensionsreduktion*, Springer, pp. 227-239.
23. Hess M. and Popov V.L., 2013, *Exakte Lösungen in drei Dimensionen für den Tangentialkontakt rotationsymmetrischer Körper*, In: Popov V.L. and Hess M. (Eds.), *Methode der Dimensionsreduktion*, Springer, pp. 227-239.

